Construction of novel optical imaging probes and their applications in bioassays

Shao, Qing

2014

Shao, Q. (2014). Construction of novel optical imaging probes and their applications in bioassays. Doctoral thesis, Nanyang Technological University, Singapore.

https://hdl.handle.net/10356/55325

https://doi.org/10.32657/10356/55325

CONSTRUCTION OF NOVEL OPTICAL IMAGING PROBES AND THEIR APPLICATIONS IN BIOASSAYS

SHAO QING

School of Physical and Mathematical Sciences

A thesis submitted to the Nanyang Technological University in partial fulfillment of the requirement for the degree of Doctor of Philosophy

2014

Acknowledgements

First, the author owes his deepest gratitude to his supervisor, Associate Professor Bengang Xing, whose continuous support and strict training enabled the author to complete the PhD course studies.

The author wishes to thank the members in Professor Xing's group for the helpful discussion and kind assistance: Dr. Jiang Tingting, Dr. Yang Yanmei, Dr. Liu Rongrong, Dr. Min Yuanzeng, Dr. Li Jinming, Mr. Liu Fang, Miss Mu Jing, Miss Lv Linna, Mr. Ai Xiangzhao, Mr. Aw Junxin, Miss Li Xi, Dr. Feng Huajun, Dr. He Yu, Dr. Ma Ying, Dr. Mo Yufei, Dr. Chen Zihui, Mr. Ling Yanwu and Mr. Song Zhijian.

The author also wishes to thank cooperators in other research groups: Prof. Yan Xiaomei and Miss Zheng Yan from Xiamen University; Prof. Cheng Zhen and Dr. Ren Gang from Stanford University Medical Center; Prof. Tang Kai and Mr. Dong Xueming from School of Biological Sciences.

The author is grateful to Nanyang Technological University for providing a research scholarship.

Finally, the author wishes to express his sincere appreciation to his family for their continuous encouragement and assistance.

Table of Contents

Abbreviations

δ	chemical shift (ppm)
Ac	acetyl
Bla	*β*-lactamase
Boc	*t*-butoxycarbonyl
br	broad singlet
CA	clavulanic acid
CFU	colony forming units
d	doublet
dd	doublet of doublets
DMAP	4-dimethylaminopyridine
DMF	N,N-dimethylformide
fLuc	firefly luciferase
FRET	fluorescent resonance energy transfer
J	coupling constants
M	concentration (mol/L)
M^+	parent ion peak (mass spectrum)
m	multiplet
MALDI-TOF	matrix-assisted laser desorption ionization-time of flight
mg	milligram
MHz	megahertz
MIC	minimum inhibitory concentration

mmol	millimole
MRSA	methicillin-resistant *Staphylococcus aureus*
MS	Mass spectrum
NMR	nuclear magnetic resonance
ns	nanosecond
PACT	photodynamic antimicrobial chemotherapy
PBPs	penicillin-binding proteins
PBS	phosphate buffered saline
PS	photosensitizer
q	quarter
ROS	reactive oxygen species
RP-HPLC	reversed phase high performance liquid chromatography
rt	room temperature
Ru	ruthenium
s	singlet
t	triplet
TFA	trifluoroacetic acid
THF	tetrahydrofuran
UV-Vis	ultraviolet-visible spectroscopy
Φ	quantum yield

Abstract

Benefited from the direct and non-invasive visualization, optical imaging has been extensively used for real-time observation of subcellular events and biochemical processes in living systems. In this technology, well-designed imaging probes are required to report the interested biological events with efficient signal contrast and specific target recognition.

In this thesis, the author describes the development of novel optical imaging probes for detection of specific biological targets (e.g. bacterial β-lactamase, antibiotic resistant bacteria and reporter enzyme firefly luciferase). Construction of these probes relies on characteristic biological reactions to ensure signal specificity, also involves particular strategies to confer these probes with attractive properties such as covalent labeling activity, photosensitizing capability or spatiotemporal control.

Chapter 2 presents enzyme responsive covalent probes for imaging and fast screening of antibiotic resistant bacteria. These probes are designed as pre-quenched. They are activated by endogenous β-lactamase, a resistance-related bacterial enzyme, to generate the fluorescent protein labeling. The covalent labeling property can reduce the fluorescence background by minimizing probe diffusion, thus provides quantitative analysis of the resistant bacterial population (down to as low as 5%) by flow cytometry, also allows single-cell detection and direct observation of bacterial enzyme activity in resistant pathogenic species.

Chapter 3 describes the construction of a luminescent Ru(II) probe for intracellular imaging and lethal photosensitization of drug resistant bacteria. By combining enzyme

recognizing specificity and photosensitizing function, this probe displays promising imaging and photokilling capabilities to the drug resistant strains, including pathogenic species like clinically isolated methicillin-resistant *Staphylococcus aureus*.

Chapter 4 presents the preliminary results of an ongoing study on the development of fluorescent probes for detection and identification of bacterial *β*-lactamases through the approach of activity-based protein labeling.

Chapter 5 presents the photocaged bioluminescent probes for selective imaging of firefly luciferase reporter gene expression in living mice with simple and controlled photoactivation. With the photocage strategy, the firefly bioluminescence can provide great opportunities for monitoring biological events *in vivo* with spatial and temporal control.

Chapter 1

General Introduction

1.1 Optical imaging

With the improvement of microscopy and probe techniques, an increasing number of investigations on the basis of bio-imaging techniques have provided critical insights into the fundamental nature of cellular and tissue functions, which contribute greatly to the preclinical investigations with early and precise diagnosis. This visualization of cellular events and molecular processes is enabled by the molecular imaging techniques, such as optical imaging, magnetic resonance imaging, ultrasound imaging, positron emission tomography (PET) and single photon emission computed tomography (SPECT). Among them, optical imaging is recently established with light source as imaging signals. This imaging technique involves the production of light emissions, usually fluorescence or bioluminescence, and capture of the optical signals by a charge-coupled device (CCD) camera for image generation.[1] By using light for image generation, optical probe does not involve the use of radiation which is more desirable than radionuclide based imaging modalities such as PET and SPECT. [2-4]

In general, optical imaging can be divided into fluorescent imaging and bioluminescent imaging according to the light signals. Fluorescence is produced by illuminating a fluorophore with excitation light. One most important parameter to conduct fluorescent imaging is the brightness of the emission, which is usually dependent on the photophysical properties of the fluorophore and influenced more or less by the surrounding microenvironment. The intrinsic brightness of a

fluorophore can be defined as the product of molar extinction coefficient (ε) and fluorescence quantum yield (Φ), which describes the ability of the fluorophore to absorb and emit light respectively.

Fluorescent microscopy imaging is one of the most widely used microscopy due to the feasibility of observing specific cellular components through targeted and specific fluorescent signals.[5] This imaging technique can provide high spatial resolution on the nanometer and sub-hundred nanometer scales for imaging cellular components and proteins with short acquisition time, thus ensures realtime monitoring of protein functions and dynamics in living cells.[6,7]

Meanwhile, fluorescent imaging still has potential limitations. For example, some imaging results are compromised by the probe photobleaching during image acquisition.[8] In addition, in living animal applications, the intrinsic light scattering and absorption by endogenous biomolecules such as hemoglobin will inevitably limit the light penetration depth in tissues, for example, only a few millimeters of fluorescence at visible wavelength.[1] Moreover, endogenous tissue autofluorescence from NADPH and flavin biomolecules may cause a dramatic loss of signal specificity and sensitivity when using the fluorophores of samiliar photophysical properties.[9] To improve fluorescent imaging for *in vivo* applications, the near infrared (NIR) light is preferentially appreciated. In this region (700-900 nm), light scattering and absorption coefficient is considerably lower (Figure 1.1), thus the NIR light can penetrate deeply to depths of several centimeters for small animal imaging.[10]

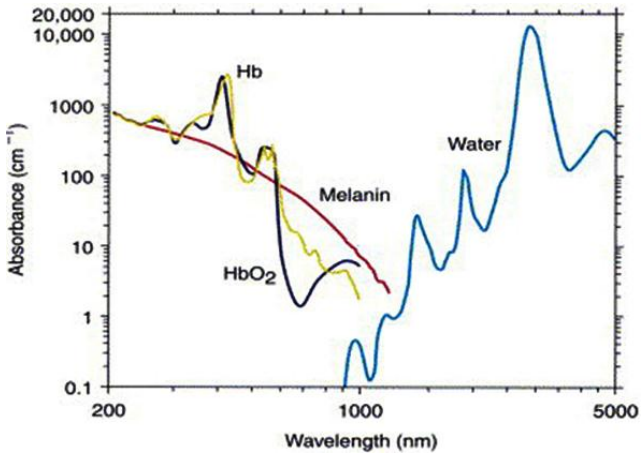

Figure 1.1 Absorption spectra of tissue components. (Hb = hemoglobin; HbO_2 = oxyhemoglobin).

Another optical imaging technique utilizes bioluminescence for image generation, which emits during specific enzymatic reactions. As the production of bioluminescence does not require excitation light, there is no autofluorescence background in tissues. In addition, the bioluminescent luciferase enzyme does not exist in mammalian cells, thus bioluminescence has nearly zero background for *in vivo* imaging.[11] Meanwhile, the generation of bioluminescence is highly efficient. For example, the quantum yield of firefly bioluminescence based on D-luciferin substrate and firefly luciferase reaches ~ 41.0% as recently determined,[12] affording great sensitivity for detection of attomole amounts of the luciferase protein.[13] With high sensitivity and specificity, bioluminescent imaging has been widely used for non-invasive visualization of biological events in living cells and animals.[14]

Up to now, the continuous technical improvement and imaging reagent development has enabled real-time investigation of three-dimensional structures and dynamic processes in living cells and small animals without sacrifice of experimental subjects.[15] Optical imaging, due to operational simplicity, tremendous adaptability and

substantial cost benefits, has become a mainstay technique in a wide variety of studies like cellular trafficking,[16] gene function,[17] drug discovery[18] and disease diagnosis.[19]

1.2 Optical imaging strategies

Optical imaging enables real time visualization of biological events of interest, such as native biomolecules or genetically modified organisms, where imaging probes are delivered to produce contrast signals specifically to these events.

1.2.1 Imaging of endogenous targets

To study native biological events, some imaging strategies utilize the probes to produce higher signal intensity over nonspecific background as a result of strong binding affinity to the biological targets (Figure 1.2B).

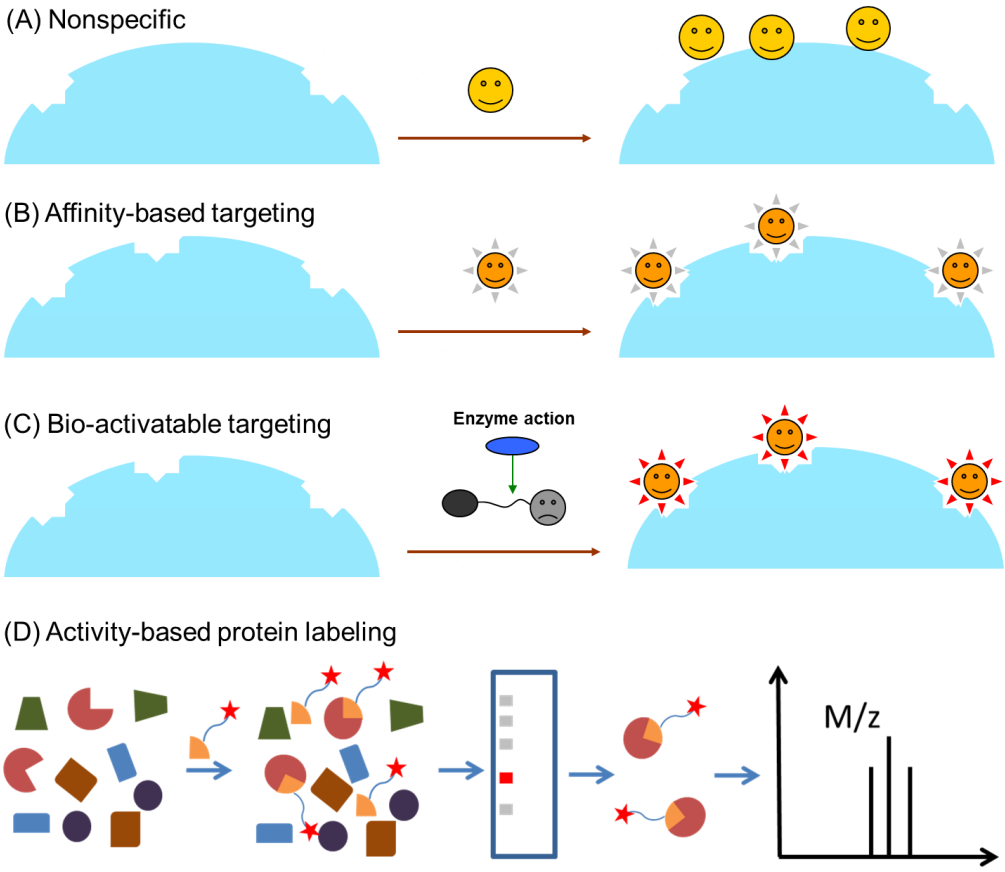

Figure 1.2 Illustration for general fluorescent imaging strategies and probe design.

Some other strategies detect the distinguished emission changes, where the probe is involved to report specific biological events or reporters with characteristic emission shift or on-off switch (Figure 1.2C). Besides, the imaging probe can be constructed with the ability to identify targeted protein in the presence of complex proteome mixtures (Figure 1.2D).

1.2.1.1 Affinity-based targeting

Cellular investigation of biological events usually requires well-designed imaging probes based on both molecular biology and cell biology. Although some simple fluorophores, such as indocyanine green, have been approved as contrast agents for cardiac and hepatic function testing in clinical investigations,[20,21] the heterogeneity and complexity of biological events still requires unique probes to generate specific and essential signal contrasts. For this purpose, one useful feature is the binding affinity of the probe to specific biological targets.

A few fluorescent small molecules naturally possess the binding affinities, such as 4',6-diamidino-2-phenylindole (DAPI), which binds strongly with DNA molecules and becomes more fluorescent upon binding, thus labels the cell nuclei. Such fluorescent staining of cellular structures has been widely used to determine the localization of the studied biological process.

However, most fluorophores are nonspecific and not able to bind cellular components. In order to improve the signal specificity in living systems, a simple and feasible way is to conjugate the fluorophores to the ligand moieties with strong binding affinities to specific molecular targets.

This strategy has been extensively used to image living cells and animals. The affinity ligands can be proteins, peptides and small biomolecules, which possess strong non-covalent bindings to specific biological targets with molecular recognitions. Incorporation of the dye molecule requires careful design to retain the binding affinities. Upon binding, the fluorescent probes are trapped in the target area, with the unbound fluorescent probes easily eliminated through the circulation process, thus provides a simple method to minimize the nonspecific binding and improve the signal contrast.

Some of these approaches involve well-known proteins of high-affinity interactions, like antibody-antigen complexes, membrane protein receptors, etc. Such tumor-targeting monoclonal antibodies[22] and epidermal growth factors[23] have been employed to conjugate NIR dyes for real-time imaging of tumor growth in living animals due to efficient binding and long tissue retention.

In terms of potential immune response from the large size of proteins, this approach has been significantly improved by the findings of important peptide sequences with specific binding affinities. Due to the smaller size, the targeting peptides have several advantages over the large protein molecules in optical imaging, such as fast clearance of non-bound molecules. Moreover, with synthetic chemistry and commercial peptide synthesizer, it is easy to develop a large combinatorial peptide library for bioactivity screening, providing much more possibilities for potent biological and chemical discoveries. For example, the Arg-Gly-Asp (RGD) sequence (Figure 1.3), which is discovered from phage display technique and serves for cell attachment by cell surface

reporter integrins,[24] has been extensively used for *in vivo* tumor imaging by targeting the high expression of $\alpha_v\beta_3$ integrin in tumors.[25,26]

Some small biomolecules also display specific interactions to biological targets which are particularly highly expressed in tumor cells (Figure 1.3). For example, folic acid has high binding affinity with folate receptor protein, which is overexpressed on certain cancer cells and regarded as an emerging imaging and therapeutic target.[27] Meanwhile, the folate linked contrast agents can be delivered cellularly through the folate receptor-mediated endocytosis, not restricted to the normal permeability barriers.[28,29] Besides, 2-deoxy-D-glucose (2-DG) has also been used in targeted optical imaging due to the upregulation of glucose transporters (GLUTs) in cancer cells.[30] The NIR fluorescent Cy5.5-2DG molecule has been successfully developed to visualize the location of tumor cells in living mice.[31] Interestingly, it is also indicated in this work that although with the tumor-targeting abilities, the enhanced uptake of Cy5.5-2DG is

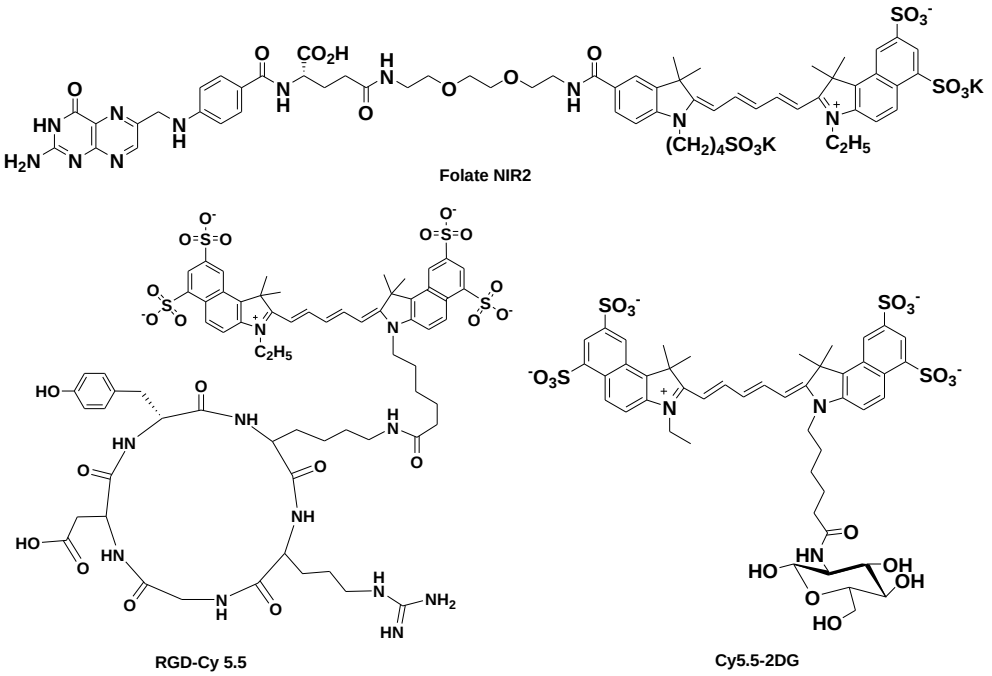

Figure 1.3 Representative fluorescent contrast agents based on small biomolecules.

not through GLUTs. Thus it is critical to select a fluorophore with reasonable size for efficient cellular uptake.

In addition, some other affinity-based probes are fluorescent derivatives of drugs or toxins with binding properties to cellular structures. For example, phallotoxins are originally isolated from mushrooms and bind tightly to the polymerized filamentous actin. Fluorescently conjugated phalloidin is now used to stain actin fibers in mammalian cells. Due to the specific binding ability, these fluorescent stains are commercially available and have been widely used in cell biology (Figure 1.4).

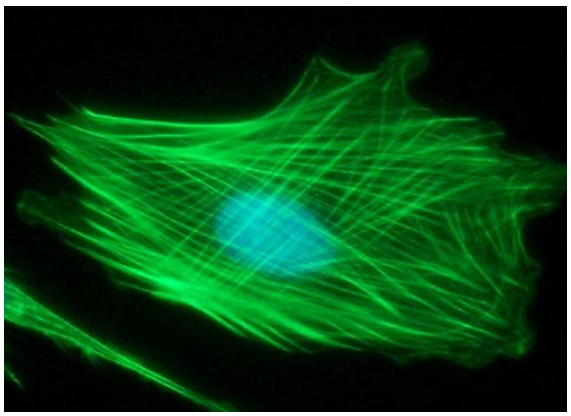

Figure 1.4 Fluorescent staining of cellular structures. The cells are stained with DAPI to stain nucleus (blue) and Alexa Fluor 488 conjugated phalloidin to stain intracellular actin filaments (green).

With specific target recognition, these affinity-based probes have become promising tools for monitoring molecular events and biological pathways. Especially the small biomolecules and peptides, with essential signal contrasts and attractive pharmacokinetics, have been successfully used for non-invasive imaging of tumor growth and therapy assessment. However, the presence of inevitable non-specific binding in living systems will limit the extensive applications of some affinity ligands

in preclinical practices. The signal-to-noise ratio dependent on the accumulation of imaging probes may be relatively low compared to tissue background and compromise the sensitivity, especially when the biological target of interest is naturally expressed in low level, thus requires the strategy of an activatable imaging to produce distinctive signal contrasts specific to the biological targets.

1.2.1.2 Bio-activatable targeting

The bio-activatable targeting can report the molecular specificity of the biological targets by the controlled manipulation of emission output as a response to the consequent change of a probe in structural conformation and chemical environments. This process normally involves the significantly amplified fluorescent signals by specific target activation, which has been extensively used for the functional imaging of enzyme activities.[32-34]

The mostly used application is monitoring protease activity, which is abundant in nature and essential for many important biological processes including diseases. Development of sensitive probes to study proteases distribution and inhibition is important not only in understanding the mechanism of diseases, such as HIV, cancer, Alzheimer's and heart diseases, but also in monitoring the progression and therapy of these diseases.[35-37]

Construction of these bio-activatable probes is usually based on enzyme substrates with the design principle of pre-quenching, such as fluorescent resonance energy transfer (FRET) to achieve low signal background. The biological activation will produce significant emission enhancement or signal regeneration. Such approach has

been used for imaging matrix metalloproteinase-7 (MMP-7)[38] and caspases[39] in cells and *in vivo*. In these studies, FRET pairs are connected with enzyme responsive peptides to construct NIR-labeled pre-quenched targeting probes, which can penetrate into cells with the fluorescent signal activated by the overexpression of targeted enzymes, thus providing high signal-to-noise ratio for *in vivo* imaging of tumor cells with target protein expressions.

1.2.1.3 Activity-based protein labeling

With the improvement of our understanding of cell signaling, the protein functions in their natural habitat have attracted much attention. Specific labeling of these proteins without introduction of recombinant tag is ideal for this purpose. Such approach of activity-based protein profiling (ABPP) has been developed for specific protein identification, including oxidoreductases, kinases, proteases, phosphatases and glycosidases.[40] The ABPP study requires well-designed probes to selectively label target protein residues in a complicated microenvironment. These probes are usually composed of two functional components: a targeting group to bind the protein of interest with covalent bonding and an analytical handle to report the bonding (Figure 1.5). The targeting group works as a mechanism-based inhibitor to direct the probe to the enzyme, thus ensures the binding specificity. The labeling event can be analyzed through Mass spectrum or visualized in gel analysis by the fluorescent signal from the analytical handle.

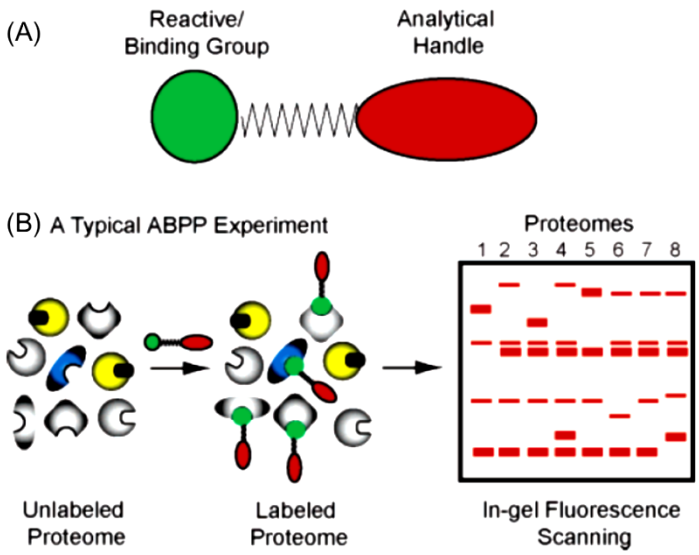

Figure 1.5 Activity-based protein profiling: (A) Construction of a typical activity-based probe, consisting of an recognition group (green) with reactivity to subsets of the proteome, and an analytical handle (red, e.g., fluorophore, biotin) for the visualization or characterization of labeling events; (B) a schematic representation of a typical ABPP experiment, consisting of a labeling step in complex proteomes and an analytical step to characterize the activity-dependent labeling events.[40]

For example, this approach has been extended for *in vivo* optical imaging of protease expression in tumor cells with a prequenched activity-based probe.[41,42] Design of this probe is based on the covalent inhibition of a cysteine protease by an acyloxymethyl ketone. In this probe, a Cy5-labeled peptide is connected to an acyloxy leaving group bearing a QSY21 quencher. This probe is cell-permeable. It is selectively cleaved at the acyloxy linkage by protease and covalently bonded to the thiol group of enzyme active site, thus has been used for intracellular imaging of protease dynamics and direct monitoring of protease functions in living animals (Figure 1.6).

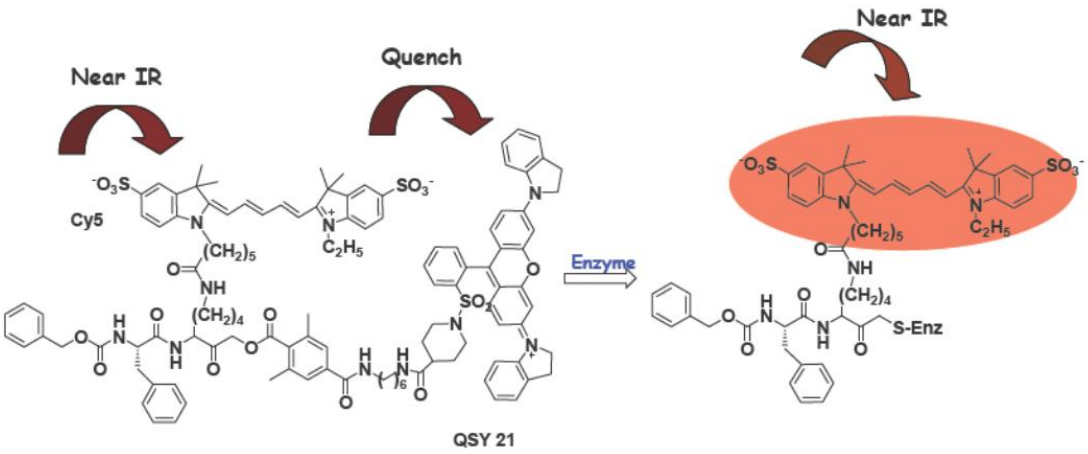

Figure 1.6 Mechanism of pre-quenched activity-based probes for cysteine protease labeling.[42]

With these imaging strategies, the endogenous biomolecules can be readily imaged to facilitate the biological and preclinical studies. Meanwhile, another strategy for investigation of biological events of interest is through the introduction of genetically encodable exogenous reporters, which has also provided promising opportunities in imaging applications.

1.2.2 Imaging of exogenous reporters

The incorporation of exogenous reporters has allowed real-time monitoring of cell tracking and protein activities in living subjects.[43] Reporter genes can be directly transferred into cells of organ systems or fused to endogenous genes of interest. And the gene product can be easily detected by intrinsic fluorescence or by a reporter probe, which is converted to a metabolite selectively trapped within targeted cells during the period of image acquisition.[44] The ideal reporter gene should be non-toxic and non-immunogenic, and the expression product should not cause significant biological

effect on the transfected cells. The reporter probes should be stable in living conditions and not metabolized before reaching the target. In addition, the probe and the metabolic products should be biocompatible and not cytotoxic. Currently, the mostly used reporter genes for optical imaging include fluorescent protein, bioluminescent luciferase, β-lactamase and β-galactosidase, as well as other recombinant tags for small-molecule labeling.

1.2.2.1 Fluorescent proteins

Fluorescent proteins (FPs) are the most common genetic reporters in cell biology because of versatile applications and relative easy manipulations. They are genetically encoded and the fusion proteins become highly fluorescent spontaneously, thus provides intrinsic signals for fluorescent observation without delivery of additional imaging probes.[45] In addition, with extensive efforts in improving FP stability and photophysical property, many new FP variants have been developed, which cover a broad emission range from blue to near infrared and allow more specific and practical applications for live cell imaging and biosensor development.[46] Most fluorescent proteins have moderate fluorescence quantum yields (Φ) and molar extinction coefficients (ε) (Figure 1.7), while the brightness is also affected by the protein folding efficiency and protein microenvironment.[45]

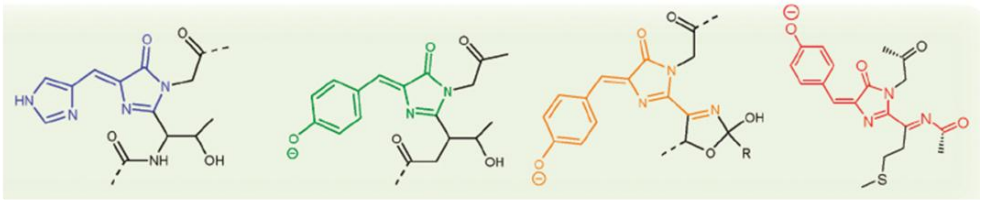

EBFP	EGFP	mOrange	mKate
Ex/Em: 383/445 nm	484/507 nm	548/562 nm	588/635 nm
Φ/ε: 0.31/29900	0.6/56000	0.69/71000	0.33/45000

Figure 1.7 Chromophore structures and photophysical properties of selective fluorescent protein color variants.

The discovery of FP color variants has also benefited the design principle of FRET for quantitative analysis of cellular biomolecules and environments such as ATP, lipid, sugar, membrane potential and proteins, as well as the real-time visualization of protein-protein interactions *in situ*.[45,46] In these studies, the most popular FRET pair is cyan fluorescent protein as energy donor and yellow fluorescent protein as energy acceptor, of which the efficiency of energy transfer is sensitive to the conformational change of the probe caused by specific ligand binding or post-translational modification, with resultant change in emission spectrum (Figure 1.8).

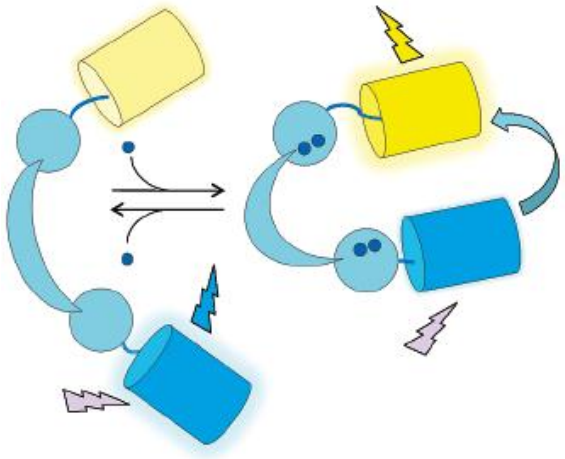

Figure 1.8 Design principle of FRET-based probe containing FP variants.[45]

1.2.2.2 Fusion tags with small-molecule targeting

With the interests in protein kinetics and functions, the FP genes may potentially interfere with the structure and function of some fused proteins under investigation due to the large size.[47,48] Such perturbation has been observed, for example when the fluorescent protein is fused to membrane proteins[49] or tubulin proteins,[50] which in turn can be avoided by replacing the large FP fusion protein with small-molecule tags in some cases.[51,52] Thus various strategies have been developed for specific protein targeting by employing small-molecule probes. These approaches usually require the combination of genetically encoded tags for site specific molecular recognition.[53] Among them, the mostly used probes are developed on the basis of tetracysteine/biarsenical interactions and fluorophore-tag conjugates.

Tetracysteine/biarsenical system is based on the high affinity interactions between trivalent arsenic compounds and the genetically encoded tetracysteine motif (CCXXCC, C is cysteine, X is any amino acid).[54] These arsenic probes are usually cell permeable and coadministrated with 1,2-ethanedithiol (EDT) antidote to reduce cytotoxicity in living cell study. Among them, the [4'-5'-bis(1,3,2-dithioarsolan-2-yl)]-fluorescein (FlAsH) and resorufin (ReAsH) have been widely used due to the high binding affinities (K_D = ~10^{-11}-10^{-12} M) and dramatic enhancement of respective green and red fluorescence (Figure 1.9).[55] The fast formation (k_a = ~10^5 $M^{-1}s^{-1}$) and slow dissociation (k_d = ~10^{-7} $M^{-1}s^{-1}$) of the organoarsenic chelators ensures the selectivity of the targeting process in the complicated chemical environment of EDT antidote and cellular thiol groups. In addition, as the unbound probes are

nonfluorescent, the background is quite low compared to the generated fluorescent signal upon binding, thus has been used in cellular imaging.[51,52]

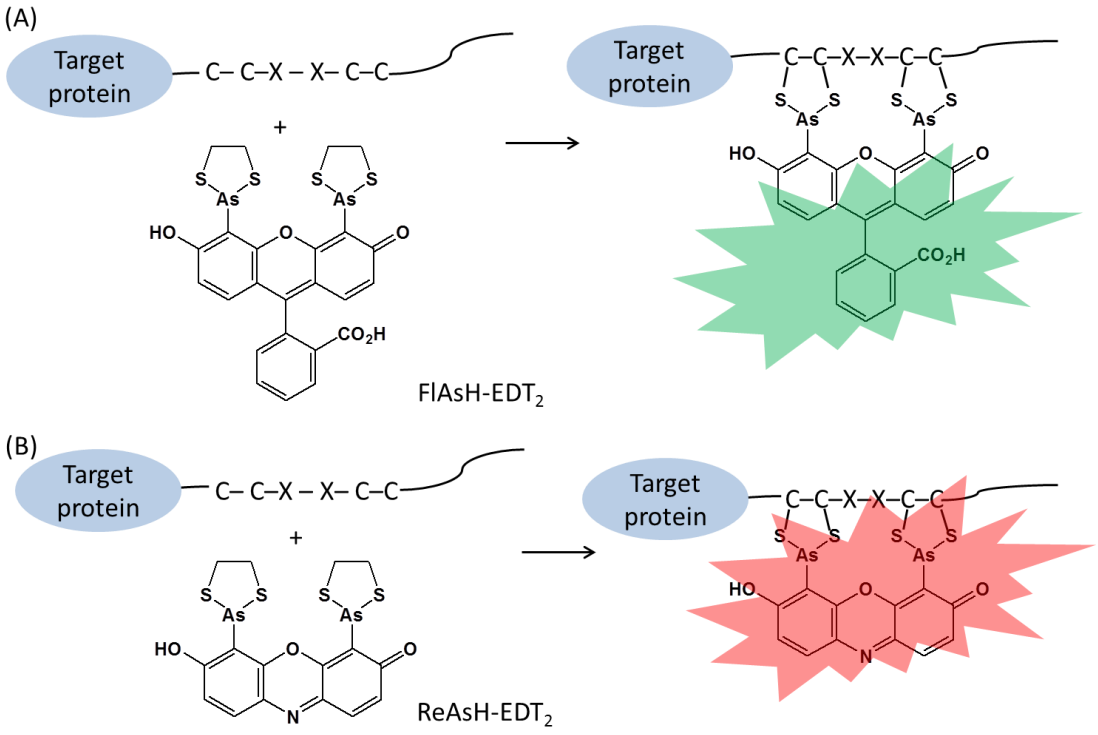

Figure 1.9 Strategy of tetracysteine/biarsenical for protein labeling with (A) FlAsH and (B) ReAsH probes.

The fluorophore-tag conjugates represent the Snap-tag and Halotag strategies that employ enzymes, such as O^6-alkylguanine-DNA-alkyltransferase (hAGT)[56] or a mutated bacterial halogene dehalogenase,[57] to irreversibly transfer their substrates into covalent labeling. This process involves the nucleophilic attack of O^6-benzylguanine (BG) by an activated cysteine residue of hAGT with the benzene ring covalently attached to the enzyme (Figure 1.10).[56,58] And in the mutated halogene dehalogenase, the hydrolysis step of a formed ester intermediate is prohibited by replacing the active His272 with Phe.[57,59] As the labeling is exclusively activated by the fusion tags, these labeling processes are highly specific and suitable for living cell study. It should also

be mentioned that compared with the tetracysteine motif, the fusion tag of hAGT and halogene dehalogenase may still represent the size considerations (182 and 293 amino acids respectively), which require further explorations.

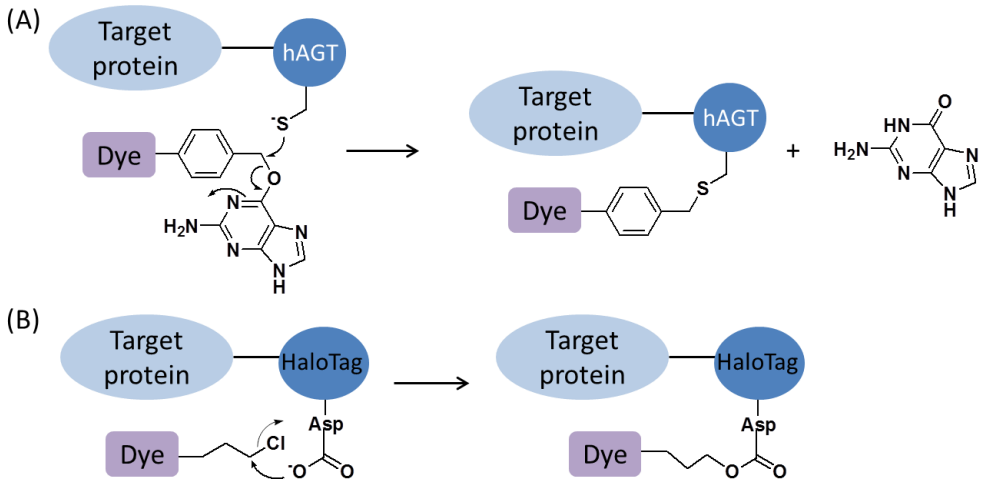

Figure 1.10 Genetically targetable tags for small-molecule labeling. (A) Snap-tag/BG system and (B) Halotag system.

With the selective incorporation of a fluorescent tag, such as fluorescent protein and small-molecule targeting fusion tag, this reporter strategy has enabled the real-time tracking of intracellular signaling pathways in living cells. Besides, the strategy of exogenous reporter also appreciates the catalytic signal amplification for improved sensitivity, such as incorporation of luciferase, β-lactamase and β-galactosidase, which can be imaged by specific probes with characteristic emissions.

1.2.2.3 Luciferase

Luciferases are oxidative enzymes found in some living creatures like bacteria, fungi, insects and marine organisms, which can naturally emit light. Among them, the *Firefly* (FLuc), *Renilla* (RLuc) and bacterial luciferases are extensively used in bioluminescent imaging as the reporter genes (Table 1.1). As cells and tissues without

luciferase expression do not emit during normal cellular functions, bioluminescence is highly sensitive and specific for visualization of cell trafficking and signaling pathways in small animals.[60]

Reporter	Advantages	Disadvantages
Firefly and click beetle luciferases D-luciferin substrate	• High sensitivity; • Quantitative correlation between signal strength and cell numbers; • Low background in animal tissues; • Different colors are available	• Requires exogenous luciferin; • Fast consumption of luciferin can lead to unstable signal; • ATP and oxygen dependent; • Currently not practical for large animal models
Renilla and Gaussia luciferase Coelenterazine substrate	• High sensitivity; • Quantitative correlation between signal strength and cell numbers; • Stabilized and red-shifted Renilla luciferases are available; • Secretion of Gaussia luciferase allows for subject-independent bioluminescence measurement	• Requires exogenous coelenterazine; • Low anatomic resolution; • Increased background due to oxidation of substrate by serum; • Oxygen dependent; • Fast consumption of coelenterazine can lead to unstable signal; • Currently not practical for large animal models
Bacterial luciferase	• High sensitivity; • Quantitative correlation between signal strength and cell number; • No requirement of addition of exogenous substrate; • Noninvasive and stable signal; • Rapid detection permitting real-time monitoring	• Emission at 490 nm prone to absorption in animal tissues; • Low anatomic resolution; • NADPH and oxygen dependent; • Not as bright as other luciferases; • Currently not practical for large animal models

Table 1.1 Comparison of luciferase reporter proteins.

Expression of luciferase can be imaged with the delivery of specific enzyme substrates like D-luciferin for FLuc and coelenterazine for RLuc. In this process, the expressed luciferase enzyme catalyzes the oxidation of these substrates in the presence of oxygen with concomitant emission of bioluminescence as a form of energy release (Figure 1.11), which has the emission peak at 560 nm for FLuc luminescence and 480

nm for RLuc luminescence.[61] In quantitative study, the luciferin substrates and oxygen levels are usually in large excess, thus the light intensity is directly related to the level of reporter gene production. In addition, FLuc mutants can produce red bioluminescence emission by using the same firefly luciferin substrate with good signal separation, which is suitable for dual-color reporter assays and imaging techniques,[62] thus providing more applications in biological study.

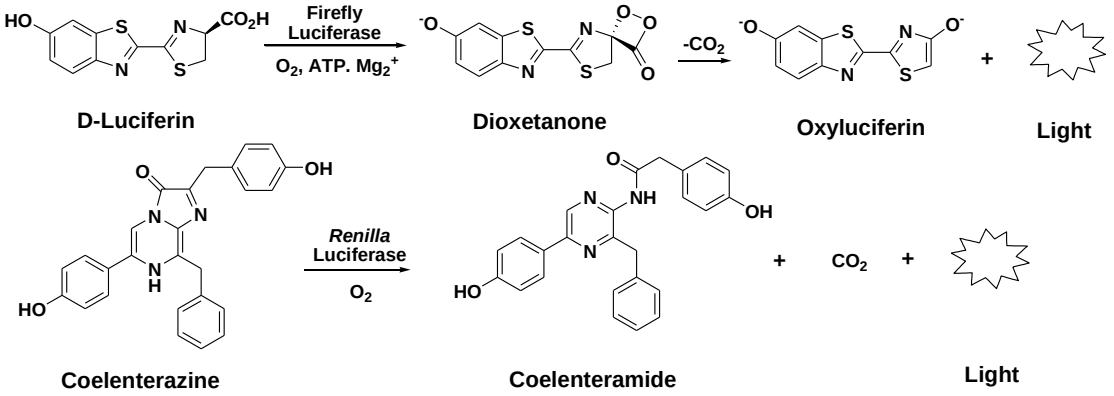

Figure 1.11 Mechanism of the bioluminescence production by oxidation of substrates.

1.2.2.4 β-Lactamase

The strategy of exogenous reporter also appreciates the catalytic signal amplification to provide brighter images with high sensitivity. This can be realized by β-lactamases (Blas), which are bacterial enzymes to render bacteria resistance to penicillin and cephalosporin antibiotics by catalyzing the hydrolysis of these drugs. Bla has not been found in mammalian cells. Expression of Bla in eukaryotic cells will not cause noticeable cell cytotoxicity and the product is not interfered by mammalian enzymes, thus has been developed as a sensitive reporter system in cell biology to monitor biological processes and protein-protein interactions.[63,64]

In vitro detection of Bla can be achieved by the colorimetric probe of Nitrocefin

with obvious colour change. Image of Bla expression in living cells requires fluorescent probes with preferred sensitivity. The first important probe is CCF2/AM, which is a cephalosporin derivative with FRET pairs. This probe is non-polar enough to cross cell membranes and trapped in the cells as a result of enzymatic hydrolysis of ester groups in the cytosol. The released structure undergoes Bla hydrolysis with characteristic emission shift from 520 nm (green fluorescence) to 477 nm (blue fluorescence) as the break of FRET, thus provides specific fluorescent signal for intracellular imaging of Bla expression (Figure 1.12).[65] This method of Bla reporter and CCF2/AM probe has been successfully applied in biological studies, such as investigation of promoter/regulator activities[66] and monitoring of protein-protein interactions in living cells.[67]

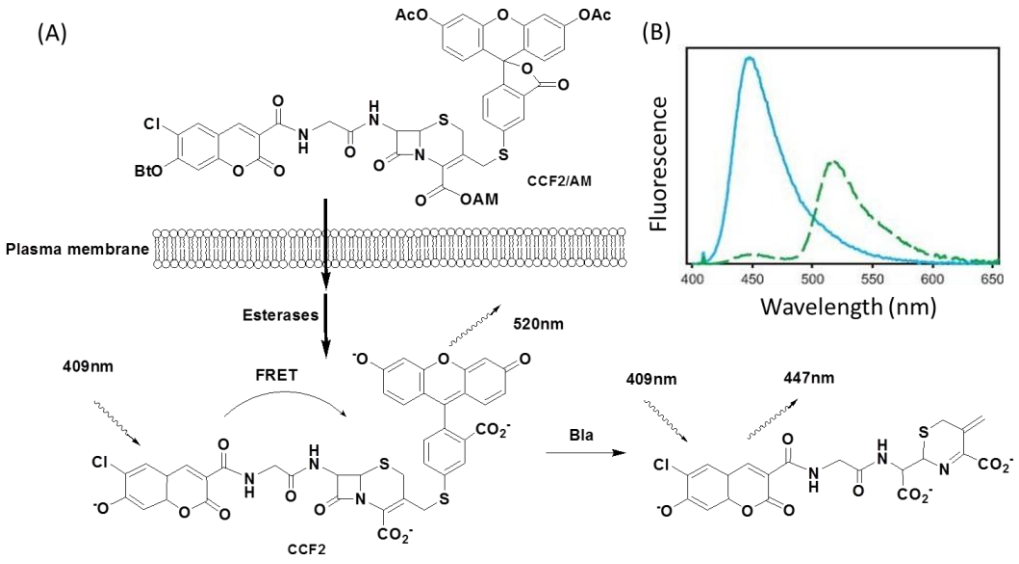

Figure 1.12 (A) Schematic presentation of CCF2/AM for Bla detection in living cells. (B) Fluorescence emission change before and after Bla activation.[65]

Development of Bla sensitive probes has now allowed *in vivo* imaging of Bla expression with FRET-quenched NIR probes[68] and bioluminescent probe[69] for

low-level background noise in living tissues (Figure 1.13). In addition, due to detection sensitivity and specificity, the Bla responsive NIR probes have also been used for imaging pathogenic bacteria with endogenous Bla production in living animals.[70]

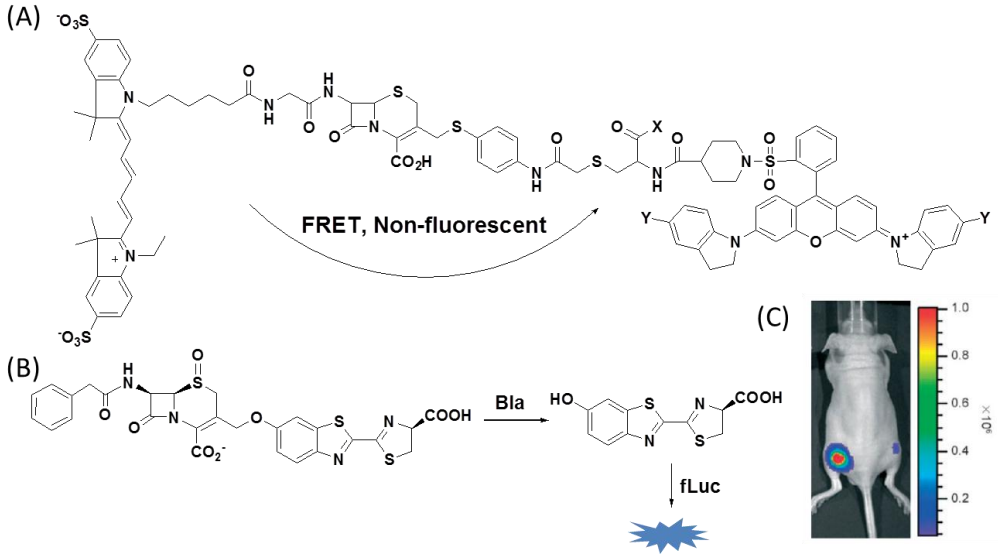

Figure 1.13 Structure of (A) NIR probes and (B) bioluminescent probe for detecting Bla activity. (C) Bioluminescent imaging of Bla expression *in vivo*.[69]

Moreover, it has also been demonstrated the applicability of specific protein labeling based on a noncatalytic Bla tag and FRET-quenched β-lactamase probe.[71] In this approach, the probe is covalently attached to the E166N mutant of TEM-1 as a result of markedly slowed probe deacylation. With fluorescent modification, the ^{E166N}TEM can be genetically encoded to label the protein of interest in living cells (Figure 1.14).

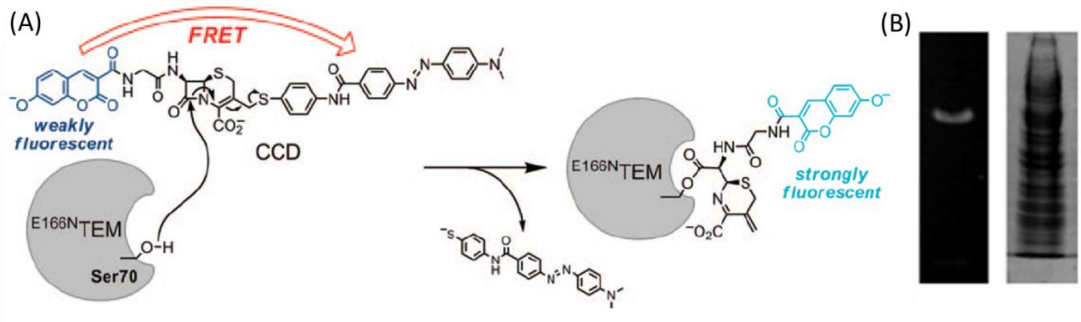

Figure 1.14 (A) Labeling mechanism of noncatalytic Bla mutant; (B) Fluorescent (left) and coomassie blue stained (right) gel image of maltose binding protein-^{E166N}TEM construct mixed with cell lysate after incubation with probe.[71]

1.2.2.5 β-Galactosidase

The catalytic signal amplification can also be achieved by β-galactosidase (β-gal), which is a hydrolase enzyme to break the β-glycosidic bond and hydrolyze various β-galactosides into monosaccharides. The *lacZ* gene of bacterial β-gal enzyme in *Escherichia coli* has been widely used as a reporter gene in molecular biology.

In gene cloning, β-gal has been conveniently used to distinguish a successful cloning product from unsuccessful ones. Cells with functional β-gal production can be visualized by X-gal, which produces a characteristic blue precipitate *in situ* (Scheme 1.1). Cells with successful ligation of a gene of interest will disrupt the functional β-gal production, resulting in white colonies.[72]

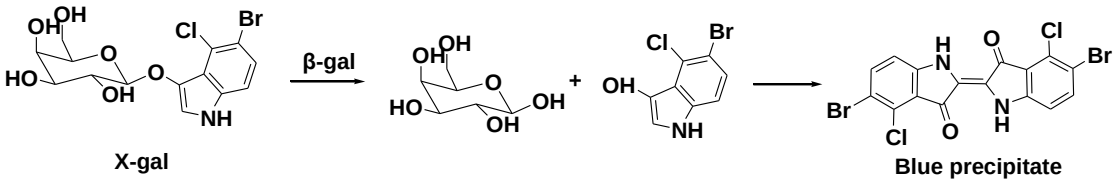

Scheme 1.1 Detection of β-gal by X-gal with blue precipitate formation.

In optical imaging, fluorescent and bioluminescent probes have been developed to

examine β-gal activity in living cells and small animals with preferred sensitivity and enzyme kinetics. For example, the nonfluorescent DDAOG molecule can penetrate the cell membrane and release the fluorophore DDAO by β-gal hydrolysis, with the recovery of far-red emission properties (Ex = 646 nm, Em = 659 nm) suitable for *in vivo* tumor imaging (Figure 1.15A,C).[73]

In vivo imaging of β-gal expression can also be realized with a dual reporter-enzyme platform with co-expression of fLuc reporter gene. This system uses a caged D-luciferin-galactoside conjugate as the probe to report β-gal with subsequent production of bioluminescent signal for *in vivo* imaging (Figure 1.15B).[17]

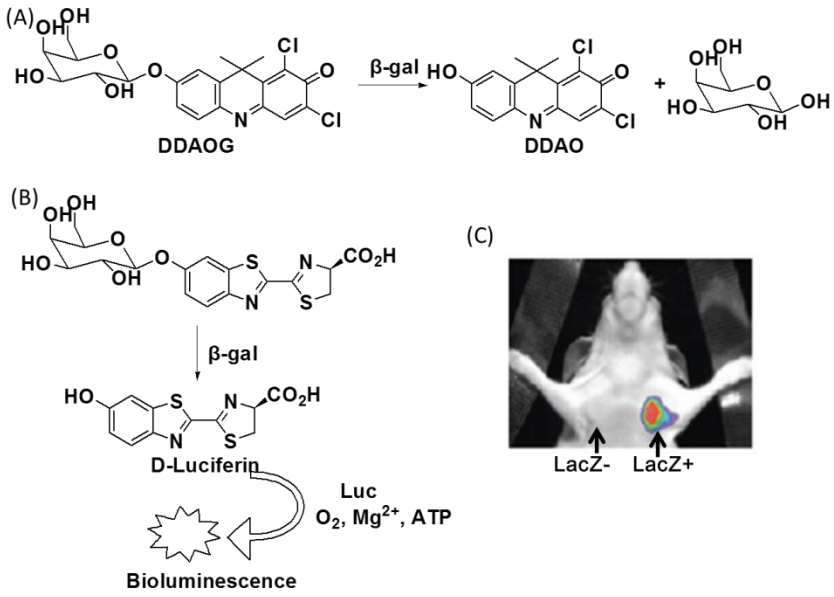

Figure 1.15 (A) fluorescent DDAOG and (B) bioluminescent probe for imaging β-gal activity. (C) *In vivo* fluorescent imaging of β-gal expression by DDAOG.[73]

1.3 Other strategies in imaging study

These imaging strategies and reporters have allowed noninvasive imaging of specific biological targets. Meanwhile, the interest of identifying the function and

dynamic of a single biomolecule in complicated environments is still in demand of novel probes and chemical biology strategies. Besides, the imaging probes are also exploited to extend the field and power of optical applications with conferred multidisciplinary functions. With these considerations, some strategies have been developed for better understanding the biological events and serving the multiple purposes in optical imaging.

1.3.1 Photocage strategy

Biomolecules often regulate their activities and dynamic properties in different conditions. Exploration of such biological functions and dynamics requires the control of surrounding microenvironments and regulation of protein activities at the molecular level, which is greatly benefited from the photocage strategy with controlled spatiotemporal modulation.[74,75] In this strategy, photolabile groups (Figure 1.16) are employed to temporarily block the biomolecules, which can be activated *in situ* upon brief illumination,[76] thus provides a promising tool in the regulation of protein activity, gene expression and cell function.[77]

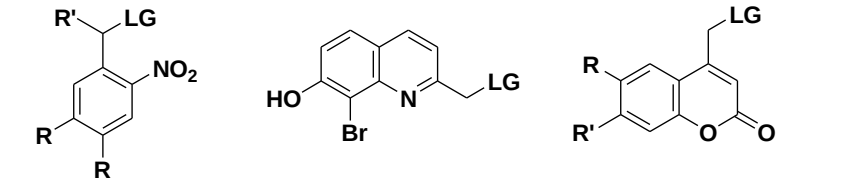

Figure 1.16 Molecular structures of selected photolabile protecting groups. (LG = leaving group)

To regulate protein activity, a caged amino acid can be genetically incorporated into natural proteins in a site-specific manner through nonsense suppression mutagenesis

and expressed protein ligation.[78] As an example, a photocaged DNA polymerase was successfully constructed through the incorporation of a caged tyrosine at the Y671 residue of enzyme activity, which allowed the precise control of DNA polymerization by brief illumination (Figure 1.17).[79]

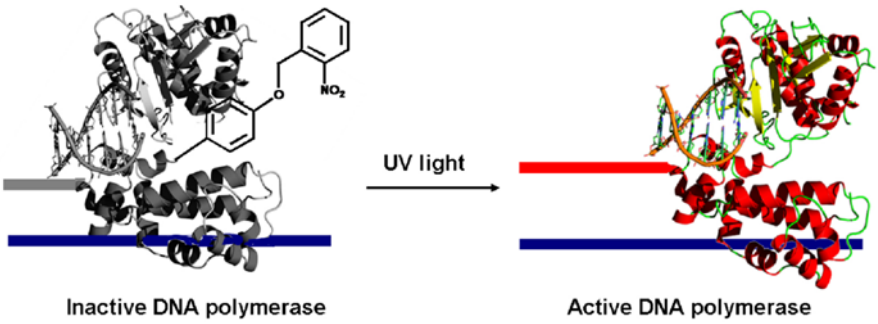

Figure 1.17 Photoactivation of DNA polymerase.[79]

However, introduction of photolabile groups to the protein of interest may not always block the protein function completely. On the contrary, photoregulation of gene expression is more direct and effective to control biological events.[80] The photoactive moieties can be directly installed onto phosphorus backbone or nucleotide base to achieve spatiotemporal regulation.[81] Moreover, the easy implementation of photocage technology and the accuracy of genetic methods have also allowed exceptional spatial control in gene regulation.[82,83]

1.3.2 Bio-activatable imaging with photosensitizer

The bio-activatable targeting strategy allows catalytic formation of activated probes to report specific biological events with high sensitivity. This strategy has also been used in the functional imaging with photosensitizers to benefit the targeting and selectivity of photodynamic therapy (PDT).

Some fluorescent molecules, like porphyrins, in their excited states are able to react with oxygen molecules and generate highly reactive singlet oxygen ($^1O_2$) during irradiation, which have been used to kill cancer cells in clinical applications.[84] These molecules, known as photosensitizers (PSs), also provide intrinsic fluorescent signals for diagnosis and treat assessment.[85]

Photosensitizers are often preferentially accumulated in neoplastic tissues. It makes them suitable for the early detection of tumor cells with fluorescence signal. In addition, PSs are also conjugated with biomolecules of specific affinities, like antibodies, lipoproteins, RGD peptide and folic acid, for improved cellular targeting and delivery.[85] The PSs normally have strong absorbance in visible wavelength and the photosensitizing process usually uses the light source of 600-800 nm range, which provides maximum light penetration and enough energy to produce singlet oxygen.[86]

However, many synthetic porphyrins have been found prolonged retention time in the skin with resultant increase in skin phototoxicity and decrease in tumor-to-tissue

Enzyme	Activatable link	Photosensitizer	Quencher	Activation fold[a]
β-galactosidase	β-galactoside	Thiazole orange	DNA-induce	N.A.
β-lactamase	β-lactam	EtNBS	Self-quenching	5
Caspase 3	GDEVDGSG	Pyropheophorbide-*a*	carotenoid	3
Caspase 3	GDEVDGSG	Pyropheophorbide-*a*	BHQ3	6
Cathepsin B	GFLG	Chlorin-e_6	Self-quenching	5
FAP	TSGPNQEQ	Pyropheophorbide-*a*	BHQ3	200
MMP7	GPLGLAR	Pyropheophorbide-*a*	BHQ3	19
thrombin	GFPIPRSGGGGG	Pyropheophorbide-*a*	Self-quenching	114

Table 1.2 Enzyme activated photosensitizers. [a] fluorescence enhancement.

contrast.[87] To improve the targeting specificity, the strategy of activatable photosensitization has been developed, where a pre-quenched photosensitizer can be selectively activated for imaging and therapy in living animals (Table 1.2).[88]

For example, a photodynamic molecular beacon is developed for selective treatment of tumors expressing MMP-7, an endopeptidase commonly expressed by epithelial cancer cells.[89] In this design, the fluorescence emission and $^1O_2$ production of the photosensitizer is quenched by a dark quencher (Figure 1.18A). Activated by MMP-7, the released fluorescence signal is used to visualize the localization of tumor cells,

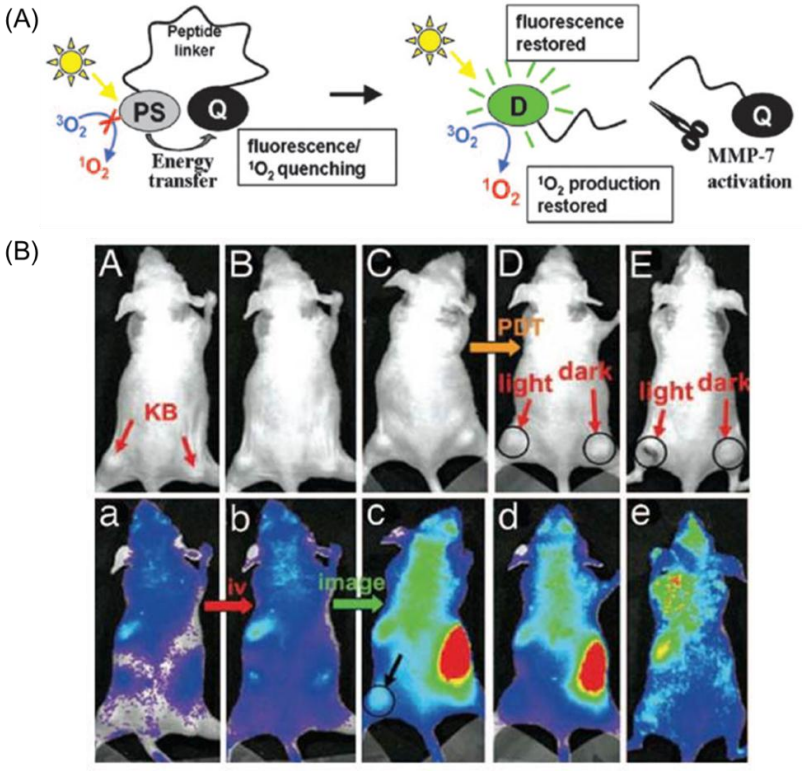

Figure 1.18 Activatable photosensitization. (A) Mechanism of the MMP-7 activated photosensitization. (B) Bright field (A-E) and fluorescent (a-e) images of photodynamic molecular beacon administered mouse (A, prescan; B, 10 min after injection; C, 3 h after injection; D, 5 h after injection and 1 h after photosensitization; E, 3 d after PDT).[89] Light-treated tumors are marked as ‘‘light’’ and nonlight-treated tumors as ‘‘dark.’’

where the $^1O_2$ productivity is recovered simultaneously and a ray of light is selectively directed for photosensitizing treatment (Figure 1.18B), thus serves both therapeutic and diagnostic purposes *in vivo*.

1.4 Background and research goals

Optical imaging has been extensively used for non-invasive visualization of biological molecules and processes in living systems. This technique relies on imaging probes to report the biological targets with specificity and sensitivity. Based on both molecular biology and cell biology, more and more probes have been developed to help our understanding of protein functions, gene functions and disease diagnosis.

In this thesis, the author aims to develop novel optical probes for biological reporters such as *β*-lactamase and firefly luciferase. These biological targets are selected due to their importance in biological study and human health concerns. Both are useful reporter genes for *in vivo* imaging. Moreover, *β*-lactamase is the endogenous enzyme to confer bacteria drug resistance. Hence study of these proteins will benefit the reporter gene techniques, as well as the antimicrobial diagnosis and therapy. In these studies, the probes are developed not only as simple image contrast agents, but also endowed with additional functions such as covalent labeling, photocage activity and photosensitizing function, serving particular research purpose.

Imaging study of the resistant bacterial species and proteins provides a simple method to improve our understanding towards antibiotic resistance in the molecular level. Usually, bacterial strains can be fluorescently labeled to monitor their survival or inhibition in the presence of antibiotics through the incorporation of reporter genes

such as fluorescent proteins.[90,91] Meanwhile, study of endogenous resistance in native bacterial species can be facilitated by imaging methods through fluorescent staining, which is mediated by various affinity groups such as zinc cations, bacteria-binding peptides, antibodies and bacteriophages to target bacterial subcellular structures through electrostatic adsorption or specific biological interactions. According to the involved mechanism of binding, these modifications usually display different ranges of selectivity.

As bacteria surface containing negative charges from lipopolysaccharides or teichoic acids, the cationic zinc dipicolylamine complexes bind strongly to the anionic surfaces of bacteria, providing distinctive fluorescence to investigate bacterial infection in living animals (Figure 1.19A).[92]

This kind of electrostatic adsorption can take effect with both gram positive and gram negative bacteria. In the studies where selective staining is required, the biomolecules or biopolymers with specific interaction to subcellular targets are often involved in the design of imaging probes. For example, some antimicrobial peptides with strong binding affinities to lipopolysaccharide in gram negative bacteria have been used for fluorescent detection and imaging of gram negative pathogens with high selectivity over gram positive species and mammalian cells (Figure 1.19B).[93] The targeting specificity can also be realized through antibody-antigen recognition, where the fluorescently labeled antibodies have been developed to identify specific bacterial proteins with imaging methods.[94] Others employ bacteriophage-mediated assays to sense and detect microbial targets due to the natural ability of a phage to infect specific

bacterial host targets. For imaging purposes, the reporter phages carrying genes of firefly luciferase or fluorescent proteins have been developed, which will be expressed within infected host bacteria upon productive infections.[95]

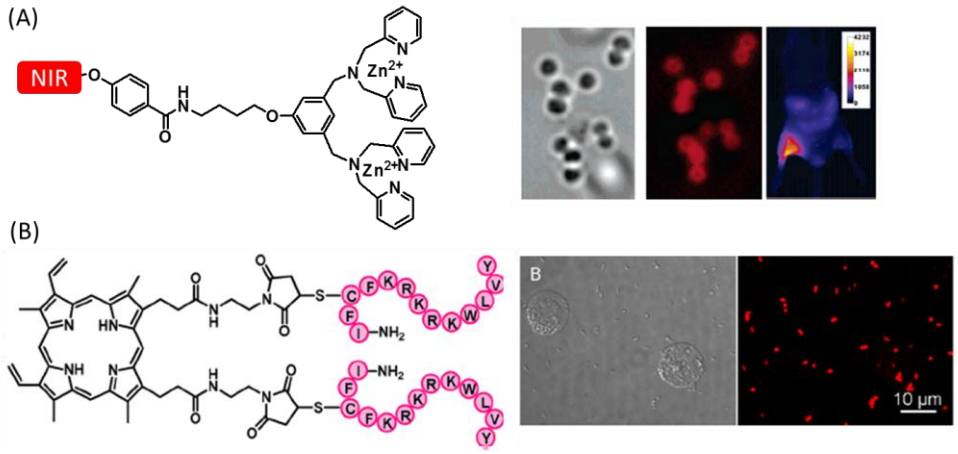

Figure 1.19 Bacterial imaging through modification with fluorescently tagged affinity groups such as (A) zinc dipicolylamine complexes[92] and (B) antimicrobial peptides.[93]

Some of these affinity groups are specific to the resistant species by targeting biomolecules which confer bacteria resistance.[94] Besides, investigation of the resistant behavior in living bacterial cells also utilizes fluorescent derivatives of antibiotics, which display intrinsic difference during their interactions with antibiotic resistant and susceptible cells.[96-98] These reagents like fluorescent penicillin or vancomycin have provided simple and direct tools to study the mechanism of resistance, such as the decrease of drug-binding capacity in resistant species (Figure 1.20). However, the signal contrast may be interfered by the inevitable nonspecific binding and adsorption of these fluorescent conjugates in living tissues.

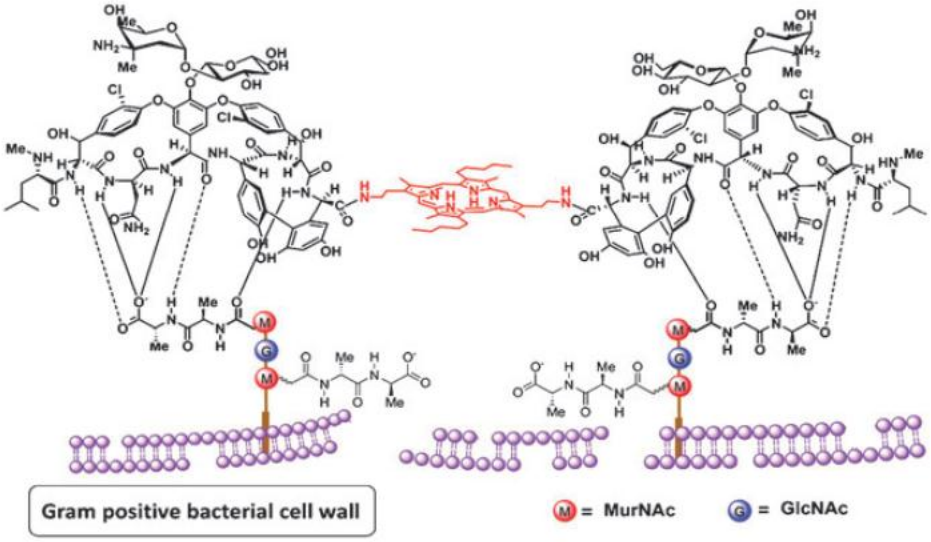

Figure 1.20 Interaction of divalent vancomycin derivative with cell wall of gram positive bacteria.[96]

To study pathogenic bacterial infections in living animals, the strategy of reporter enzyme fluorescence has been successfully employed to image antibiotic resistance with on-off fluorescence switch or distinctive emission shift.[99-101] In these approaches, the fluorescent signal can be selectively activated by the endogenous reporter of *β*-lactamases to indicate the presence of antibiotic resistance (Figure 1.21). Due to the specific presence of *β*-lactamases in antibiotic resistant bacteria, this method can easily detect and image tubercle bacilli in living mice, which is usually difficult to study with general methods due to the slow growth rate and genetic intractability.[99] Moreover, further development of these imaging probes through introduction of steric hindrance provides selectivity towards enzyme subclasses, suitable for fast screening and detection of the pathogenic species producing such enzyme subclass.[100,101]

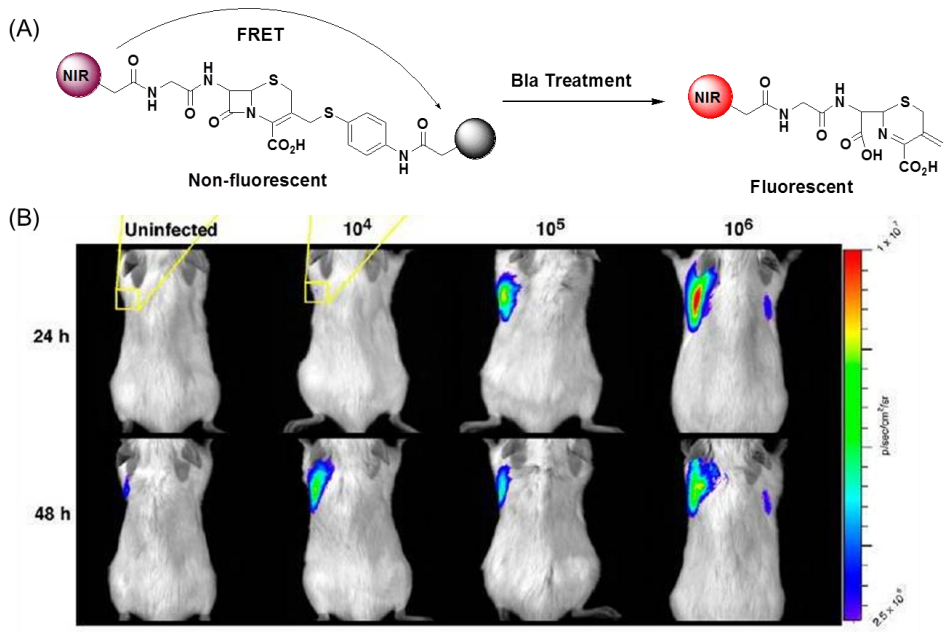

Figure 1.21 Reporter enzyme fluorescence for detection and imaging of bacterial infection in living mice. (A) mechanism of fluorescence activation and (B) signal level from mice infected with bacillus Calmette–Guérin and administered with probe.[99]

In this thesis, the author has developed a set of activatable covalent probes for imaging and fast screening of antibiotic resistant bacteria as described in Chapter 2. These probes are activated by the resistance-associated endogenous *β*-lactamases and served for covalent labeling of the resistant bacterial species with reduced background by minimizing probe diffusion.

This enzyme activation strategy is further utilized in the development of a luminescent Ru(II) probe for selective imaging and lethal photosensitization of the drug resistant bacteria. Chapter 3 describes the construction of this multifunctional probe and the promising therapeutic effects to the drug resistant strains.

In addition, in order to better understand *β*-lactamase functions and activities in their natural habitat, an ongoing study aims to develop probes for detection and identification of bacterial *β*-lactamases through the approach of activity-based protein

labeling. The preliminary results are presented briefly in Chapter 4.

In order to improve the spatial and temporal control of bioluminescent imaging, a photocaged bioluminescent probe is developed for imaging firefly luciferase activity in living mice. Chapter 5 presents the monitoring of firefly bioluminescence *in vivo* with spatial and temporal control in the combination of photocage technology.

1.5 References

(1) Weissleder, R.; Mahmood, U. *Radiology* **2001**, *219*, 316.

(2) Mayerhofer, R.; Araki, K.; Szalay, A. A. *J. Biolumin. Chemilumin.* **1995**, *10*, 271.

(3) Bennett, J.; Duan, D. S.; Engelhardt, J. F.; Maguire, A. M. *Investig. Ophthalmol. Vis. Sci.* **1997**, *38*, 2857.

(4) Rehemtulla, A.; Stegman, L. D.; Cardozo, S. J.; Gupta, S.; Hall, D. E.; Contag, C. H.; Ross, B. D. *Neoplasia* **2000**, *2*, 491.

(5) Giepmans, B. N. G.; Adams, S. R.; Ellisman, M. H.; Tsien, R. Y. *Science* **2006**, *312*, 217.

(6) Lippincott-Schwartz, J.; Patterson, G. H. *Science* **2003**, *300*, 87

(7) Betzig, E.; Patterson, G. H.; Sougrat, R.; Lindwasser, O. W.; Olenych, S.; Bonifacino, J. S.; Davidson, M. W.; Lippincott-Schwartz, J.; Hess, H. F. *Science* **2006**, *313*, 1642.

(8) Lippincott-Schwartz, J.; Snapp, E.; Kenworthy, A. *Nat. Rev. Mol. Cell Biol.* **2001**, *2*, 444.

(9) AnderssonEngels, S.; afKlinteberg, C.; Svanberg, K.; Svanberg, S. *Phys. Med. Biol.* **1997**, *42*, 815.

(10) Petrovsky, A.; Schellenberger, E.; Josephson, L.; Weissleder, R.; Bogdanov, A. *Cancer Res.* **2003**, *63*, 1936.

(11) Wu, J. C.; Inubushi, M.; Sundaresan, G.; Schelbert, H. R.; Gambhir, S. S. *Circulation* **2002**, *105*, 1631.

(12) Ando, Y.; Niwa, K.; Yamada, N.; Enomot, T.; Irie, T.; Kubota, H.; Ohmiya, Y.; Akiyama, H. *Nat. Photonic.* **2008**, *2*, 44.

(13) Lundin, A. In *Bioluminescence and Chemilunescence: Status Report*; Szalay, A., Kricka, L. J., Stanley, P. E., Eds.; John Wiley: Chichester, UK, 1993, p 291.

(14) Close, D. M.; Xu, T. T.; Sayler, G. S.; Ripp, S. *Sensors* **2011**, *11*, 180.

(15) Huang, B.; Bates, M.; Zhuang, X. W. *Annu. Rev. Biochem.* **2009**, *78*, 993.

(16) Contag, C. H.; Bachmann, M. H. *Annu. Rev. Biomed. Eng.* **2002**, *4*, 235.

(17) Wehrman, T. S.; von Degenfeld, G.; Krutzik, P.; Nolan, G. P.; Blau, H. M. *Nat. Methods* **2006**, *3*, 295.

(18) Licha, K.; Olbrich, C. *Adv. Drug Deliver. Rev.* **2005**, *57*, 1087.

(19) Rothman, D. M.; Shults, M. D.; Imperiali, B. *Trends Cell Biol* **2005**, *15*, 502.

(20) Haglund, M. M.; Berger, M. S.; Hochman, D. W. *Neurosurgery* **1996**, *38*, 308.

(21) Ntziachristos, V.; Yodh, A. G.; Schnall, M.; Chance, B. *Proc. Nat. Acad. Sci. USA* **2000**, *97*, 2767.

(22) Ramjiawan, B.; Maiti, P.; Aftanas, A.; Kaplan, H.; Fast, D.; Mantsch, H. H.; Jackson, M. *Cancer* **1999**, *89*, 1134.

(23) Ke, S.; Wen, X. X.; Gurfinkel, M.; Charnsangavej, C.; Wallace, S.; Sevick-Muraca, E. M.; Li, C. *Cancer Res.* **2003**, *63*, 7870.

(24) Ruoslahti, E. *Annu. Rev. Cell Dev. Biol.* **1996**, *12*, 697.

(25) Brooks, P. C.; Montgomery, A. M. P.; Rosenfeld, M.; Reisfeld, R. A.; Hu, T. H.; Klier, G.; Cheresh, D. A. *Cell* **1994**, *79*, 1157.

(26) Schottelius, M.; Laufer, B.; Kessler, H.; Wester, H. J. *Acc. Chem. Res.* **2009**, *42*, 969.

(27) Low, P. S.; Henne, W. A.; Doorneweerd, D. D. *Acc. Chem. Res.* **2008**, *41*, 120.

(28) Low, P. S.; Kularatne, S. A. *Curr. Opin. Chem. Biol.* **2009**, *13*, 256.

(29) Lin, Y. H.; Weissleder, R.; Tung, C. H. *Bioconjugate Chem.* **2002**, *13*, 605.

(30) Macheda, M. L.; Rogers, S.; Best, J. D. *J. Cell. Physiol.* **2005**, *202*, 654.

(31) Cheng, Z.; Levi, J.; Xiong, Z. M.; Gheysens, O.; Keren, S.; Chen, X. Y.; Gambhir, S. S. *Bioconjugate Chem.* **2006**, *17*, 662.

(32) Funovics, M.; Weissleder, R.; Tung, C. H. *Anal. Bioanal. Chem.* **2003**, *377*, 956.

(33) Weissleder, R.; Tung, C. H.; Mahmood, U.; Bogdanov, A. *Nat. Biotechnol.* **1999**, *17*, 375.

(34) Edgington, L. E.; Berger, A. B.; Blum, G.; Albrow, V. E.; Paulick, M. G.; Lineberry, N.; Bogyo, M. *Nat. Med.* **2009**, *15*, 967.

(35) Cravatt, B. F.; Sorensen, E. J. *Curr. Opin. Chem. Biol.* **2000**, *4*, 663.

(36) Lecaille, F.; Kaleta, J.; Bromme, D. *Chem. Rev.* **2002**, *102*, 4459.

(37) Selkoe, D. J. *Physiol. Rev.* **2001**, *81*, 741.

(38) Pham, W.; Choi, Y. D.; Weissleder, R.; Tung, C. H. *Bioconjugate Chem.* **2004**, *15*, 1403.

(39) Bullok, K.; Piwnica-Worms, D. *J. Med. Chem.* **2005**, *48*, 5404.

(40) Evans, M. J.; Cravatt, B. F. *Chem. Rev.* **2006**, *106*, 3279.

(41) Blum, G.; Mullins, S. R.; Keren, K.; Fonovic, M.; Jedeszko, C.; Rice, M. J.; Sloane, B. F.; Bogyo, M. *Nat. Chem. Biol.* **2005**, *1*, 203.

(42) Blum, G.; von Degenfeld, G.; Merchant, M. J.; Blau, H. M.; Bogyo, M. *Nat. Chem. Biol.* **2007**, *3*, 668.

(43) Kircher, M. F.; Gambhir, S. S.; Grimm, J. *Nat. Rev. Clin. Oncol.* **2011**, *8*, 677.

(44) Massoud, T. F.; Gambhir, S. S. *Genes Dev.* **2003**, *17*, 545.

(45) Newman, R. H.; Fosbrink, M. D.; Zhang, J. *Chem. Rev.* **2011**, *111*, 3614.

(46) Wang, L.; Jackson, W. C.; Steinbach, P. A.; Tsien, R. Y. *Proc. Nat. Acad. Sci. USA* **2004**, *101*, 16745.

(47) Marguet, D.; Spiliotis, E. T.; Pentcheva, T.; Lebowitz, M.; Schneck, J.; Edidin, M. *Immunity* **1999**, *11*, 231.

(48) Tsien, R. Y. *Annu. Rev. Biochem.* **1998**, *67*, 509.

(49) Vilardaga, J. P.; Bunemann, M.; Krasel, C.; Castro, M.; Lohse, M. J. *Nat. Biotechnol.* **2003**, *21*, 807.

(50) Carminati, J. L.; Stearns, T. *J. Cell Biol.* **1997**, *138*, 629.

(51) Hoffmann, C.; Gaietta, G.; Bunemann, M.; Adams, S. R.; Oberdorff-Maass, S.; Behr, B.; Vilardaga, J. P.; Tsien, R. Y.; Eisman, M. H.; Lohse, M. J. *Nat. Methods* **2005**, *2*, 171.

(52) Andresen, M.; Schmitz-Salue, R.; Jakobs, S. *Mol. Biol. Cell* **2004**, *15*, 5616.

(53) Chen, I.; Ting, A. Y. *Curr. Opin. Biotech.* **2005**, *16*, 35.

(54) Martin, B. R.; Giepmans, B. N. G.; Adams, S. R.; Tsien, R. Y. *Nat. Biotechnol.*

2005, *23*, 1308.

(55)Adams, S. R.; Campbell, R. E.; Gross, L. A.; Martin, B. R.; Walkup, G. K.; Yao, Y.; Llopis, J.; Tsien, R. Y. *J. Am. Chem. Soc.* **2002**, *124*, 6063.

(56)Keppler, A.; Gendreizig, S.; Gronemeyer, T.; Pick, H.; Vogel, H.; Johnsson, K. *Nat. Biotechnol.* **2003**, *21*, 86.

(57)Janssen, D. B. *Curr. Opin. Chem. Biol.* **2004**, *8*, 150.

(58)Komatsu, T.; Johnsson, K.; Okuno, H.; Bito, H.; Inoue, T.; Nagano, T.; Urano, Y. *J. Am. Chem. Soc.* **2011**, *133*, 6745.

(59)Los, G. V.; Encell, L. P.; McDougall, M. G.; Hartzell, D. D.; Karassina, N.; Zimprich, C.; Wood, M. G.; Learish, R.; Ohane, R. F.; Urh, M.; Simpson, D.; Mendez, J.; Zimmerman, K.; Otto, P.; Vidugiris, G.; Zhu, J.; Darzins, A.; Klaubert, D. H.; Bulleit, R. F.; Wood, K. V. *Acs Chem. Biol.* **2008**, *3*, 373.

(60)Yu, Y. A.; Timiryasova, T.; Zhang, Q.; Beltz, R.; Szalay, A. A. *Anal. Bioanal. Chem.* **2003**, *377*, 964.

(61)Wilson, T.; Hastings, J. W. *Annu. Rev. Cell Dev. Biol.* **1998**, *14*, 197.

(62)Branchini, B. R.; Southworth, T. L.; Khattak, N. F.; Michelini, E.; Roda, A. *Anal. Biochem.* **2005**, *345*, 140.

(63)Xing, B. G.; Rao, J. H.; Liu, R. R. *Mini-Rev. Med. Chem.* **2008**, *8*, 455.

(64)Wehrman, T.; Kleaveland, B.; Her, J. H.; Balint, R. F.; Blau, H. M. *Proc. Nat. Acad. Sci. USA* **2002**, *99*, 3469.

(65)Zlokarnik, G.; Negulescu, P. A.; Knapp, T. E.; Mere, L.; Burres, N.; Feng, L. X.; Whitney, M.; Roemer, K.; Tsien, R. Y. *Science* **1998**, *279*, 84.

(66) Day, J. R.; Munk, C.; Guatelli, J. C. *J. Virol.* **2004**, *78*, 1069.

(67) Spotts, J. M.; Dolmetscht, R. E.; Greenberg, M. E. *Proc. Nat. Acad. Sci. USA* **2002**, *99*, 15142.

(68) Xing, B. G.; Khanamiryan, A.; Rao, J. H. *J. Am. Chem. Soc.* **2005**, *127*, 4158.

(69) Yao, H.; So, M. K.; Rao, J. *Angew. Chem. Int. Ed.* **2007**, *46*, 7031.

(70) Kong, Y.; Yao, H. Q.; Ren, H. J.; Subbian, S.; Cirillo, S. L. G.; Sacchettini, J. C.; Rao, J. H.; Cirillo, J. D. *Proc. Nat. Acad. Sci. USA* **2010**, *107*, 12239.

(71) Mizukami, S.; Watanabe, S.; Hori, Y.; Kikuchi, K. *J. Am. Chem. Soc.* **2009**, *131*, 5016.

(72) Alam, J.; Cook, J. L. *Anal. Biochem.* **1990**, *188*, 245.

(73) Tung, C. H.; Zeng, Q.; Shah, K.; Kim, D. E.; Schellingerhout, D.; Weissleder, R. *Cancer Res.* **2004**, *64*, 1579.

(74) Lee, H. M.; Larson, D. R.; Lawrence, D. S. *Acs Chem. Biol.* **2009**, *4*, 409.

(75) Ellis-Davies, G. C. R. *Nat. Methods* **2007**, *4*, 619.

(76) Pelliccioli, A. P.; Wirz, J. *Photochem. Photobiol. Sci.* **2002**, *1*, 441.

(77) Shao, Q.; Xing, B. G. *Chem. Soc. Rev.* **2010**, *39*, 2835.

(78) Hahn, M. E.; Muir, T. W. *Angew. Chem. Intl. Ed.* **2004**, *43*, 5800.

(79) Chou, C. J.; Young, D. D.; Deiters, A. *Angew. Chem. Intl. Ed.* **2009**, *48*, 5950.

(80) Tang, X. J.; Dmochowski, I. J. *Mol. BioSyst.* **2007**, *3*, 100.

(81) Monroe, W. T.; McQuain, M. M.; Chang, M. S.; Alexander, J. S.; Haselton, F. R. *J. Bio. Chem.* **1999**, *274*, 20895.

(82) Tang, X. J.; Dmochowski, I. J. *Angew. Chem. Intl. Ed.* **2006**, *45*, 3523.

(83) Shestopalov, I. A.; Sinha, S.; Chen, J. K. *Nat. Chem. Biol.* **2007**, *3*, 650.

(84) Huang, Z. *Technol. Cancer Res. Treat.* **2005**, *4*, 283.

(85) Celli, J. P.; Spring, B. Q.; Rizvi, I.; Evans, C. L.; Samkoe, K. S.; Verma, S.; Pogue, B. W.; Hasan, T. *Chem. Rev.* **2010**, *110*, 2795.

(86) Detty, M. R.; Gibson, S. L.; Wagner, S. J. *J. Med. Chem.* **2004**, *47*, 3897.

(87) Sharman, W. M.; Allen, C. M.; van Lier, J. E. *Drug Discov. Today* **1999**, *4*, 507.

(88) Lovell, J. F.; Liu, T. W. B.; Chen, J.; Zheng, G. *Chem. Rev.* **2010**, *110*, 2839.

(89) Zheng, G.; Chen, J.; Stefflova, K.; Jarvi, M.; Li, H.; Wilson, B. C. *Proc. Nat. Acad. Sci. USA* **2007**, *104*, 8989.

(90) Golding, I.; Paulsson, J.; Zawilski, S. M.; Cox, E. C. *Cell* **2005**, *123*, 1025.

(91) Zhao, M.; Yang, M.; Baranov, E.; Wang, X.; Penman, S.; Moossa, A. R.; Hoffman, R. M. *Proc. Natl. Acad. Sci. U.S.A.* **2001**, *98*, 9814.

(92) Leevy, W. M.; Gammon, S. T.; Jiang, H.; Johnson, J. R.; Maxwell, D. J.; Jackson, E. N.; Marquez, M.; Piwnica-Worms, D.; Smith, B. D. *J. Am. Chem. Soc.* **2006**, *128*, 16476.

(93) Liu, F.; Ni, A. S. Y.; Lim, Y.; Mohanram, H.; Bhattacharjya, S.; Xing, B. G. *Bioconjugate Chem.* **2012**, *23*, 1639.

(94) Hujer, A. M.; Keslar, K. S.; Dietenberger, N. J.; Bethel, C. R.; Endimiani, A.; Bonomo, R. A. *BMC Microbiol.* **2009**, *9*, 46.

(95) Smartt, A. E.; Ripp, S. *Anal. Bioanal. Chem.* **2011**, *400*, 991.

(96) Xing, B. G.; Jiang, T. T.; Bi, W. G.; Yang, Y. M.; Li, L. H.; Ma, M. L.; Chang, C. K.; Xu, B.; Yeow, E. K. L. *Chem. Commun.* **2011**, *47*, 1601.

(97) Galleni, M.; Lakaye, B.; Lepage, S.; Jamin, M.; Thamm, I.; Joris, B.; Frere, J. M. *Biochem. J.* **1993**, *291*, 19.

(98) Pereira, P. M.; Filipe, S. R.; Tomasz, A.; Pinho, M. G. *Antimicrob. Agents Chemother.* **2007**, *51*, 3627.

(99) Kong, Y.; Yao, H. Q.; Ren, H. J.; Subbian, S.; Cirillo, S. L. G.; Sacchettini, J. C.; Rao, J. H.; Cirillo, J. D. *Proc. Nat. Acad. Sci. USA* **2010**, *107*, 12239.

(100) Xie, H. X.; Mire, J.; Kong, Y.; Chang, M. H.; Hassounah, H. A.; Thornton, C. N.; Sacchettini, J. C.; Cirillo, J. D.; Rao, J. H. *Nat. Chem.* **2012**, *4*, 802.

(101) Zhang, J. X.; Shen, Y.; May, S. L.; Nelson, D. C.; Li, S. W. *Angew. Chem., Int. Ed.* **2012**, *51*, 1865.

Chapter 2

Covalent Probes for Imaging *β*-Lactamase Activity and Fast Screening of Antibiotic Resistant Bacteria

2.1 Introduction

Construction of fluorescent probes for living cell imaging requires the fluorescence signal localized in the cells of interest. Normally, the probe can be built with appropriate lipophilicity to cross cell membrane and activated by cellular events to release the hydrophilic fluorophore trapped inside cells. Alternatively, a covalent labeling property can be introduced for living cell imaging as minimizing the diffusion of probe into surrounding medium. With this consideration, we select the antibiotic resistant bacteria as the target to design specific probes for living cell imaging.

The purpose of this study is to develop probes for rapid detection of the resistant strains and understanding the biological basis, because antibiotic resistance represents an emerging concern regarding human health. Normally, the drug resistance is studied by the culture and growth method, which is labor intensive and difficult to determine the heterogeneous in individual cells. On the contrary, optical imaging as a powerful method to enable rapid and sensitive visualization of biological events in single cells, is limited for the direct observation of antibiotic resistance due to lack of imaging probes to report the resistant events with essential signal contrasts. In this chapter, we describe the rational design of novel optical probes for resistant bacteria detection based on the endogenous reporter enzyme of *β*-lactamase. This reporter enzyme is a main mechanism to confer antibiotic resistance and exclusively produced to destroy

antibiotic drugs. By targeting this endogenous reporter, this study employs the strategy of bio-activatable targeting to develop β-lactamase sensitive probes for detection and imaging of the resistant bacteria through covalent fluorescent labeling.

2.1.1 Bacteria and cell wall structure

There are a large number of bacteria in the human body. Most of them live together with human cells at peace. A few are beneficial to human physiological processes such as digestion, growth and self-defense. However, some bacterial species are pathogenic and involved in serious infectious diseases such as fatal tuberculosis.[1] Thus the understanding of bacteria cell structure and biological behavior is necessary for both clinical treatment and antibacterial drug development.

Bacteria are single-celled prokaryotic microbes surrounded by a lipid cell membrane (also known as cytoplasmic membrane) to hold the cellular contents like nucleoid, ribosomes, proteins and other essential components within the cell. On the outside of cytoplasmic membrane, a cell wall is present and essential for maintaining cell shape and protection against osmotic lysis. There are generally two large groups of bacteria based on the cell wall structure, Gram positive and Gram negative, as determined by Gram staining.[2] The cell wall of Gram positive bacteria is relatively thick and composed of many layers of peptidoglycan and teichoic acids. In contrast, the cell wall of Gram negative bacteria is relatively thin and composed of a few layers of peptidoglycan coated by an outer membrane containing lipopolysaccharides and lipoproteins (Figure 2.1).

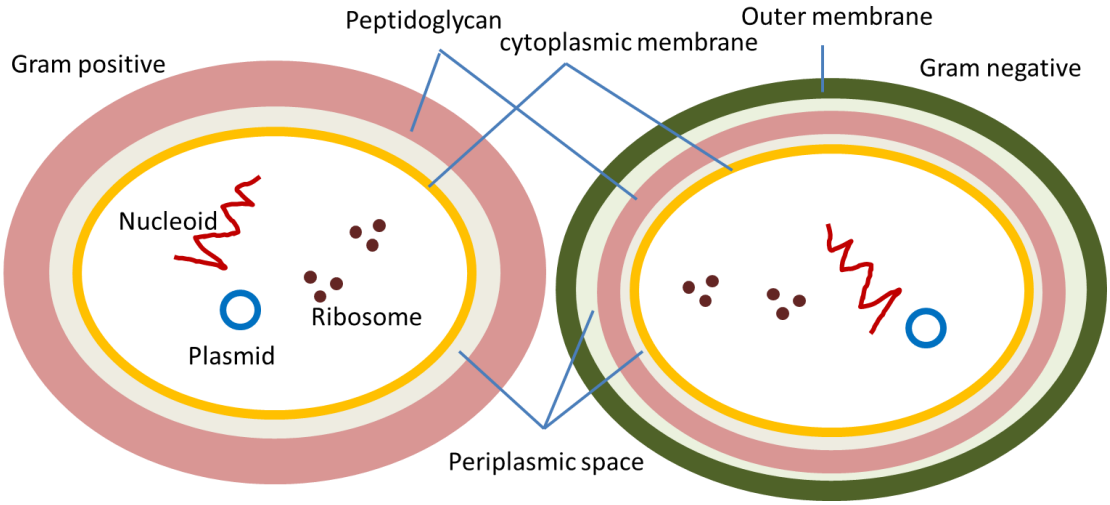

Figure 2.1 Structure of Gram positive and Gram negative bacterial cell wall.

2.1.2 *β*-Lactam antibiotics

The discovery and development of antibiotics and antimicrobial agents have saved many lives from infectious diseases. The antibiotics are natural products with high efficiency to destroy bacteria by attacking bacterial cell walls, plasma membranes, proteins or nucleic acids (Figure 2.2).[3] Many of them are produced by microorganisms as a survival mechanism to keep other organisms away and protect the supply of

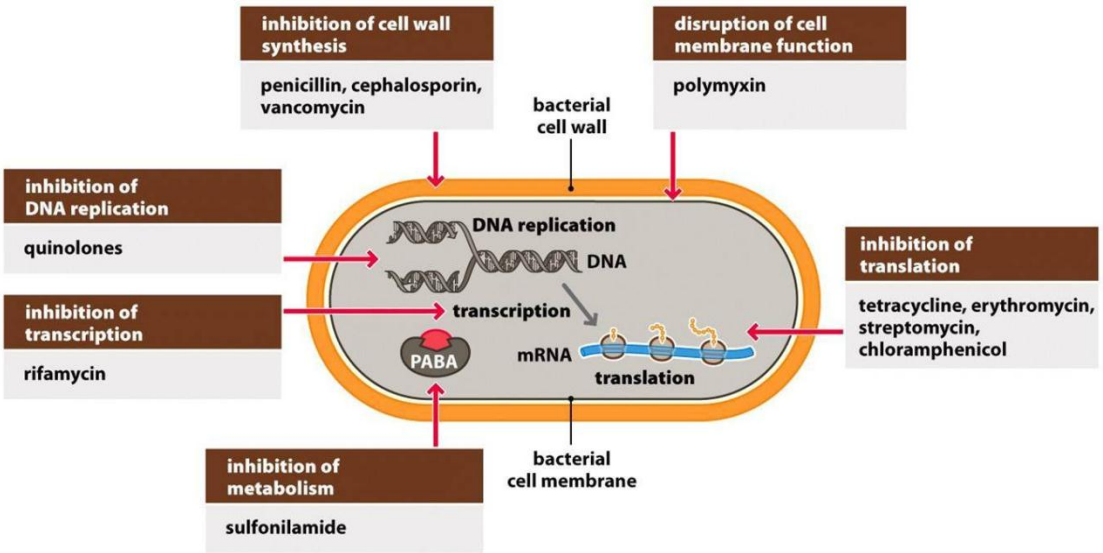

Figure 2.2 Antibiotics and their biological targets.

nutrients.[4] In addition, more and more antimicrobial agents have been developed with improved efficacy through chemical modification.

Among them, *β*-lactam antibiotics are widely used due to the antibacterial efficacy and good safety profile. These antibiotics, including penicillins, cephalosporins, monobactams and carbapenems, have same *β*-lactam ring in their molecular structures (Figure 2.3). This core structure mimics the D-Ala-D-Ala unit in peptidoglycan and inhibits the formation of peptidoglycan layer in bacterial cell wall synthesis with resultant cell death.[5]

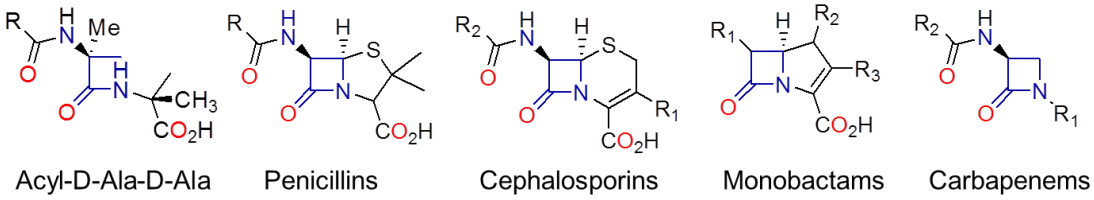

Figure 2.3 Structure of typical *β*-lactam antibiotics.

The peptidoglycan layer is the major component of cell wall and essential for cell wall integrity. Formation of this layer involves a series of steps in the final stages of peptidoglycan biosynthesis, including the translocation of a peptidoglycan unit to the outside of the cell and attachment to the polysaccharide chain, followed by cross-linking with peptide bond inside the cell and removal of the D-alanine (Figure 2.4).

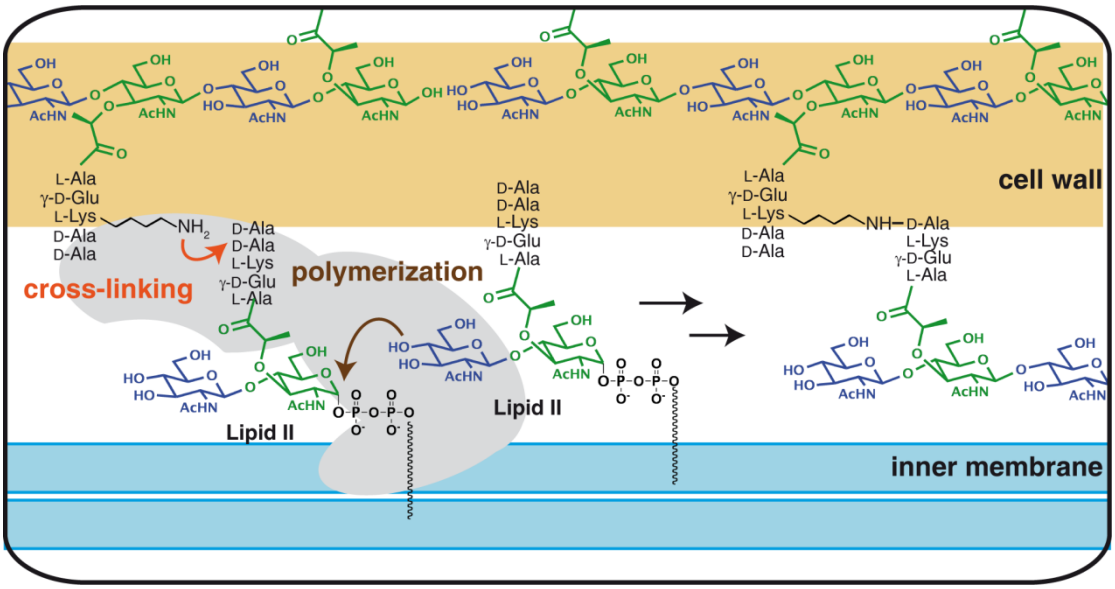

Figure 2.4 Polymerization and cross-linking of peptidoglycan in cell wall biosynthesis.

The cross-linking of peptidoglycan is catalyzed by D-Ala-D-Ala-transpeptidases, which are also called penicillin-binding proteins (PBPs) due to their binding capacity to penicillin antibiotics.[6] These antibiotics resemble the D-Ala-D-Ala unit of the peptidoglycan with the *β*-lactam structure and irreversibly bind to the PBP active site, thus prevent the cross-linking of peptidoglycan layer and disrupt cell wall synthesis.[7]

Because bacterial cell wall does not exist in animal cells, the β-lactam antibiotics are quite safe to human beings. Together with their broad-spectrum efficacy, β-lactams have become the most frequently prescribed antibiotics in clinical practice.[8]

Benefited from these antibiotic drugs, the mortality of infectious diseases dropped dramatically from 797 per 100,000 persons in 1900 to 36 per 100,000 persons in 1980.[9] However, the mortality raises higher recently to 148 per 100,000 persons in 2004, especially in less-developed countries.[10] This is mostly due to the prevalence of antibiotic resistance.

2.1.3 Antibiotic resistance and detection methods

The overuse of antibiotic drugs has led to the prevalence of antibiotic resistant bacteria. The environment of high-concentration antibiotics has increased the pressure by natural selection, where resistant cells survived and rapidly multiplied with the resistant genes passed on to other bacteria. The resistance may come from different mechanisms, such as production of enzymes to inactivate the drugs, alteration of drug targets, or increased permeability barrier to reduce drug accumulation.[11]

Understanding of the molecular basis of resistance has presented an important topic in microbiological study. This knowledge is essential for the development of novel antimicrobial methods and agents to overcome the resistance. In addition, it is also important in clinical diagnosis to select more effective drugs to the resistant pathogens, which requires a fast and sensitive detection method to identify antibiotic resistance.

The resistant genes of pathogenic species can be readily identified by polymerase chain reaction (PCR), but restricted to the well-characterized genes.[12] Meanwhile, the complexity and multiplicity of resistance mechanisms still requires phenotypic testing to evaluate bacteria susceptibility to antibiotics, especially for treatment of serious infectious diseases. The resistance is usually observed and determined through culture and growth, which is labor intensive and time-consuming, leading to an unexpected delay in the early diagnosis. In addition, this method cannot offer direct observation of intrinsic resistance of individual cells in a mixed population.[11]

Optical imaging is widely used in biological study to provide rapid and direct visualization of biological events in living systems. Benefited from the non-invasive

operation and subcellular resolution, optical imaging is powerful in the monitoring of bacterial protein dynamics and understanding of pathogen-host interactions.[13]

Used in the study of antibiotic resistance, optical imaging is limited mostly due to the lack of appropriate probe to report the resistance and produce essential signal contrast. Incorporation of fluorescent proteins has been successfully applied in the cellular detection of resistant genes[14] and monitoring of antibiotic response to bacterial infections in living animals.[15] But the laboratory strains expressing foreign genes are not identical to native bacterial samples because such fluorescent tags may potentially cause unpredictable perturbation in protein functions or levels due to the large size (~27 kDa).[16]

Imaging studies of drug resistance in native bacterial strains usually involve the step of fluorescent staining to assist the observation of bacteria survival or inhibition in the presence of antibiotics. These approaches utilize the affinity groups such as zinc cations,[17] bacteria-binding peptides,[18] antibodies[19] and bacteriophages[20,21] to target bacterial subcellular structures with fluorescence combination. This kind of fluorescent staining has also been used in rapid analysis of drug resistance in mixed cultures through flow-cytometric (FCM) study.[22,23] But these modifications are not always specific to the pathogens with potent resistance.[20]

Direct observation of bacterial resistance has been reported by utilizing fluorescent antibiotic derivatives, like fluorophore-coupled penicillin or vancomycin, based on the intrinsic difference during their interactions toward antibiotic resistant and susceptible cells.[24-26] But the signal contrast may be interfered by the inevitable nonspecific

binding and adsorption of these drug conjugates.[26] More powerful design is required to effectively report the antibiotic resistance.

Recently, reporter enzyme fluorescence has been successfully used to detect antibiotic resistance with tunable emission enhancement or distinctive shift, [27-30] also to image pathogenic bacterial infections in living animals (Figure 2.5).[27,28] In these approaches, a fluorescent probe can be selectively activated by the endogenous reporter of β-lactamase and used to image the resistance.

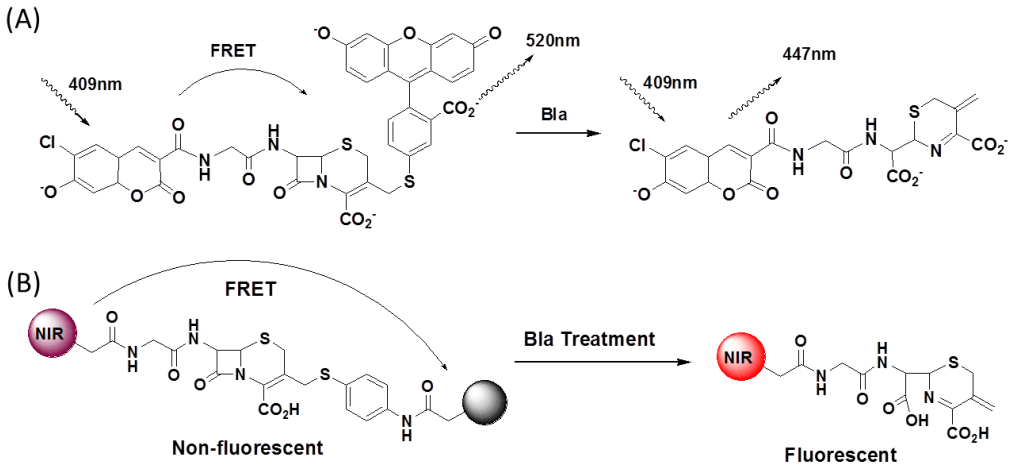

Figure 2.5 Mechanism of fluorescent probes for Bla detection with (A) emission shift[30] or (B) on-off switch.[27]

Production of β-lactamases (Blas) is a main mechanism to keep bacteria survive in the presence of β-lactam drugs.[31] These enzymes catalyze the hydrolysis of β-lactam ring and destroy the drugs with high efficiency.[32] Also with the exclusive production in antibiotic resistant bacteria, Blas are almost naturally suitable as the biological targets to ensure signal specificity in resistance detection.

Moreover, due to academic interest and clinical importance, some β-lactamases have been intensively studied, including the most commonly encountered class A

β-lactamases like *Escherichia coli* TEM-1, a plasmid mediated bacterial enzyme.[33] The enzymatic hydrolysis of penicillin antibiotic is proposed in Scheme 2.1, where acylation and deacylation steps are involved. In the enzyme structure, the Glu166 activates a water molecule for assisting the nucleophilic attack of the Ser70 on the *β*-lactam carbonyl group. This high-energy intermediate changes into lower energy covalent acyl-enzyme after protonation of the *β*-lactam nitrogen and cleavage of the amide bond. This structure is attacked by a catalytic water molecule with resultant deacylation, which releases enzyme molecule and regenerates enzyme activity.

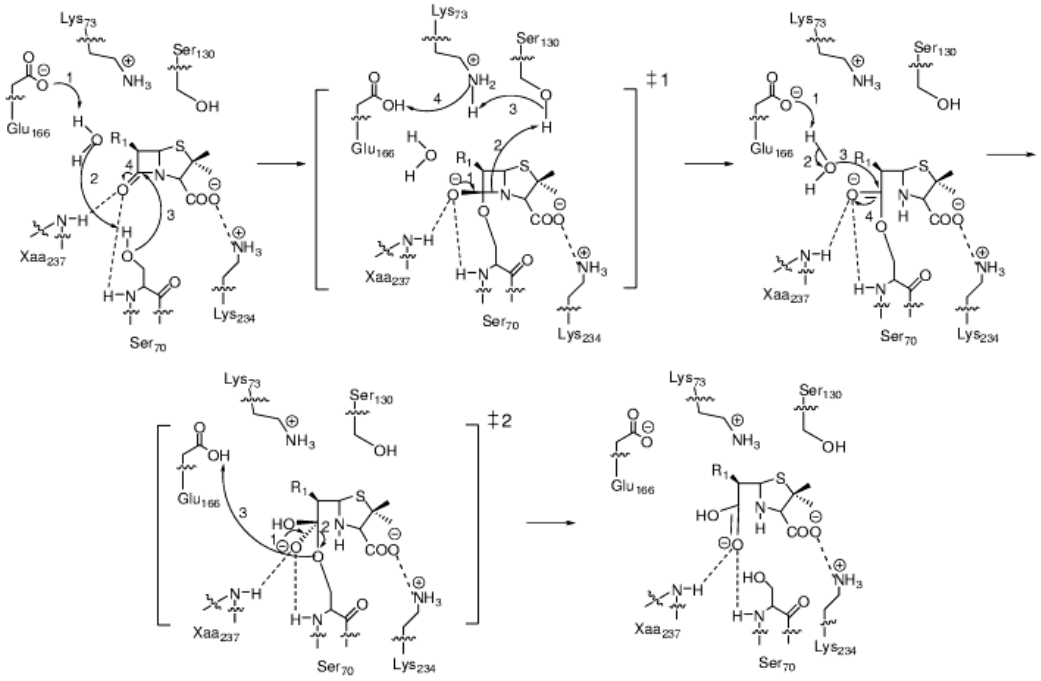

Scheme 2.1 Proposed reaction mechanism of a penicillin substrate by class A Bla enzyme. Dashed lines represent hydrogen bonds.

With the characterization of this report enzyme and understanding of molecular mechanism, imaging probes have been developed to facilitate the detection of the resistant enzyme with improved sensitivity and specificity, such as noninvasive identification of the recombinant Bla as an exogenous reporter (see Section 1.2.2.4)

and detection of endogenous Blas in bacterial pathogens.[34-38] Design of these molecules usually combines the sensitive enzyme substrates and well-suited fluorescence resonance energy transfer (FRET) pairs, where the enzyme activity in recombinant cells or native bacterial species can be clearly visualized from the on-off fluorescence switch or emission shift upon enzyme activation. However, the inevitable probe diffusion in the living tissues may still cause the perturbation in detection sensitivity, especially when the studied targets are in low level.

In order to avoid probe diffusion and provide *in situ* recognition of endogenous Bla reports, here we introduce a covalent labeling capability into Bla probes. By minimizing the diffusion of activated probes, this β-lactamase-responsive bacterial labeling (LRBL) approach can greatly reduce the nonspecific background and enable rapid and reliable differentiation of clinical resistance, suitable for systematic investigation of antibiotic resistance of individual cells in a mixed population.

2.2 Experimental sections

2.2.1 Design, synthesis and characterization

The labeling ability is derived from the highly reactive quinone-methide intermediate, which acts as a nucleophilic trap to bond the surrounding nucleophiles like enzyme serine and cysteine residues. As shown in Scheme 2.2, a precursor of labile *p*-hydroxybenzylic ester is tagged with a FRET-quenched fluorophore and connected to a Bla-sensitive cephalosporin, where the sulfide bond is oxidized to sulfoxide for improved stability. In resistant bacteria, the endogenous β-lactamases catalyze the hydrolysis of LRBL probes and release the *p*-hydroxybenzylic derivatives,

which can rearrange spontaneously to generate fluorescent quinone-methides for covalent labeling with recovered fluorescence for direct observation.

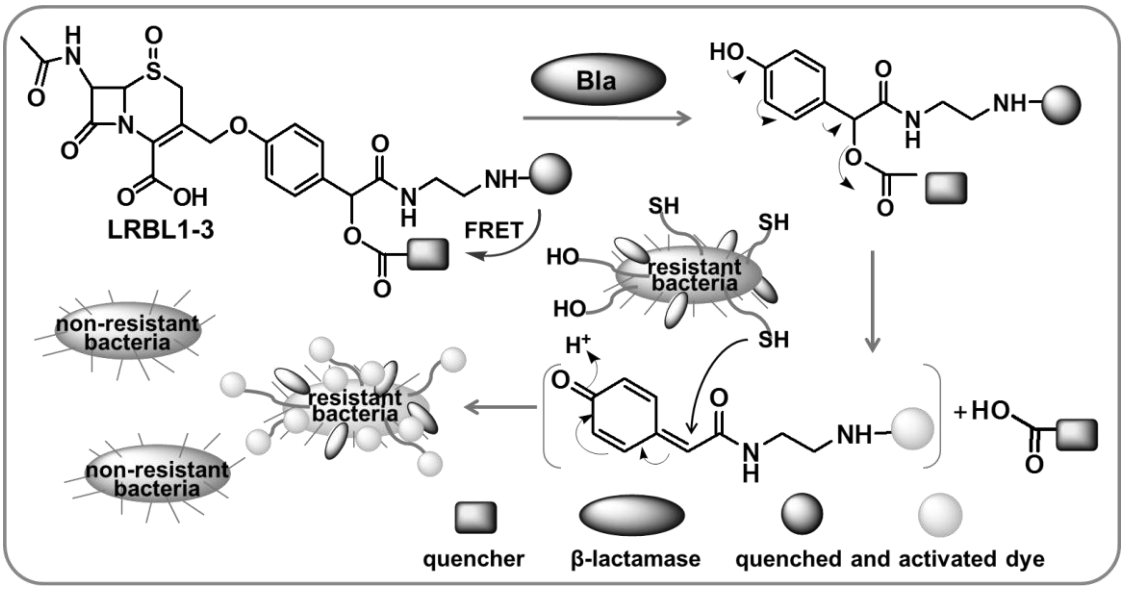

Scheme 2.2 Design of the β-lactamase-responsive bacterial labeling.

Three fluorophores with different emission properties were used, including fluorescein (Em = 520 nm, green), Cy3 (Em = 580 nm, yellow) and near-infrared Cy5.5 (Em = 680 nm), to facilitate microscopic imaging and flow cytometry analysis. The fluorescence was prequenched by DABCYL, BHQ2 and BHQ3 molecules respectively. These LRBL probes were synthesized according to Scheme 2.3 and the products were characterized by Mass spectra and HNMR spectra as shown below.

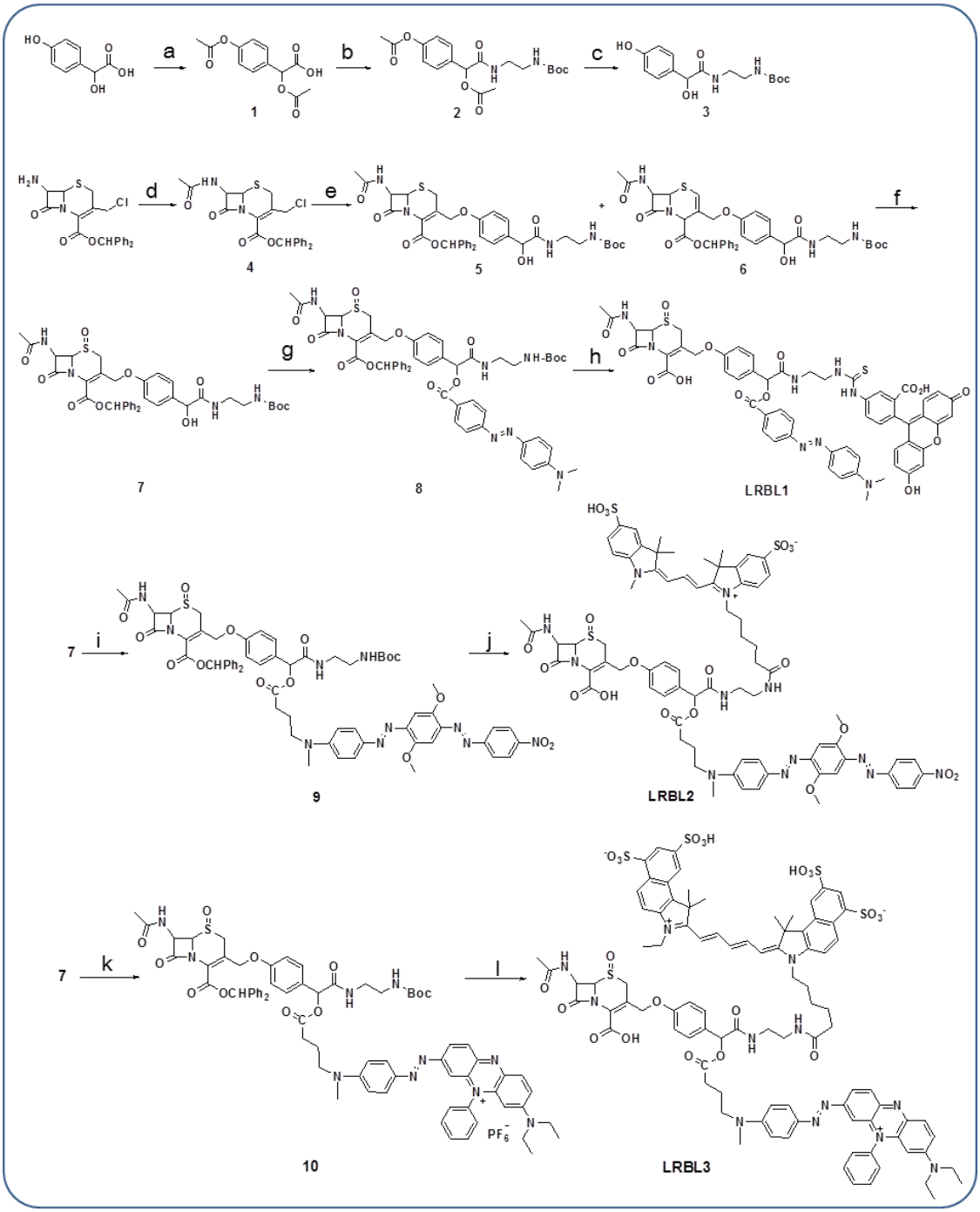

Scheme 2.3 Synthesis of LRBL1-3. Conditions: (a) acetic anhydride/pyridine; (b) EDC, TEA, N-Boc-ethylenediamine/DCM; (c) DBU/MeOH; (d) acetyl chloride/DCM; (e) i) NaI/Acetone, ii) compound 3/Acetonitrile; (f) mCPBA/DCM; (g) DCC, DABCYL acid/DCM; (h) i) TFA, anisole/DCM, ii) FITC, DIPEA/DMF; (i) BHQ2 carboxylic acid, DCC/DCM; (j) i) TFA, anisole/DCM, ii) Cy3 *N*-Hydroxysuccinimide (NHS) ester, DIPEA/DMF; (k) BHQ3 carboxylic acid, DCC/DCM; (l) i) TFA, anisole/DCM, ii) Cy5.5 NHS ester, DIPEA/DMF.

Compound 1. Acetic anhydride (2.5 ml, 26.5 mmol) was added to a cooled solution of 4-hydroxymandelic acid monohydrate (1.77 g, 9.5 mmol) in 2.5 ml of pyridine. The mixture was stirred for 30 min, then dissolved in DCM and washed with water. After drying, the solvent was removed at reduced pressure to give 2.21 g of white solid. Yield: 92.2%. ^{1}HNMR (400 MHz, $CDCl_3$) δ (ppm): 7.51 (d, J = 8.72 Hz, 2H), 7.13 (d, J = 8.72 Hz, 2H), 5.94 (s, 1H), 2.31 (s, 3H), 2.20 (s, 3H); HRMS (ESI) m/z: calcd for $C_{12}H_{13}O_6$: 253.0712; $[M+H]^+$ found: 253.0720.

Compound 2. To a solution of compound **1** (1.26 g, 5.0 mmol) in 30 ml of DCM, N-Boc-ethylenediamine (800 mg, 5.0 mmol), EDC (1.15 g, 6.0 mmol) and TEA (1.4 ml, 10.0 mmol) was added. The mixture was stirred for 5 hrs, washed with water and dried over Na_2SO_4. After concentration, the residue was purified by column chromatography on silica gel to give 1.83 g of product. Yield: 92.9%. ^{1}HNMR (400 MHz, $CDCl_3$) δ (ppm): 7.43 (d, J = 8.72 Hz, 2H), 7.05 (d, J = 8.72 Hz, 2H), 6.02 (s, 1H), 5.10 (m, 1H), 3.29 (m, 2H), 3.23 (m, 2H), 2.26 (s, 3H), 2.18 (s, 3H), 1.43 (s, 9H); HRMS (ESI) m/z: calcd for $C_{19}H_{27}N_2O_7$: 395.1818; $[M+H]^+$ found: 395.1803.

Compound 3. Compound **2** (0.85 g, 2.16 mmol) was dissolved in 20 ml of MeOH. Then DBU (1.64 g, 10.8 mmol) was added and the mixture was stirred for 30 min. After concentration, the residue was purified by column chromatography on silica gel to give 387 mg of white solid. Yield: 57.8%. ^{1}HNMR (400 MHz, MeOH-d4) δ (ppm): 8.18 (br, 1H), 7.23 (m, 2H), 6.73 (m, 2H), 6.56 (br, 1H), 4.90 (s, 1H), 3.29 (m, 2H), 3.16 (m, 2H), 1.42 (s, 9H); HRMS (ESI) m/z: calcd for $C_{15}H_{23}N_2O_5$: 311.1607; $[M+H]^+$ found: 311.1602.

Compound 4. 7-Amino-3-chloromethyl-3-cephem-4-carboxylic acid diphenylmethyl ester hydrochloride (400 mg, 0.89 mmol) was added in 30 ml of DCM, followed by addition of acetyl chloride (70 mg, 0.89 mmol) and 2,6-lutidine (191 mg, 1.78 mmol). The mixture was stirred for 2 hrs and concentrated. The residue was purified by column chromatography on silica gel to give 365 mg of white solid. Yield: 89.7%. ^{1}HNMR (400 MHz, $CDCl_3$) δ (ppm): 7.42-7.44 (m, 2H), 7.28-7.37 (m, 8H), 6.98 (s, 1H), 6.31 (d, J = 9.16 Hz, 1H), 5.89 (dd, J = 5.04 Hz, 9.16 Hz, 1H), 4.99 (d, J = 5.04 Hz, 1H), 4.39 (d, J = 1.40 Hz, 2H), 3.62 (d, J = 18.32 Hz, 1H), 3.48 (d, J = 18.32 Hz, 1H), 2.04 (s, 3H); HRMS (ESI) m/z: calcd for $C_{23}H_{21}ClN_2O_4SNa$: 479.0808; $[M+Na]^+$ found: 479.0824.

Compound 5. Sodium iodide (600 mg, 4.00 mmol) was added to a solution of compound **4** (300 mg, 0.66 mmol) in 10 ml acetone and stirred for 1 hr. After concentration, the residue was dissolved in EA, washed and dried over Na_2SO_4. After concentration, the crude product was dissolved in 10 ml of anhydrous CH_3CN, followed by addition of compound **3** (205 mg, 0.66 mmol) and potassium carbonate (140 mg, 1.01 mmol). The reaction mixture was stirred for 16 hrs and purified by column chromatography on silica gel to give 45 mg of **5** and 97 mg of **6.** Yield: 9.3%. ^{1}HNMR (400 MHz, Acetone-d6) δ (ppm): 7.93 (d, J = 8.72 Hz, 1H), 7.67 (m, 1H), 7.50 (d, J = 1.84 Hz, 2H), 7.48 (d, J = 1.84 Hz, 2H), 7.28-7.37 (m, 9H), 6.98 (s, 1H), 6.76 (d, J = 8.24 Hz, 2H), 6.13 (br, 1H), 5.91 (dd, J = 5.04 Hz, 8.68 Hz, 1H), 5.18 (d, J = 4.60 Hz, 1H), 4.99 (s, 1H), 4.84 (s, 2H), 3.72 (d, J = 8.68 Hz, 2H), 3.32 (m, 2H), 3.21 (m, 2H), 2.03 (s, 3H), 1.40 (s, 9H); HRMS (ESI) m/z: calcd for $C_{38}H_{43}N_4O_9S$:

731.2751; $[M+H]^+$ found: 731.2744.

Compound 6. Yield: 20.1%. ^{1}HNMR (400 MHz, Acetone-d6) δ (ppm): 7.97 (d, J = 8.24 Hz, 1H), 7.64 (m, 1H), 7.25-7.43 (m, 13H), 6.90 (s, 1H), 6.82 (d, J = 8.24 Hz, 2H), 6.73 (s, 1H), 6.10 (br, 1H), 5.58 (m, 1H), 5.27 (m, 2H), 4.97 (s, 1H), 4.60 (s, 2H), 3.29 (m, 2H), 3.19 (m, 2H), 2.02 (s, 3H), 1.38 (s, 9H); HRMS (ESI) m/z: calcd for $C_{38}H_{43}N_4O_9S$: 731.2751; $[M+H]^+$ found: 731.2744.

Compound 7. *m*-Chloroperbenzoic acid (41 mg, 85%, 0.20 mmol) was added to a cooled solution of compound **6** (97 mg, 0.13 mmol) in 1 ml of DCM and stirred at 0˚C for 1 hr. Then the mixture was diluted with 40 ml of EA, washed with 10% $NaHCO_3$ and dried over Na_2SO_4. After evaporation, the residue was purified by column chromatography on silica gel to afford 63 mg of white solid. Yield: 64.9%. ^{1}HNMR (400 MHz, Acetone-d6) δ (ppm): 7.69 (br, 1H), 7.56 (d, J = 8.24 Hz, 2H), 7.48 (d, J = 7.36 Hz, 2H), 7.25-7.38 (m, 9H), 7.01 (s, 1H), 6.73 (d, J = 8.72 Hz, 2H), 6.14 (br, 1H), 6.10 (m, 1H), 5.29 (m, 1H), 5.11 (d, J = 13.28 Hz, 1H), 4.97 (m, 2H), 4.78 (d, J = 13.72 Hz, 1H), 4.10 (d, J = 19.24 Hz, 1H), 3.67 (d, J = 18.80 Hz, 1H), 3.31 (m, 2H), 3.20 (m, 2H), 2.08 (s, 3H), 1.40 (s, 9H); HRMS (ESI) m/z: calcd for $C_{38}H_{43}N_4O_{10}S$: 747.2700; $[M+H]^+$ found: 747.2703.

Compound 8. Compound **7** (20 mg, 0.027 mmol) was dissolved in 2 ml of DCM. Then 4-(Dimethylaminoazo)benzene-4-carboxylic acid (DABCYL acid, 7 mg, 0.026 mmol), 4-(dimethylamino) pyridine (5 mg, 0.041 mmol) and DCC (16 mg, 0.078 mmol) was added and the mixture was stirred overnight. The solvent was removed under reduced pressure and the residue was purified by column chromatography on

silica gel to afford 13 mg product. Yield: 48.2%. ^{1}HNMR (400 MHz, Acetone-d6) δ (ppm): 8.28 (d, J = 8.24 Hz, 2H), 7.88-7.94 (m, 5H), 7.46-7.56 (m, 6H), 7.24-7.38 (m, 7H), 7.02 (s, 1H), 6.87 (d, J = 9.16 Hz, 2H), 6.82 (d, J = 8.72 Hz, 2H), 6.19 (s, 1H), 6.09-6.15 (m, 2H), 5.16 (d, J = 13.28 Hz, 1H), 4.99 (d, J = 3.68 Hz, 1H), 4.81(d, J = 13.28 Hz, 1H), 4.12 (d, J = 19.24 Hz, 1H), 3.71 (d, J = 18.80 Hz, 1H), 3.35 (m, 2H), 3.23 (m, 2H), 3.14 (s, 6H), 2.08 (s, 3H), 1.38 (s, 9H); HRMS (ESI) m/z: calcd for $C_{53}H_{56}N_7O_{11}S$: 998.3759; $[M+H]^+$ found: 998.3748.

LRBL1. 300 ul of TFA and 100 ul of anisole were added to a solution of compound **8** (10 mg, 0.010 mmol) in 1 ml of DCM and the mixture was stirred at room temperature for 1 hr. The solvent was removed at reduced pressure and the residue was dissolved in 1 ml of DMF, followed by addition of FITC (6.0 mg, 0.015 mmol) and N,N-diisopropylethylamine (4.0 μl, 0.023 mmol). The mixture was stirred for 3 hrs and purified by reverse-phase HPLC to give 3.8 mg of red product after lyophilization. Yield: 33.9%. ^{1}HNMR (400 MHz, Acetone-d6) δ (ppm): 11.83 (br, 1H), 10.20 (br, 1H), 8.44 (s, 1H), 8.25 (d, J = 7.80 Hz, 2H), 8.17 (m, 1H), 7.84-7.91 (m, 5H), 7.57 (m, 2H), 7.21 (d, J = 9.64 Hz, 1H), 7.15 (d, J = 8.24 Hz,1H), 6.94 (m, 2H), 6.85 (d, J = 9.16 Hz, 2H), 6.71-6.74 (m, 4H), 6.62 (m, 2H), 6.20 (s, 1H), 6.03 (m, 1H), 5.27 (d, J = 12.84 Hz, 1H), 4.91 (d, J = 3.64 Hz, 1H), 4.82 (t, J = 11.92 Hz, 1H), 4.05 (d, J = 19.24 Hz, 1H), 3.86 (m, 1H), 3.50-3.74 (m, 3H), 3.14-3.23 (m, 10H), 2.08 (s, 3H); HRMS (ESI) m/z: calcd for $C_{56}H_{49}N_8O_{14}S_2$: 1121.2810; $[M+H]^+$ found: 1121.2822.

Compound 9. Same procedure as compound **8**. Yield: 49.8%. ^{1}HNMR (400 MHz, Acetone-d6) δ (ppm): 8.46 (d, J = 9.16 Hz, 2H), 8.13 (d, J = 9.16 Hz, 2H), 7.87 (d, J =

7.76 Hz, 2H), 7.73 (m, 1H), 7.53-7.55 (m, 3H), 7.46-7.49 (m, 3H), 7.20-7.39 (m, 9H), 7.00 (s, 1H), 6.91 (d, *J* = 7.76 Hz, 2H), 6.79 (d, *J* = 6.88 Hz, 2H), 6.06-6.09 (m, 2H), 5.93 (s, 1H), 5.10 (d, *J* = 13.28 Hz, 1H), 4.94 (d, *J* = 4.12 Hz, 1H), 4.79 (d, *J* = 12.80 Hz, 1H), 4.05-4.11 (m, 4H), 4.00 (s, 3H), 3.56-3.68 (m, 3H), 3.30 (m, 2H), 3.18 (m, 2H), 3.13 (s, 3H), 2.57 (m, 2H), 2.08 (s, 3H), 1.54 (m, 2H), 1.40 (s, 9H); HRMS (ESI) m/z: calcd for $C_{63}H_{67}N_{10}O_{15}S$: 1235.4508; $[M+H]^+$ found: 1235.4546.

LRBL2. Same procedure as compound **LRBL1**. Yield: 33.5%. ^{1}HNMR (400 MHz, DMSO-d6) δ (ppm): 8.44 (d, *J* = 8.72 Hz, 2H), 8.30 (m, 2H), 8.22 (d, *J* = 8.24 Hz, 1H), 8.05 (d, *J* = 9.16 Hz, 2H), 7.76-7.80 (m, 5H), 7.66 (d, *J* = 7.76 Hz, 2H), 7.44 (s, 1H), 7.33-7.38 (m, 5H), 6.93 (d, *J* = 8.24 Hz, 2H), 6.88 (d, *J* = 9.64 Hz, 2H), 6.43 (dd, *J* = 3.24 Hz, 13.76 Hz, 2H), 5.80 (m, 2H), 5.04 (d, *J* = 12.40 Hz, 1H), 4.90 (d, *J* = 3.68 Hz, 1H), 4.76 (d, *J* = 12.80 Hz, 1H), 4.05 (m, 2H), 3.99 (s, 3H), 3.94 (s, 3H), 3.66 (s, 1H), 3.62 (s, 6H), 3.05 (m, 8H), 2.54 (s, 2H), 2.02 (t, *J* = 6.88 Hz, 2H), 1.94 (s, 2H), 1.91 (s, 1H), 1.85 (t, *J* = 6.88 Hz, 1H), 1.67 (m, 14H), 1.53 (m, 2H), 1.33 (m, 2H); HRMS (ESI) m/z: calcd for $C_{75}H_{83}N_{12}O_{20}S_3$: 1567.5009; $[M+H]^+$ found: 1567.4967.

Compound 10. Same procedure as compound **8**. Yield: 36.5%. ^{1}HNMR (400 MHz, Acetone-d6) δ (ppm): 8.40 (d, *J* = 9.12 Hz, 1H), 8.26 (dd, *J* = 9.16 Hz, 1.84 Hz, 1H), 8.20 (d, *J* = 10.04 Hz, 1H), 8.07 (m, 1H), 7.96-8.00 (m, 3H), 7.83 (m, 2H), 7.78 (dd, *J* = 9.16 Hz, 1.36 Hz, 2H), 7.54 (m, 2H), 7.44 (m, 3H), 7.26-7.38 (m, 8H), 6.98 (d, *J* = 4.60 Hz, 1H), 6.91 (d, *J* = 9.64 Hz, 2.72 Hz, 2H), 6.77 (m, 2H), 6.08 (d, *J* = 4.60 Hz, 1H), 6.00 (d, *J* = 2.72 Hz, 1H), 5.91 (d, *J* = 2.28 Hz, 1H), 5.09 (dd, *J* = 13.28 Hz, 7.32 Hz, 1H), 4.95 (m, 1H), 4.76 (m, 1H), 4.03 (d, *J* = 19.2 Hz, 1H), 3.96 (br, 1H),

3.56-3.69 (m, 4H), 3.28 (m, 2H), 3.16 (m, 5H), 2.59 (m, 2H), 2.09 (s, 3H), 2.01 (m, 1H), 1.40 (s, 9H), 1.15 (m, 2H); HRMS (ESI) m/z: calcd for $C_{71}H_{75}N_{10}O_{11}S^+$: 1275.5338; $[M\text{-}PF_6]^+$ found: 1275.5419.

LRBL3. Same procedure as compound **LRBL1**. Yield: 36.9%. ^{1}HNMR (400 MHz, DMSO-d6) δ (ppm): 8.99 (m, 2H), 8.35-8.42 (m, 5H), 8.19-8.27 (m, 4H), 8.12 (m, 2H), 7.86-7.94 (m, 5H), 7.65-7.76 (m, 8H), 7.35 (d, J = 8.24 Hz, 2H), 7.15 (s, 1H), 6.91 (d, J = 7.76 Hz, 2H), 6.81 (d, J = 9.16 Hz, 2H), 6.54 (m, 1H), 6.28 (m, 2H), 5.80 (m, 2H), 5.67 (s, 1H), 5.02 (d, J = 10.04 Hz, 1H), 4.90 (d, J = 3.68 Hz, 1H), 4.73 (d, J = 11.92 Hz, 1H), 4.24 (m, 2H), 4.14 (m, 2H), 3.94 (d, J = 18.32 Hz, 1H), 3.79 (m, 2H), 3.64 (d, J = 17.84 Hz, 1H), 3.05 (m, 7H), 2.04 (m, 2H), 1.94 (s, 3H), 1.91 (m, 12H), 1.85 (m, 1H), 1.72 (m, 2H), 1.53 (m, 2H), 1.33 (m, 6H), 1.19 (m, 4H), 0.96 (m, 2H); HRMS (ESI) m/z: calcd for $C_{94}H_{99}N_{12}O_{22}S_5$: 1907.5600; $[M+H]^+$ found: 1907.5679.

2.2.2 Enzyme activity and fluorescent labeling

Fluorescence measurement. Reaction mixtures (200 μL each) containing LRBL probes (10 μM) and TEM-1 Bla in phosphate buffered saline (PBS) were incubated at 37˚C and subjected to fluorescence measurement. In control experiments, probes were incubated with PBS buffer at 37˚C. The excitation wavelength for LRBL1, 2 and 3 was 488, 525 and 650 nm respectively.

Enzyme kinetic study. The enzyme kinetics was carried out in PBS (pH 7.2) at 37 ˚C. A series of different concentrations of LRBL probes were prepared and incubated with TEM-1 Bla in PBS buffer (pH 7.2) at 37˚C. The enzymatic hydrolysis rates were determined and plotted against probe concentrations.

Sensitivity of LRBL probes. Reaction mixtures (200 μL each) containing LRBL probes (10 μM) and TEM-1 Bla (1 to 200 pM) in PBS buffer (pH 7.2) were incubated at 37˚C for 30 min and subjected to fluorescence measurement. In control experiments, probes were incubated with PBS buffer at 37˚C for 30 min. All the tests were performed in triplicate.

Fluorescent labeling. The labeling ability was examined with gel electrophoresis. The reaction mixture of 1 μg of Bla and 2 μM of probe was loaded on a 10%-polyacrylamide/SDS gel and then subjected to 1 h of separation. In the competition assay, Bla enzyme was pretreated with Bla inhibitor clavulanic acid (CA). The labeling profile was further examined with molecular weight analysis on the ABI 4800 MALDI-TOF.

Bla activity assay. The Bla activity after LRBL labeling was examined by the conventional hydrolysis assay using benzylpenicillin as the substrate.[39] TEM-1 Bla (0.5 μM) was incubated with LRBL probes (50 μM) for 30 mins respectively. Then the reaction mixture was added to benzylpenicillin (0.5 mM in PBS) with 1 : 200 dilution and the enzymatic hydrolysis of benzylpenicillin was monitored based on the absorbance change at 232 nm. The efficient Bla inhibitor CA (50 μM) was used for comparison.

2.2.3 Detection and Imaging of resistant bacteria

Material. Several strains have been used to examine the resistance, including penicillin resistant *E. coli* JM109/pUC19, antibiotic resistant *B. cereus*, methicillin resistant *S. aureus* and antibiotic susceptible *S. aureus*. The penicillin susceptible *E.*

coli JM109 without Bla production was used as the negative control. Single colonies of bacterial strains on solid Luria-Bertani (LB) plates were transferred to liquid LB culture medium and grown at 37 ˚C for 12h. Bacterial cells were harvested by centrifuging and washed with sterile PBS for further use.

Bacterial susceptibility to LRBL probes (MIC). The bacterial culture of a single colony was washed and resuspended in PBS buffer to 10^7 CFU/ml. A 10 μl bacterial solution was added to 1 ml LB solution containing LRBL probes (from 0.5 μM to 120 μM) with the final bacterial concentration of 10^5 CFU/ml. The cultures were shaken at 37 ˚C for 24 h and the bacterial growth was determined with naked eye. The reported MIC was the lowest concentration of compound that prevented cell growth. Each measurement was performed in triplicate.

Enzyme detection in cell lysates. *E. coli* JM109 and JM109/pUC19 cells (10^8 CFU/ml) were lysed in 1 ml of PBS by sonication with a Vibra-Cell Sonics (3 × 10 min), pulsed at 70% max. LRBL1 (10 μM) was incubated with the bacterial lysates at 37 ˚C for fluorescence measurement with 488 nm excitation and 520 nm emission.

Fluorescent imaging. Imaging of bacterial cells was conducted on a Nikon Eclipse TE2000 Confocal Microscope. The overnight culture of bacterial suspensions were diluted to 10^8 cells/ml and incubated with LRBL probes (10 μM). After washing with PBS, the bacterial cells were spotted on poly-L-lysine pretreated glass slides and immobilized with coverslips for image acquisition. To study the enzyme specificity, the cells were pretreated with enzyme inhibitor CA and labeled with LRBL probes for imaging study. In addition, the various depths of bacterial imaging were scanned to

prove probe cell permeability in different strains.

Flow cytometric study. All FCM experiments were carried out by cooperators in Xiamen University. The overnight cultures of bacterial strain were washed with PBS and diluted to 10^8 cells/ml respectively. The bacterial cells were incubated with LRBL1 (10 μM) for 60 min, washed with PBS and directly subjected to FCM analysis. Fluorescence of the cells was detected by a laboratory-built high-sensitivity flow cytometer with a solid-state 488 nm continuous-wave laser as excitation source.[40] The emitted light was collected and splitted into two light paths for side scatter and green fluorescence detection respectively. To study the labeling specificity, the bacteria cells were preincubated with Bla inhibitor clavulanic acid for 1 h, then stained with LRBL1 and subjected to FCM analysis. The bacterial cells without LRBL1 labeling were used as negative control. For experiments with fixation and permeabilization treatment, bacterial cells were first fixed with 1% PFA for 5 min and washed with PBS. The fixed cells were then incubated with permeating solution (25 mM Tris-HCl, 1.8 % glucose and 10 mM EDTA, pH 7.4) for 20 min. After washing with PBS, the treated cells were incubated with LRBL1 (2 μM) for 20 min, washed with PBS and subjected to FCM study.

2.3 Results and discussion

2.3.1 Enzyme activation and covalent labeling

Strong fluorescence enhancement was observed in the LRBL probes after incubated with TEM-1 Bla (38-, 110- and 80-fold for LRBL1, 2 and 3, Figure 2.6), indicating the break of FRET status and cleavage of the quencher. And the control sample without

Bla addition indicated that these probes were quite stable in aqueous conditions, thus allowed the determination of Bla detection limit as low as 1.5, 10 and 50 pM by LRBL1, 2 and 3 respectively.

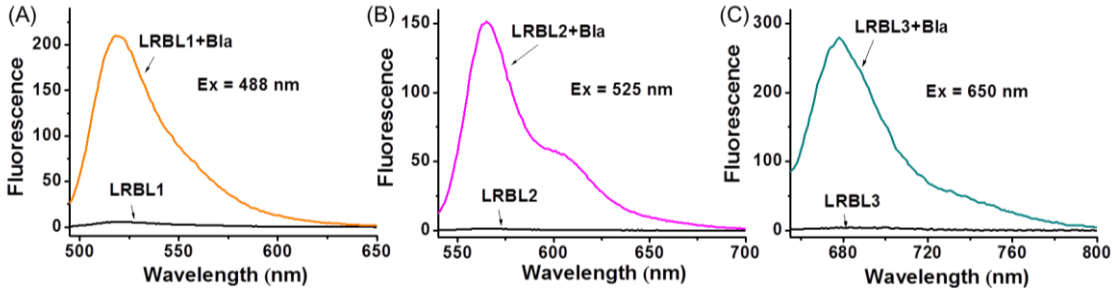

Figure 2.6 Fluorescence emission of LRBL1 - 3 (10 μM) in the absence or presence of Bla hydrolysis (PBS, pH 7.2).

The catalytic constants (k_{cat} = 4.92, 2.16, 1.49 min^{-1}) and Michaelis constants (K_m = 3.08, 4.28, 5.24 μM) for LRBL1, 2 and 3 were determined (Figure 2.7), from which the catalytic efficiencies (k_{cat}/K_m) were calculated to be 2.66, 0.84 and 0.47 × 10^4 $M^{-1}s^{-1}$ respectively, comparable to the values of reported Bla probes containing similar oxidized cephalosporin cores.[35,36]

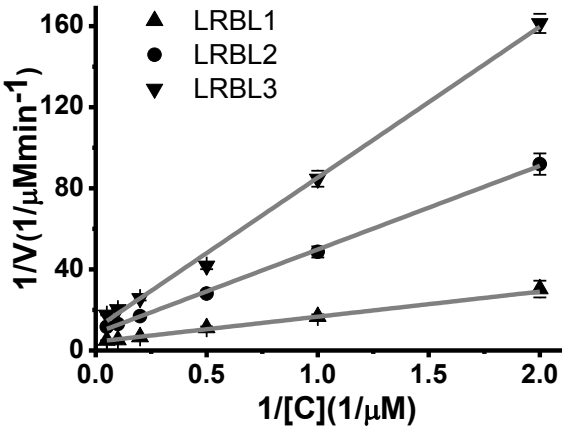

Figure 2.7 Enzyme kinetics of LRBL probes to TEM-1 Bla.

The labeling capability was examined with SDS-PAGE analysis, from which the labeled enzyme could be directly observed from the tagged fluorescence signal. In contrast, the competition assay with Bla inhibitor pretreatment did not fluoresce, thus clearly proved the specificity of the labeling activity (Figure 2.8).

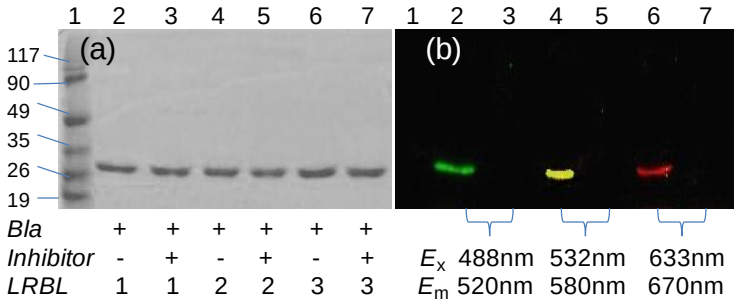

Figure 2.8 SDS-PAGE analysis of Bla labeling. (a) Coomassie Blue staining and (b) fluorescence image of merged green, yellow and NIR channels. Lane 1: Mw marker; lane 2: Bla+LRBL1; Lane 4: Bla+LRBL2; Lane 6: Bla+LRBL3; Lane 3, 5 and 7: clavulanic acid inhibited Bla with LRBL1, 2 and 3 respectively.

To further examine the labeling profile, the incubated protein mixture was analyzed with MALDI-TOF Mass spectrum. Besides the Mw peak of 28985 from parent Bla enzyme, the observed molecular weight peaks of 29572, 29800 and 30081 indicated the attachment of quinone-methide intermediates (Mw: 581, 813 and 1090 for LRBL1, LRBL2+Na and LRBL3) into TEM-1 Bla (Figure 2.9). In addition, multiple labeling was also observed in MALDI-TOF analysis. In LRBL2, the molecular weight peaks of 30616, 31459 and 32309 were assigned to the TEM-1 lactamase labeled with two, three, and four reactive molecules respectively. In LRBL3, the molecular weight of 31151 and 32255 indicated that the enzyme structure was attached with two and three molecules (Figure 2.9).

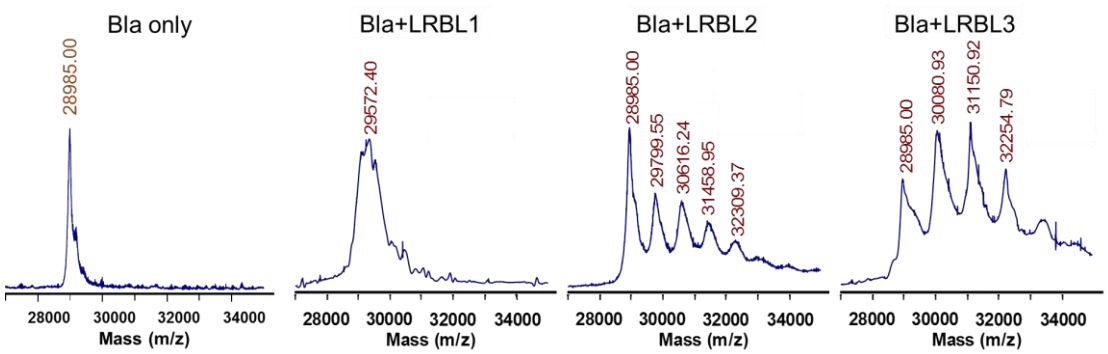

Figure 2.9 MALDI-TOF analysis of TEM-1 Bla enzyme by LRBL labeling.

This result demonstrated the difference of this LRBL labeling to the conventional activity-based probes that directly bond the catalytic amino acid residues in enzyme structure (see Section 1.3.1). Normally, formation of quinone-methide nucleophilic trap requires the cleavage of a precursor and successive spontaneous elimination.[41-44] During these cascade reactions, the activated probes may not work as suicide inhibitors and the enzyme activity still remains. This hypothesis was examined by the conventional hydrolysis assay using benzylpenicillin as enzyme substrate. As shown in Figure 2.10, the absorbance change of benzylpenicillin hydrolysis by LRBL labeled Bla mixtures was almost same as that by pure Bla, indicating that LRBL labeling did not disturb enzyme activity. As a control, the enzyme activity was significantly suppressed in the presence of an effective Bla inhibitor, clavulanic acid. With the enzyme activity remains, more quinone-methide fragments can be produced and captured by nucleophilic amino acids, thus would ideally facilitate the localized amplification of fluorescent signals for real-time imaging of enzyme activity and screening of antibiotic resistant bacteria.

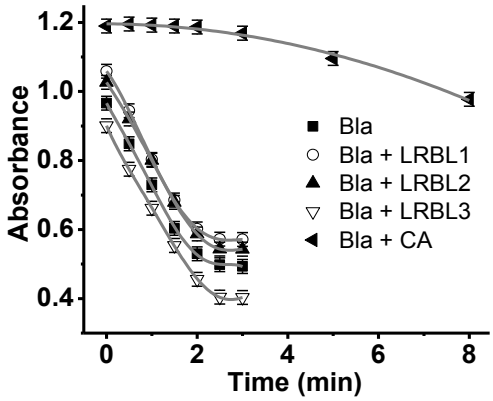

Figure 2.10 Activity of TEM-1 Bla after incubation with LRBL1-3. Enzymatic hydrolysis of benzylpenicillin based on absorbance decrease at 232 nm after incubation with LRBL probes or enzyme inhibitor CA.

2.3.2 Labeling of Gram negative bacteria

With these exciting results, we studied the detection of antibiotic resistant bacteria by fluorescent labeling. A Gram-negative penicillin resistant *E. coli* JM109/pUC19 was selected as our target due to the high production of Bla enzyme in this strain. The antibiotic susceptible *E. coli* JM109 without Bla production was used as the negative control. These bacterial cells were lysed and the Bla activity was examined by LRBL1. As shown in Figure 2.11, Bla production of the resistant *E. coli* JM109/pUC19 was

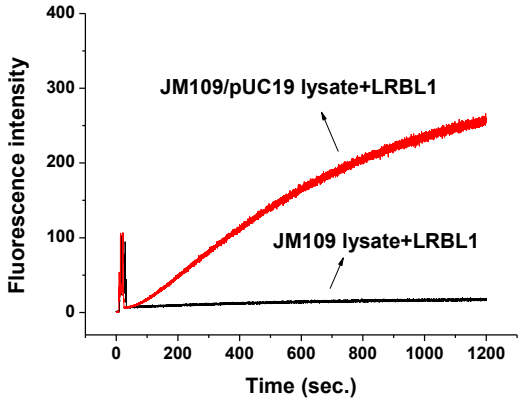

Figure 2.11 Fluorescence of LRBL1 with bacterial lysates of *E. coli* JM109 and *E. coli* JM109/pUC19.

easily detected with fluorescence enhancement. Meanwhile, there was no obvious fluorescence in the lysates of antibiotic susceptible *E. coli* JM109, indicating the specific enzyme reaction and stability of LRBL probes in the presence of other bacterial proteins.

It is also with noting that some *β*-lactam probes can be cleaved by the penicillin binding proteins (PBPs) theoretically with consequent release of fluorophores as illustrated in Scheme 2.4. Considering the number of PBP molecules in *E. coli* (reported as ~2481 per cell)[45] and the non-catalytic nature, the activated fluorescent molecules can be around 2.5 nM at cell density of 10^8 CFU/ml and may not be readily detectable from 10 μM of quenched probes in cell lysate.

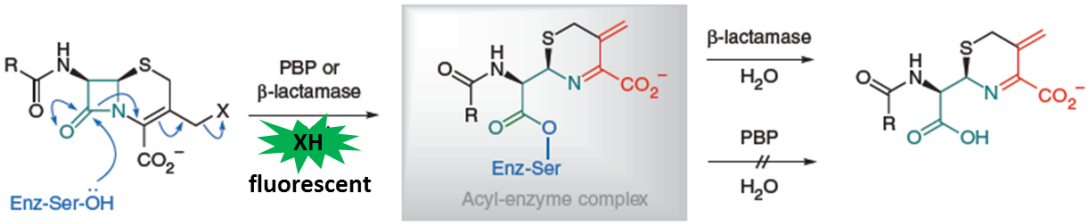

Scheme 2.4 Reaction of Bla and penicillin-binding protein with *β*-lactam probes.

Meanwhile, the bacteria growth of antibiotic susceptible *E. coli* JM109 (MIC study) was examined in the presence of LRBL probes, where no obvious inhibition was observed with 120 μM of LRBL probes. This result demonstrated that the functions of penicillin binding proteins were not affected by LRBL probes, probably due to limited binding capacity and steric hindrance.[46]

The antibiotic resistance was easily detected with living cell imaging. As shown in Figure 2.12, after incubation with LRBL probes, the resistant *E. coli* JM109/pUC19 bacterial cells displayed strong fluorescence emission, while there was no fluorescence

in the cells pretreated with Bla inhibitor as well as the negative control of susceptible *E. coli* JM109.

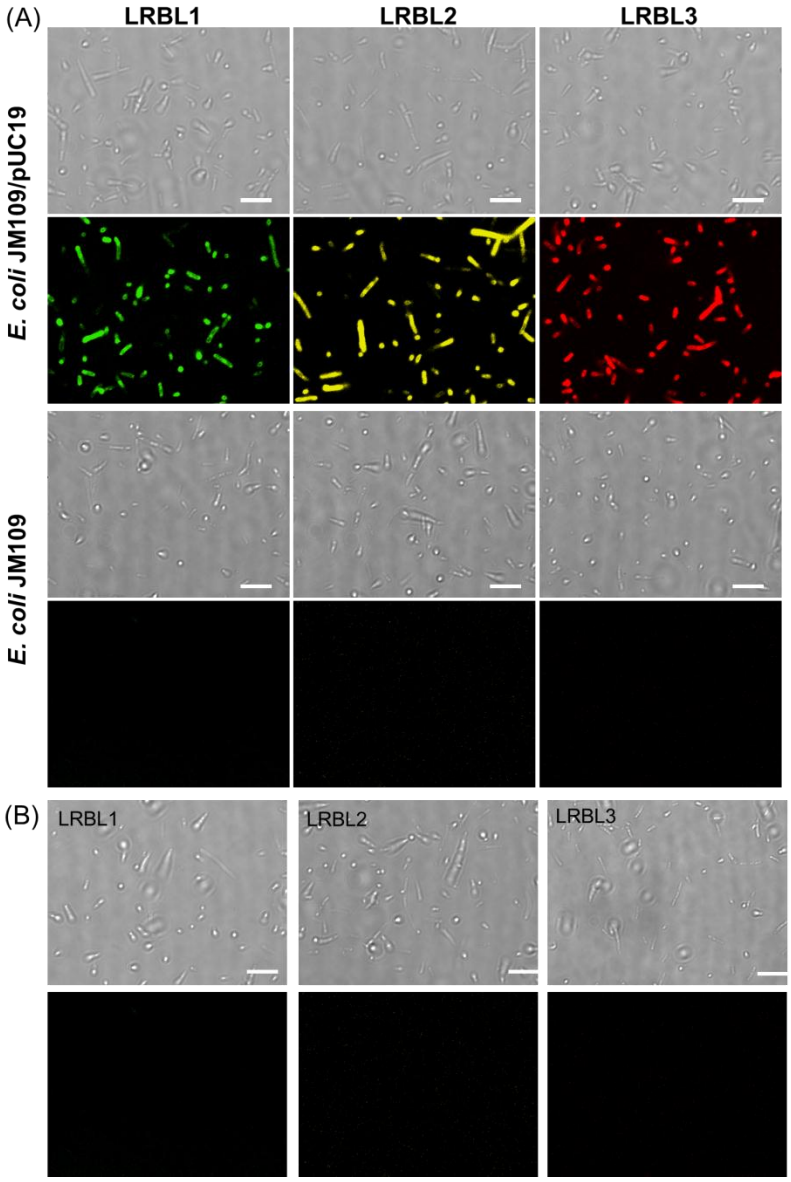

Figure 2.12 (A) Imaging of penicillin resistant *E. coli* JM109/pUC19 (top) and penicillin susceptible *E. coli* JM109 (bottom) incubated with LRBL1, 2 and 3 respectively (10 μM) upon 30 min incubation. (B) Imaging of the resistant *E. coli* JM109/pUC19 cells pretreated with enzyme inhibitor. Scale bar: 10 μm.

In living cell imaging, good membrane permeability is often required to ensure the cellular uptake of probe to study the biological events. In antibiotic resistant bacteria,

Bla enzymes are usually produced in periplasmic space; some can be excreted outside the cell wall in a free and/or membrane-bound form.[47] If the probe is activated by the excreted enzyme in surrounding medium, the fluorescent quinone-methide may stain the outer membrane before entering into cell wall. But such extracellular activation may cause the loss of sensitivity to a large extent due to the probe diffusion in medium and hydroxylation of quinone-methide by water. Thus the cells were washed before probe incubation to remove the excreted free enzyme. In addition, the membrane permeability of LRBL probes was also proved by imaging the labeled cells at various depths with even distribution of fluorescence inside cells (Figure 2.13).

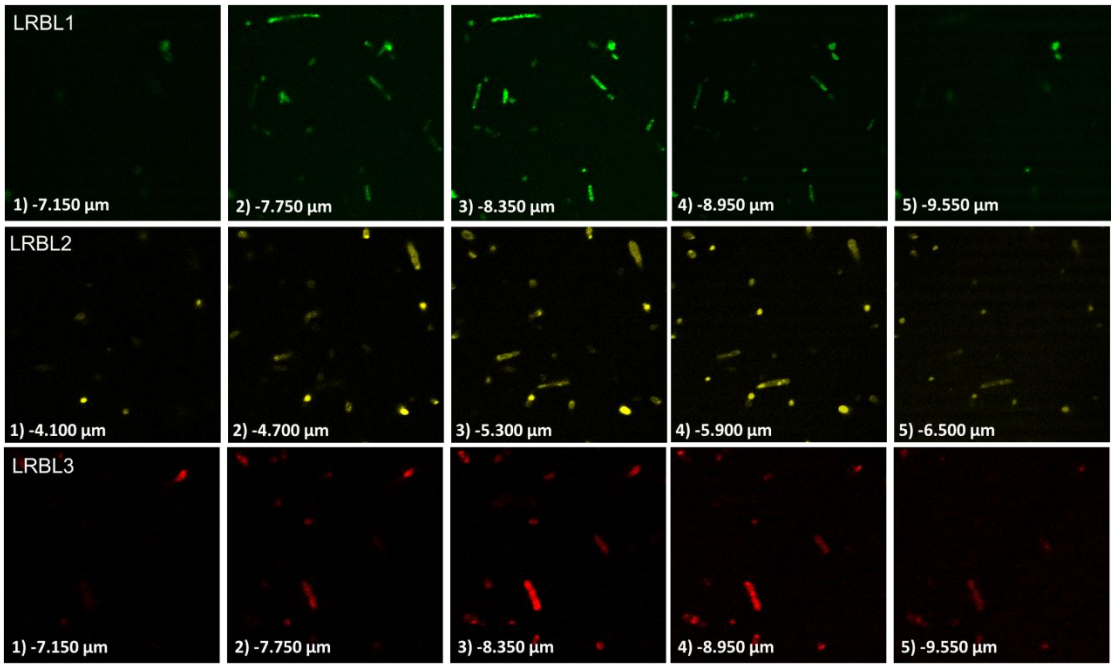

Figure 2.13 Fluorescent imaging of *E. coli* JM109/pUC19 cells at various depths.

As bacteria usually coexist in natural environments, early detection of the resistant subpopulation is helpful to the control of their predominance under antibiotic pressure. To examine the labeling specificity in bacteria mixtures, the Bla-positive *E. coli* JM109/pUC19 cells were mixed with Bla-negative *E. coli* ER2566 cells expressing

green fluorescent protein (GFP). Then the bacteria mixture was incubated with LRBL3 and subjected to fluorescent imaging. As shown in Figure 2.14, the antibiotic resistant *E. coli* JM109/pUC19 cells with Bla expression exhibited distinctive NIR fluorescence by LRBL3 labeling; while the GFP-labeled *E. coli* ER2566 cells without Bla expression did not produce any NIR signal. This result proved that the activated probes would predominately accumulate in the targeted bacteria as the large extent retention in the cellular context would significantly prevent the leakage from cell wall structure, therefore greatly facilitating the specificity in detection and imaging. This study also demonstrated the feasibility of imaging probes with color variants in biological study.

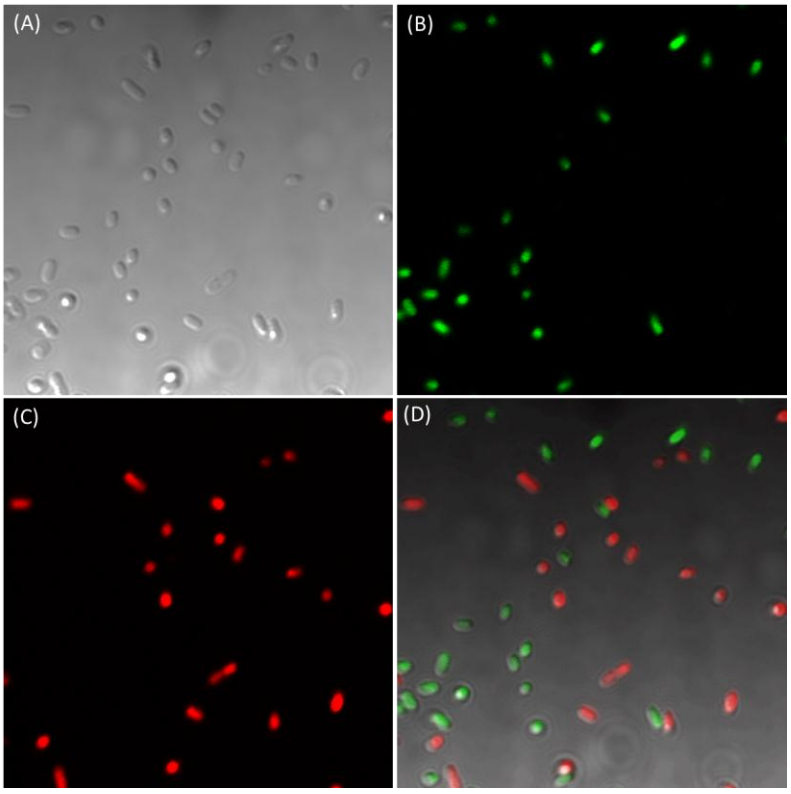

Figure 2.14 Labeling of antibiotic resistant bacteria in mixed population. (A) White light; (B) Green channel displayed the *E. coli* ER2566 cells with GFP expression; (C) NIR channel displayed the resistant *E. coli* JM109/pUC19 cells with LRBL3 labeling; (D) the merged image demonstrated the specificity of labeling.

The feasibility of labeling and fast screening of the resistant strains was also exploited with flow-cytometric (FCM) analysis, which could perform rapid analysis of individual cellular functions with excellent statistics in asynchronous cultures. However, FCM study of antibiotic resistance is usually based on the determination of antibiotic susceptibility without exploiting resistance mechanism. Recent studies utilizing antibiotic-target interactions still cannot identify different mechanisms,[22,48] like lack of the binding target or production of the protective enzyme. With this LRBL labeling, it will directly distinguish the production of Bla and facilitate a clear insight into population heterogeneity in terms of drug resistance with quantitative analysis.

First we determined the respective fluorescence of these two *E. coli* strains after incubation with LRBL1, where a strong increase (~ 20-fold) was observed in the drug resistant *E. coli* JM109/pUC19 cells (red, strain 3) compared to antibiotic susceptible *E. coli* JM109 (green, strain 1) with the populations completely separated (Figure 2.15). Meanwhile, the competition assay with CA inhibition further proved the signal specificity with expected low fluorescence (blue, strain 2).

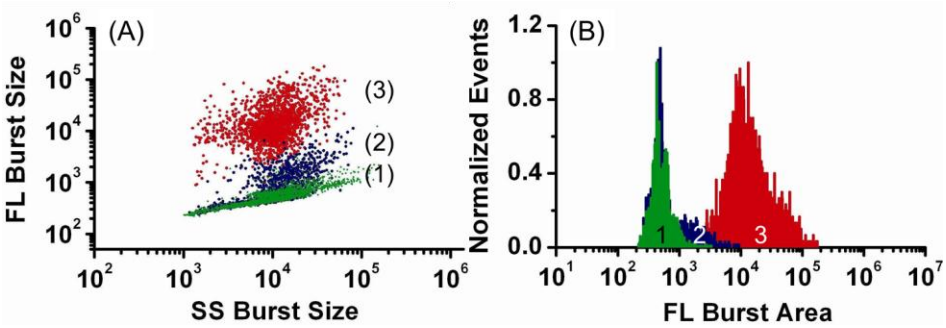

Figure 2.15 FCM analysis of (A) bivariate dot-plot of fluorescence (FL) burst area versus side scattering (SS) burst area and (B) histograms of the fluorescence burst area distribution. *E. coli* JM109 (green, 1), *E. coli* JM109/pUC19 (red, 3) and CA treated *E. coli* JM109/pUC19 (blue, 2).

Next, the *E. coli* JM109 and JM109/pUC19 cells were mixed in various proportions and the mixtures were incubated with LRBL1. The resistance was easily observed in the mixed samples from the bivariate dot-plot with a clear separation between the resistant and susceptible species (Figure 2.16). In addition, the proportion of the detected bacteria with high fluorescence intensity was directly correlated to that of added JM109/pUC19 cells. When the prevalence of JM109/pUC19 in the mixture was 5, 20, 50, 80 and 100%, the percentage of detected resistant bacteria was 6.6, 19.6, 40.5, 69.3 and 92.2% correspondingly. This linear relationship (R^2 = 0.990) proved the labeling specificity, also allowed quantitative analysis of the resistant cells in a mixed population down to as low as 5%. This result also confirmed the labeling specificity in bacteria mixtures.

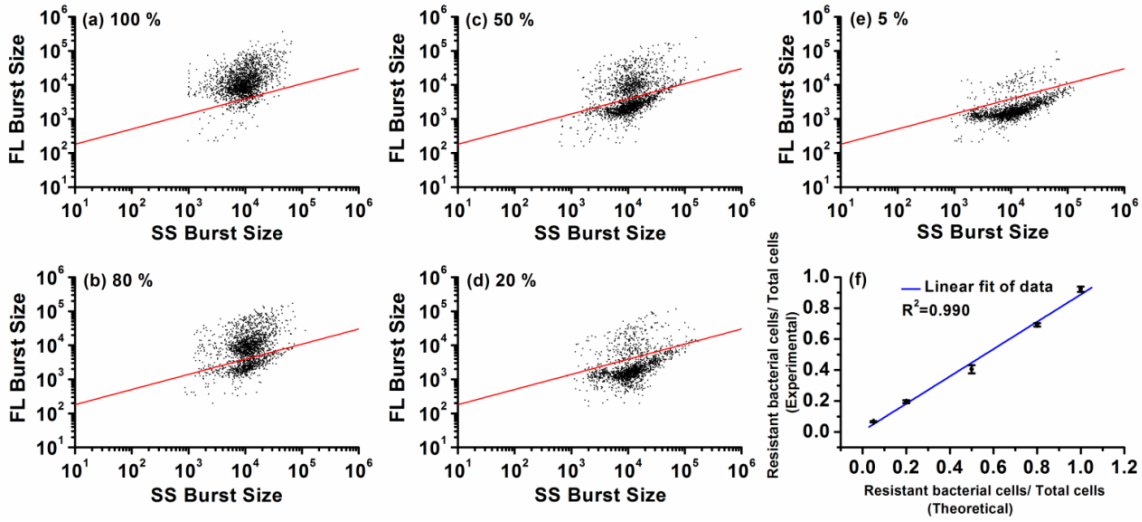

Figure 2.16 Differentiation of resistant *E. coli* JM109/pUC19 cells in bacterial mixtures. (a)-(e) FCM analysis of the antibiotic resistant and susceptible bacteria as separated by the red line. (f) Linear correspondence between the theoretical and the FCM-measured percentages of antibiotic resistant bacteria.

In comparison, a commercial fluorogenic substrate for *β*-lactamase (Fluorocillin™ Green 495/525, Invitrogen) was also used to study antibiotic resistance. This probe could be easily hydrolyzed by TEM-1 Bla, also by the endogenous *β*-lactamases from *E. coli* JM109/pUC19 (Figure 2.17d). However, the fluorescent products could not retain within the bacteria without labeling ability, thus making the FCM analysis difficult (Figure 2.17a-c). These experiments clearly demonstrated the distinctive advantage of the covalent nature in LRBL probes.

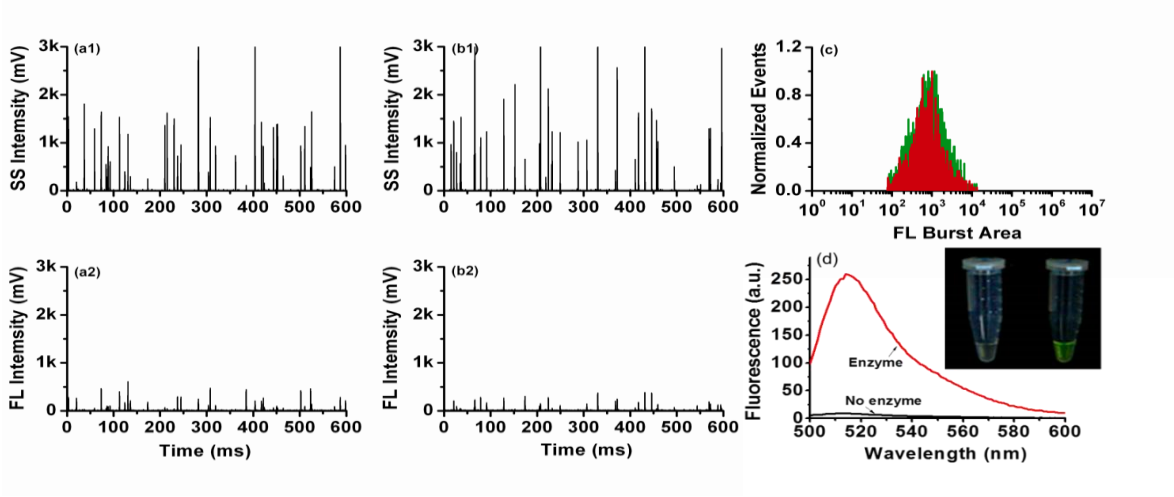

Figure 2.17 FCM study of side scattering (SS, a1, b1) and fluorescence burst traces (FL, a2, b2) for *E. coli* JM109 and *E. coli* JM109/pUC19 cells upon incubation with Fluorocillin™ Green 495/525 (20 μM). (c) Fluorescence burst area distribution of *E. coli* JM109 (green) and *E. coli* JM109/pUC19 (red). (d) Fluorescence enhancement of Fluorocillin Green upon enzyme hydrolysis. Inset shows the picture of bacterial suspensions with Fluorocillin Green incubation prior to PBS washing. *E. coli* JM109 (left), *E. coli* JM109/pUC19 (right).

With the advantage of fluorescent labeling, these probes were further studied the applicability for fast screening of enzyme inhibitor. Normally, the inhibition efficacy is measured through the culture and growth method containing both antibiotic and Bla

inhibitor, which is labor intensive and time consuming. Our probe targets the Bla activity directly with the advantage of signal specificity and fast analysis. As a proof of concept, the resistant *E. coli* JM109/pUC19 cells with high Bla production were incubated with Bla inhibitor including clavulanic acid (CA) and sulbactam (SUL), and the antibiotic aztreonam (ATM) was used as control. After one hour, the cells were incubated with LRBL1 probe for another one hour and subjected to FCM analysis. As shown in Figure 2.18, the bacterial fluorescence decreased significantly due to the suppression of Bla activity by CA and SUL, while the antibiotic aztreonam could not inhibit class A Bla activity efficiently. As the efficacy of Bla inhibitors varies with different enzyme classes and different strains,[30] fast readings of inhibitory efficiency through the enzyme responsive covalent labeling may thus facilitate a simple and overall inspection of chemical-microbe interactions. This approach of enzyme responsive bacterial labeling is thus useful to provide promising applications in clinical tests and new drug development.

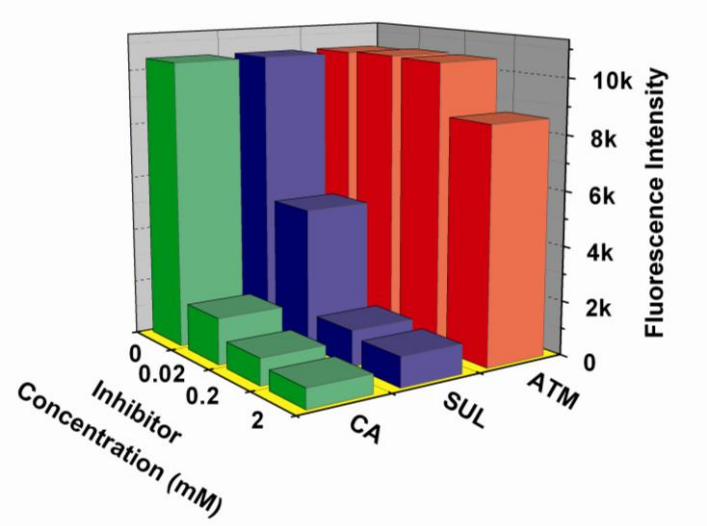

Figure 2.18 Examination of Bla inhibitory activity through fluorescent labeling.

2.3.3 Labeling of Gram positive pathogenic bacteria

The general applicability of fluorescent labeling was further studied with the pathogenic Gram positive *Bacillus cereus* and *Staphylococcus aureus*. These species are involved in various infections like brain abscesses and pneumonia, and represent a therapeutic challenge in terms of drug resistance with complicated mechanisms.[49,50] Three pathogenic species, including one clinically isolated methicillin-resistant *S. aureus* (MRSA, ATCC BAA39), one penicillin resistant *B. cereus* 5/B (ATCC 13061), and one penicillin susceptible *S. aureus* (ATCC 29213), were used in this study as the different ability to produce Bla. As shown in Figure 2.19, strong fluorescent emission could be observed in the penicillin resistant *B. cereus* and MRSA cells upon probe incubation, demonstrating the production of Bla enzyme in these drug resistant strains. Meanwhile the fluorescent signal in *S. aureus* was much weaker due to the low-level Bla production in this strain.[51]

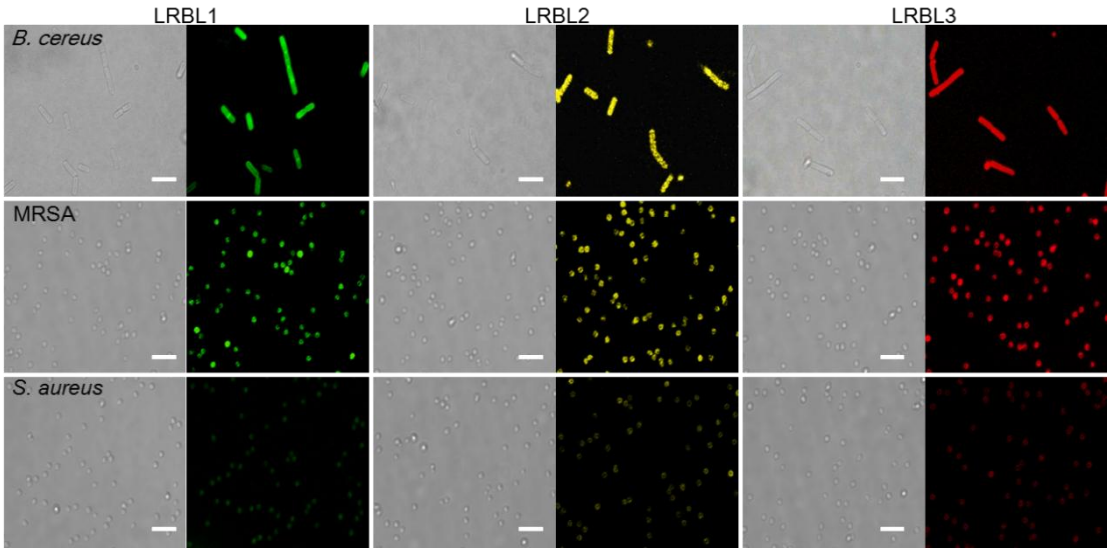

Figure 2.19 Fluorescent imaging of Gram positive *B. cereus*, MRSA and *S. aureus* after incubation with LRBL1, 2 and 3 respectively (10 μM). Scale bar: 10 μm.

The fluorescent labeling of Gram positive species were also investigated with FCM analysis. These bacterial cells were incubated with LRBL1 (2 μM) and subjected to FCM analysis. The resistant strains of MRSA and *B. cereus* both exhibited intense fluorescent signal, which confirmed the efficient covalent labeling. These species were readily detectable due to the good distribution of fluorescence burst area and significant fluorescence enhancement over autofluorescence background (Figure 2.20). Meanwhile, FCM analysis also indicated 10-fold fluorescence enhancement between the resistant MRSA and the susceptible *S. aureus* (Figure 2.20A), which was in accordance with the imaging measurements, clearly suggesting the quantitative distinguishing of Bla activities in naturally existing bacterial pathogens. In addition, FCM analysis also proved the suppression of Bla activity by enzyme inhibitor in these pathogenic species with obvious fluorescence decrease (Figure 2.20B), providing a simple method to screen suitable enzyme inhibitors for clinical applications.

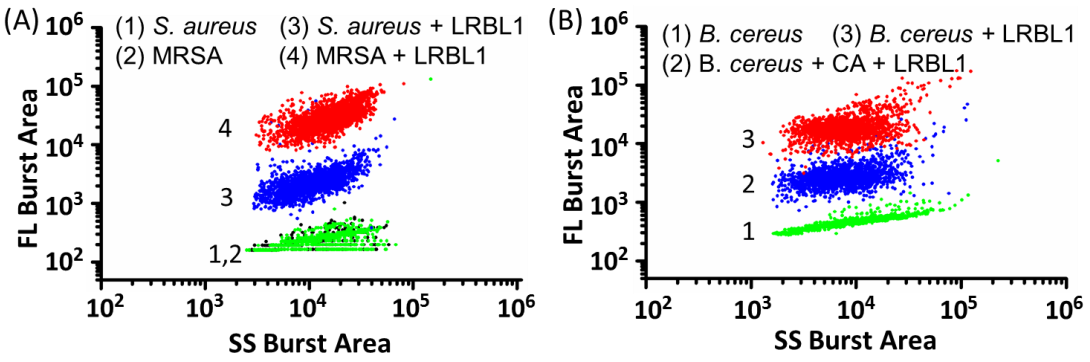

Figure 2.20 FCM analysis of bacteria resistance in Gram positive bacteria. (A) bivariate dot-plot of fluorescence burst area versus side scatter burst area for *S. aureus* (1: unlabeled; 3: labeled) and MRSA (2: unlabeled; 4: labeled). (B) *B. cereus* by LRBL1 labeling. *B. cereus* (1: unlabeled; 2: CA pretreated and labeled; 3: labeled).

2.4 Conclusion

In this chapter, we have presented the development of novel optical imaging probes for specific covalent labeling and fast screening of antibiotic resistant bacteria. These probes target the endogenous production of *β*-lactamases in the resistant strains and form fluorescent quinone-methide intermediates serving as reactive electrophiles for covalent labeling of drug resistant bacteria. With these probes, the Gram negative antibiotic resistant *E. coli* JM109/pUC19 and the Gram positive pathogenic *B. cereus* and MRSA can be easily detected by microscopic imaging and flow cytometry with specificity and sensitivity. This specific *β*-lactamase activation and covalent fluorescent labeling, also allows quantitative analysis of resistant species in a mixed sample down to as low as 5%, thus offers great possibility for clinical investigation and microbiological research, such as high-throughput screening of enzyme inhibitor, real-time diagnosis of bacterial infection and assessment of therapeutic efficacy *in vitro* and *in vivo.*

2.5 References

(1) Sears, C. L. *Anaerobe* **2005**, *11*, 247.

(2) Austrian, R. *Bacteriol. Rev.* **1960**, *24*, 261.

(3) von Nussbaum, F.; Brands, M.; Hinzen, B.; Weigand, S.; Habich, D. *Angew. Chem. Int. Ed.* **2006**, *45*, 5072.

(4) Walsh, C. *Nat. Rev. Microbiol.* **2003**, *1*, 65.

(5) Bugg, T. D. H.; Braddick, D.; Dowson, C. G.; Roper, D. I. *Trends Biotechnol.* **2011**, *29*, 167.

(6) Waxman, D. J.; Strominger, J. L. *Annu. Rev. Biochem.* **1983**, *52*, 825.

(7) Page, M. I. *Acc. Chem. Res.* **1984**, *17*, 144.

(8) Elander, R. P. *Appl. Microbiol. Biotechnol.* **2003**, *61*, 385.

(9) K. E. Nelson; Williams, C. M. *Infectious Disease Epidemiology*; Jones & Bartlett Publishers, 2012.

(10) World Health Organization. *Age-standardized DALYs per 100,000 by cause, and Member State: 2004.* Geneva, WHO, 2009.

(11) Levy, S. B.; Marshall, B. *Nat. Med.* **2004**, *10*, S122.

(12) Deurenberg, R. H.; Vink, C.; Kalenic, S.; Friedrich, A. W.; Bruggeman, C. A.; Stobberingh, E. E. *Clin. Microbiol. Infect.* **2007**, *13*, 222.

(13) Kentner, D.; Sourjik, V. *Annu. Rev. Microbiol.* **2010**, *64*, 373.

(14) Golding, I.; Paulsson, J.; Zawilski, S. M.; Cox, E. C. *Cell* **2005**, *123*, 1025.

(15) Zhao, M.; Yang, M.; Baranov, E.; Wang, X.; Penman, S.; Moossa, A. R.; Hoffman, R. M. *Proc. Natl. Acad. Sci. U.S.A.* **2001**, *98*, 9814.

(16) Tsien, R. Y. *Annu. Rev. Biochem.* **1998**, *67*, 509.

(17) Leevy, W. M.; Gammon, S. T.; Jiang, H.; Johnson, J. R.; Maxwell, D. J.; Jackson, E. N.; Marquez, M.; Piwnica-Worms, D.; Smith, B. D. *J. Am. Chem. Soc.* **2006**, *128*, 16476.

(18) Liu, F.; Ni, A. S. Y.; Lim, Y.; Mohanram, H.; Bhattacharjya, S.; Xing, B. G. *Bioconjugate Chem.* **2012**, *23*, 1639.

(19) Hujer, A. M.; Keslar, K. S.; Dietenberger, N. J.; Bethel, C. R.; Endimiani, A.; Bonomo, R. A. *BMC Microbiol.* **2009**, *9*, 46.

(20) Smartt, A. E.; Ripp, S. *Anal. Bioanal. Chem.* **2011**, *400*, 991.

(21) Edgar, R.; McKinstry, M.; Hwang, J.; Oppenheim, A. B.; Fekete, R. A.; Giulian, G.; Merril, C.; Nagashima, K.; Adhya, S. *Proc. Natl. Acad. Sci. U.S.A.* **2006**, *103*, 4841.

(22) Jarzembowski, T.; Wisniewska, K.; Jozwik, A.; Bryl, E.; Witkowski, J. *Curr. Microbiol.* **2008**, *57*, 167.

(23) Alvarez-Barrientos, A.; Arroyo, J.; Canton, R.; Nombela, C.; Sanchez-Perez, M. *Clin. Microbiol. Rev.* **2000**, *13*, 167.

(24) Xing, B. G.; Jiang, T. T.; Bi, W. G.; Yang, Y. M.; Li, L. H.; Ma, M. L.; Chang, C. K.; Xu, B.; Yeow, E. K. L. *Chem. Commun.* **2011**, *47*, 1601.

(25) Galleni, M.; Lakaye, B.; Lepage, S.; Jamin, M.; Thamm, I.; Joris, B.; Frere, J. M. *Biochem. J.* **1993**, *291*, 19.

(26) Pereira, P. M.; Filipe, S. R.; Tomasz, A.; Pinho, M. G. *Antimicrob. Agents Chemother.* **2007**, *51*, 3627.

(27) Kong, Y.; Yao, H. Q.; Ren, H. J.; Subbian, S.; Cirillo, S. L. G.; Sacchettini, J. C.; Rao, J. H.; Cirillo, J. D. *Proc. Nat. Acad. Sci. USA* **2010**, *107*, 12239.

(28) Xie, H. X.; Mire, J.; Kong, Y.; Chang, M. H.; Hassounah, H. A.; Thornton, C. N.; Sacchettini, J. C.; Cirillo, J. D.; Rao, J. H. *Nat. Chem.* **2012**, *4*, 802.

(29) Zhang, J. X.; Shen, Y.; May, S. L.; Nelson, D. C.; Li, S. W. *Angew. Chem., Int. Ed.* **2012**, *51*, 1865.

(30) Zlokarnik, G.; Negulescu, P. A.; Knapp, T. E.; Mere, L.; Burres, N.; Feng, L. X.; Whitney, M.; Roemer, K.; Tsien, R. Y. *Science* **1998**, *279*, 84.

(31) Drawz, S. M.; Bonomo, R. A. *Clin. Microbiol. Rev.* **2010**, *23*, 160.

(32) Sanders, C. C.; Sanders, W. E. *Clin. Infect. Dis.* **1992**, *15*, 824.

(33) Jelsch, C.; Mourey, L.; Masson, J. M.; Samama, J. P. *Proteins: Struct., Funct., Genet.* **1993**, *16*, 364.

(34) Xing, B. G.; Khanamiryan, A.; Rao, J. H. *J. Am. Chem. Soc.* **2005**, *127*, 4158.

(35) Yao, H.; So, M. K.; Rao, J. *Angew. Chem. Int. Ed.* **2007**, *46*, 7031.

(36) Gao, W. Z.; Xing, B. G.; Tsien, R. Y.; Rao, J. H. *J. Am. Chem. Soc.* **2003**, *125*, 11146.

(37) Mizukami, S.; Watanabe, S.; Hori, Y.; Kikuchi, K. *J. Am. Chem. Soc.* **2009**, *131*, 5016.

(38) Xing, B. G.; Rao, J. H.; Liu, R. R. *Mini-Rev. Med. Chem.* **2008**, *8*, 455.

(39) Boggio, S. B.; Roveri, O. A. *Microbiology-Sgm* **2003**, *149*, 445.

(40) Yang, L. L.; Zhou, Y. X.; Zhu, S. B.; Huang, T. X.; Wu, L. N.; Yan, X. M. *Anal. Chem.* **2012**, *84*, 1526.

(41) Janda, K. D.; Lo, L. C.; Lo, C. H. L.; Sim, M. M.; Wang, R.; Wong, C. H.; Lerner, R. A. *Science* **1997**, *275*, 945.

(42) Kurogochi, M.; Nishimura, S. I.; Lee, Y. C. *J. Biol. Chem.* **2004**, *279*, 44704.

(43) Komatsu, T.; Kikuchi, K.; Takakusa, H.; Hanaoka, K.; Ueno, T.; Kamiya, M.; Urano, Y.; Nagano, T. *J. Am. Chem. Soc.* **2006**, *128*, 15946.

(44) Zhu, Q.; Girish, A.; Chattopadhaya, S.; Yao, S. Q. *Chem. Commun.* **2004**, 1512.

(45) Dougherty, T. J.; Kennedy, K.; Kessler, R. E.; Pucci, M. J. *J. Bacteriol.* **1996**, *178*, 6110.

(46) Sauvage, E.; Kerff, F.; Terrak, M.; Ayala, J. A.; Charlier, P. *FEMS Microbiol. Rev.* **2008**, *32*, 234.

(47) Livermore, D. M. *Clin. Microbiol. Rev.* **1995**, *8*, 557.

(48) Jarzembowski, T.; Jozwik, A.; Wisniewska, K.; Witkowski, J. *Curr. Microbiol.* **2010**, *61*, 407.

(49) Bottone, E. J. *Clin. Microbiol. Rev.* **2010**, *23*, 382.

(50) Chambers, H. F.; Deleo, F. R. *Nat. Rev. Microbiol.* **2009**, *7*, 629.

(51) Nannini, E. C.; Singh, K. V.; Murray, B. E. *Clin. Infect. Dis.* **2003**, *37*, 1194.

Chapter 3

Functional Luminescent Ru(II) Probe for Intracellular Imaging and Lethal Photosensitization of Drug Resistant Bacteria

3.1 Introduction

Apart from the covalent labeling of antibiotic resistant bacteria, the strategy of bio-activatable targeting can also be extended for multiple approaches towards systematic imaging and combination of additional functions. One important feature is photosensitization, which is discovered in some fluorescent compounds and used in clinical applications. These photosensitizers produce highly reactive singlet oxygen ($^1O_2$) during irradiation, which is able to destroy cellular components and cause cell death. The combination of imaging technique and photosensitizing ability has the advantage as the localization of these lethal reagents can be imaged, where light can be selectively delivered to perform photokilling. In this chapter, this approach is used in the development of imaging probes to overcome antibiotic resistance through selective imaging and photosensitization of drug resistant bacteria.

3.1.1 β-Lactam antibiotic resistance

β-Lactam antibiotics stop bacteria growth by inactivating penicillin binding proteins (PBPs) that are required for the polymerization and cross-linking of peptidoglycan in cell wall biosynthesis.[1] These agents mimic C-terminal D-Ala-D-Ala motif of peptidoglycan, suffer nucleophilic attack from PBP and lead to the formation of an inert covalent intermediate. Due to the broad-spectrum efficacy and safety profile, β-lactams are among the most frequently prescribed antibiotics. However, the misuse

and overuse of antibiotic drugs has induced the prevalence of antibiotic resistant bacteria like the methicillin-resistant Staphylococcus aureus (MRSA), which are involved in various infections like brain abscesses and pneumonia, and represent a therapeutic challenge due to the difficulties in treatment, prolonged illness and higher risk of death.[2]

On the other hand, there are no major discoveries of naturally occurring antibiotics in recent years. And the exploration of synthetic drugs is also restricted to the chemical modification of existing antibiotics due to unpredictable difficulties and huge costs. Although many chemicals possess antimicrobial properties, the inherent toxicity make them impossible to use in clinical practice, and such toxicity testing will take years and cost millions of dollars. Even successfully used in therapy, the drugs may still face the challenge of the resistant strains and lose their efficacy in some diseases after a short period of time. Thus it is urgent to overcome the antibiotic resistance, which requires the understanding of resistant mechanism and applicable method to destroy the resistant strains.

The resistance is usually determined during the culture of bacteria in antibiotics. Meanwhile, the molecular mechanism of resistance has also been extensively studied with continuous efforts to benefit clinical diagnosis and new drug development. Production of endogenous β-lactamases is a most common mechanism to confer bacteria resistance by effectively destroying β-lactam drugs before they interact with penicillin binding proteins.[3] Study of β-lactamase activity will be helpful to the better understanding of resistance mechanisms, as well as the selection of effective

antibiotics or coadministration of β-lactamase inhibitors for successful treatment.[4] These bacterial enzymes can be readily detected *in vitro* and *in vivo* by the biological or chemical methods such as polymerase chain reactions, culture and growth method and colorimetric or fluorescent probes (See Section 1.2.2.4 and Section 2.1.3). And the development of optical imaging probes has provided great opportunity for imaging the pathogenic bacterial infection in living animals with endogenous Bla as reporter enzyme.[5,6] However, the demand of systematic investigation and thorough inactivation of drug resistant pathogenic bacteria still requires the development of effective probes to detect and destroy the resistant strains. One promising alternative is the approach of photodynamic antimicrobial chemotherapy (PACT), which employs photosensitizer (PS) to produce highly reactive $^1O_2$ and kill bacteria. With the appreciated features of fluorescent imaging and antibacterial lethality, this approach will greatly facilitate the specific detection and photokilling of the resistant strains.

3.1.2 Photosensitizing Ru(II) complex

Recently, the luminescent ruthenium (II) complexes have attracted much attention due to their attractive photophysical properties, such as high photostability, long emission lifetime (several ms), wide absorbance range and large Stokes shifts (hundreds of nm).[7] Meanwhile, their important photochemistry of generating reactive oxygen species (e.g. $^1O_2$) also ensures interesting explorations of DNA photocleavage[8] and protein photoinactivation.[9] In this process, excitation of the Ru(II)$(bpy)_3^{2+}$ photosensitizer generates the long lived luminescent metal-to-ligand charge transfer (^{3}MLCT) excited state, in which it reacts with O_2 and produces highly reactive $^1O_2$

with high quantum yield (Φ ($^1O_2$) = 0.57) to destroy cells or bacteria (Figure 3.1).[7]

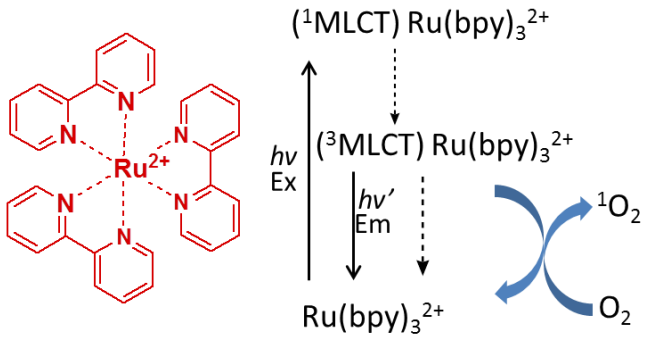

Figure 3.1 Generation of singlet oxygen and luminescent emission by photosensitizing ruthenium (II) complex.

Used in antimicrobial study, this singlet oxygen based photodynamic antimicrobial chemotherapy is capable of eradicating bacteria in a short period of time without damaging adjacent host tissues to a great extent,[10] and regarded as a promising alternative to control the microbial pathogens.[11] The killing efficacy is dependent on the localized accumulation of $^1O_2$ due to its short lifetime (on the order of 10^{-6} s) and limited diffusion distance,[12] thus the cellular uptake is essential for a photosensitizer. In Ru(II) complexes, the binding capacity can be improved by chemical modification of the peripheral ligands to balance the hydrophobic/hydrophilic properties, where higher binding capacities are usually observed in more lipophilic complexes with larger *n*-octanol-water partition coefficients.[13]

Meanwhile, much effort has been devoted to the modification of PSs for improved delivery and cellular uptake.[14] Recent studies have demonstrated the improvement of the killing efficacy by directing PS to target bacterial cells through the incorporation of high-affinity biomaterials, such as peptides,[15,16] antibodies,[17] protein cages,[18] and bacteriophages,[19] as well as multifunctional platforms like zeolite nanocrystals[20] and

conjugated polymers (Table 3.1).[21] However, the inevitable nonspecific accumulation of PSs is still a potential limitation. Thus an activatable photosensitizer for selective $^1O_2$ production is highly expected for the precise control of bacterial photokilling, which also requires a localized fluorescent signal to report such activating events and conduct the delivery of light.

Bacterial strain	Photosensitizer	Affinity ligand	Interaction mechanism
S. aureus	Chlorin e6	Poly-L-lysine	Electrostatic adsorption
E. coli	Porphyrin	Poly-L-lysine	Electrostatic adsorption
S. aureus	Tin(IV) chlorin e6	IgG	Antibody-antigen binding
S. aureus	Tin(IV) chlorin e6	Phage 75	Bacteriophage infection
E. coli	Phthalocyanine	Amino groups	Electrostatic adsorption
E. coli; B. subtilis	Porphyrin	Charges	Electrostatic adsorption

Table 3.1 Affinity groups to improve antibacterial photosensitization.

In order to improve the imaging and photokilling specificity, here we introduce a biosensitive luminescent Ru(II) (BLRu) probe to report the β-lactamase production in resistant bacteria and activate the Ru(II) photosensitization. Ideally, the activation of the photosensitizer in the resistant strains can be imaged through luminescence enhancement, where light is selectively directed for a targeted photosensitization.

3.2 Experimental section

3.2.1 Design, synthesis and characterization

The efficeint activation of imaging property and photosensitizaiton of BLRu complex is based on the cephalosporin structure and FRET principle. As shown in Figure 3.2, a 4-mercaptophenyl linker was connected to the cephalosporin core and

further conjugated with the luminescent Ru(II)$(bpy)_3^{2+}$ complex, of which both emission and photosensitization were quenched by a non-fluorescent BHQ3 in the 7′-amino of the cephalosporin structure through FRET. Upon Bla hydrolysis in resistant strains, the ruthenium complex was released with the recovery of emission property and singlet oxygen productivity for sensitive imaging and localized phototherapy.

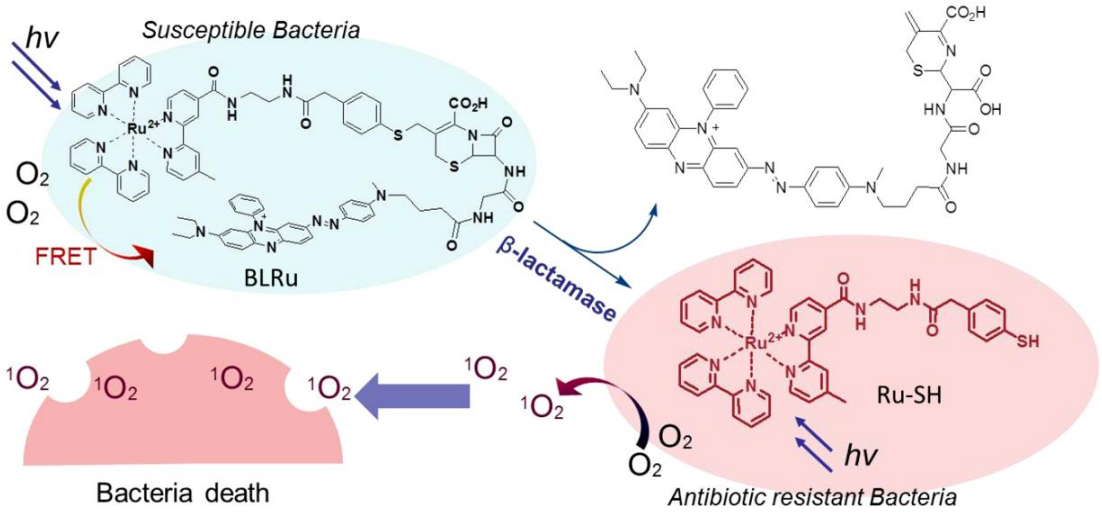

Figure 3.2 Bla responsive luminescent emission and photosensitization of Ru(II) cephalosporin complex to image and kill antibiotic resistant bacteria.

Synthesis of BLRu probe was according to Scheme 3.1. The final product was purified by reverse phase HPLC and characterized by HNMR and mass spectrometry (ESI-MS). In addition, the proposed product after enzyme reaction (Ru-SH) was also synthesized and used for comparison (Scheme 3.2).

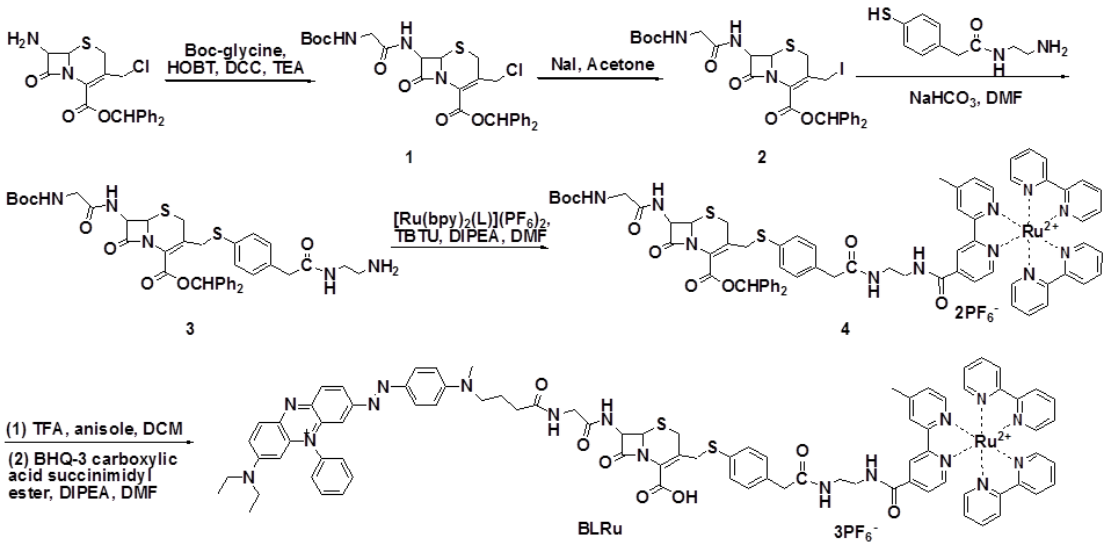

Scheme 3.1 Synthesis of BLRu.

Compound 1. 7-Amino-3-chloromethyl-3-cephem-4-carboxylic acid diphenylmethyl ester hydro-chloride (400 mg, 0.89 mmol) was added in a mixed solvent of acetonitrile and dioxane (1:1). Then TEA (140 ul, 1.00 mmol) was added, followed by addition of N-Boc-glycine (174 mg, 1.0 mmol), HOBt (270 mg, 2.0 mmol) and DCC (240 mg, 1.2 mmol). The mixture was stirred for 16 hrs and concentrated. The residue was purified by column chromatography on silica gel to give 420 mg of white solid. Yield: 82.5%. ^{1}HNMR (400 MHz, $CDCl_3$) δ (ppm): 7.27-7.46 (m, 10H), 7.00 (s, 1H), 5.90 (dd, J = 5.04 Hz, 9.26 Hz, 1H), 5.03 (d, J = 5.04 Hz, 1H), 4.42 (d, J = 5.00 Hz, 2H), 3.80-3.95 (m, 2H), 3.66 (d, J = 18.32 Hz, 1H), 3.52 (d, J = 18.32 Hz, 1H), 1.48 (s, 9H); MS (ESI) m/z: 593.97, calculated for $[M+Na]^+$: 594.14.

Compound 2. Sodium iodide (60 mg, 0.40 mmol) was added to a solution of compound **1** (25 mg, 0.044 mmol) in 10 ml acetone and the mixture was stirred for 1 hr. After concentration, the residue was dissolved in EA, washed, dried over Na_2SO_4 and directly used without purification.

Compound 3. Sodium bicarbonate (11 mg, 0.135 mmol) was added to a solution of compound **2** in 0.4 ml of DMF. Then a solution of *N*-(2-aminoethyl)-2-(4-mercapto-phenyl)acetamide (21 mg, 0.1 mmol) in 0.1 ml of DMF was added by dropwise under nitrogen atmosphere. The reaction mixture was stirred for 2 hrs and purified by reverse-phase HPLC to collect 13 mg of white solid. Yield: 39.7%. ^{1}HNMR (400 MHz, MeOH-d4) δ (ppm): 7.25-7.44 (m, 10H), 7.14(dd, *J* = 8.24 Hz, 16.04 Hz, 4H), 6.77 (s, 1H), 5.68 (d, *J* = 5.04 Hz, 1H), 5.01 (d, *J* = 4.60 Hz, 1H), 4.12 (d, *J* = 13.28 Hz, 1H), 3.87 (d, *J* = 13.28 Hz, 1H), 3.70-3.80 (m, 4H), 3.40-3.61 (m, 6H), 1.45 (s, 9H); MS (ESI) m/z: 746.10, calculated for $[M+H]^{+}$: 746.26.

Compound 4. $[Ru(bpy)_2(L)](PF_6)_2$ (L = 4'-methyl-2, 2'-bipyridine-4-carboxylic acid) (13 mg, 0.014 mmol) and compound **3** (10 mg, 0.013 mmol) were dissolved in 0.5 ml of DMF, followed by addition of TBTU (21 mg, 0.065 mmol) and DIPEA (5 μl, 0.028 mmol). The mixture was stirred for 5 hrs and purified by reverse-phase HPLC to afford 12 mg yellow solid. Yield: 56.2%. ^{1}HNMR (400 MHz, Acetone-d6) δ (ppm): 10.10 (m, 1H), 9.48 (d, *J* = 16.92 Hz, 1H), 9.00 (d, *J* = 13.72 Hz, 1H), 8.83-8.88 (m, 4H), 8.61 (m, 1H), 8.16-8.25 (m, 4H), 8.08-8.13 (m, 2H), 8.01-8.04 (m, 3H), 7.90 (m, 1H), 7.85 (dd, *J* = 3.44 Hz, 5.72 Hz, 1H), 7.51-7.61 (m, 6H), 7.25-7.43 (m, 8H), 7.20 (t, *J* = 7.80 Hz, 2H), 7.08 (d, *J* = 8.24 Hz, 1H), 7.02 (d, *J* = 8.24 Hz, 1H), 6.82 (d, *J* = 2.76 Hz, 1H), 6.38 (br, 1H), 5.81 (m, 1H), 5.09 (t, *J* = 4.12 Hz, 1H), 3.85-4.06 (m, 4H), 3.41-3.68 (m, 8H), 2.58 (d, *J* = 4.12 Hz, 3H), 1.42 (s, 9H); MS (ESI) m/z: 677.60, calculated for $[M-2PF_6]^{2+}$: 677.68.

Compound BLRu. 300 ul of TFA and 100 ul of anisole were added to a mixture of

compound **4** (4 mg, 0.0024 mmol) in 1 ml of DCM and the mixture was stirred at room temperature for 1 hr. The solvent was removed at reduced pressure and the residue was dissolved in 300 μl DMF, followed by addition of BHQ-3 carboxylic acid succinimidyl ester (2.3 mg, 0.0029 mmol) and DIPEA (2.1 μl, 0.012 mmol). The mixture was stirred for 3 hrs and purified by reverse-phase HPLC to give 1.7 mg of dark blue product after lyophilization. Yield: 34.3%. ^{1}HNMR (400 MHz, DMSO-d6) δ (ppm): 9.14 (m, 1H), 9.12 (s, 1H), 8.84 (m, 6H), 8.41 (d, J = 9.16 Hz, 1H), 8.30 (t, J = 5.72 Hz, 1H), 8.13-8.21 (m, 7H), 8.00 (dd, J = 9.60 Hz, 2.28 Hz, 1H), 7.86-7.95 (m, 4H), 7.77 (m, 6H), 7.72 (m, 3H), 7.49-7.58 (m, 5H), 7.40 (d, J = 5.96 Hz, 1H), 7.10-7.30 (m, 6H), 6.87 (d, J = 9.16 Hz, 2H), 5.70 (d, J = 2.32 Hz, 1H), 5.65 (dd, J = 8.24 Hz, 4.82 Hz, 1H), 5.06 (m, 1H), 4.09 (m, 1H), 3.92 (m, 1H), 3.81-3.87 (m, 2H), 3.38 (s, 3H), 3.25 (m, 2H), 3.09 (s, 3H), 2.54 (s, 3H), 2.21 (t, J = 6.88 Hz, 2H), 1.79 (m, 2H), 1.23 (m, 4H), 0.98 (m, 3H); MS (ESI) m/z: 539.75, calculated for $[M\text{-}3PF_6]^{3+}$: 539.50.

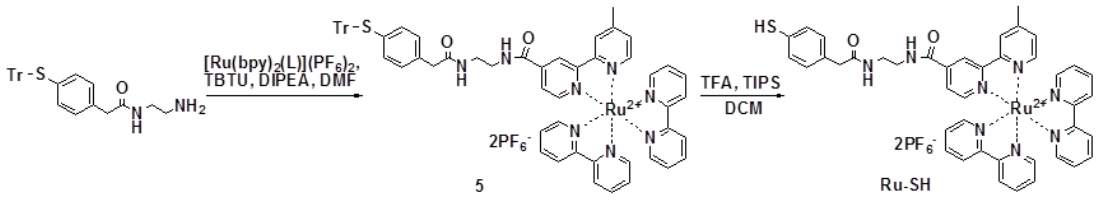

Scheme 3.2 Synthesis of enzyme cleavage product Ru-SH.

Compound 5. *N*-(2-aminoethyl)-2-(4-tritylmercaptophenyl)acetamide (8.6 mg, 0.019 mmol) and $[Ru(bpy)_2(L)](PF_6)_2$ (12 mg, 0.013 mmol) were dissolved in 0.5 ml of DMF, followed by addition of TBTU (21 mg, 0.065 mmol) and DIPEA (11 μl, 0.065 mmol). The reaction mixture was stirred overnight and purified by reverse-phase HPLC to

give 8 mg red powder. Yield: 45.5%. ^{1}HNMR (400 MHz, Acetone-d6) δ (ppm): 10.06 (br, 1H), 9.43 (s, 1H), 8.97 (s, 1H), 8.81-8.88 (m, 4H), 8.50 (br, 1H), 8.16-8.25 (m, 4H), 8.03-8.13 (m, 5H), 7.91 (d, *J* = 5.52 Hz, 1H), 7.88 (d, *J* = 5.96 Hz, 1H), 7.52-7.61 (m, 4H), 7.44 (d, *J* = 5.52 Hz, 1H), 7.31-7.34 (m, 6H), 7.19-7.26 (m, 9H), 7.02 (d, *J* = 8.24 Hz, 2H), 6.76 (d, *J* = 8.24 Hz, 2H), 3.55 (m, 2H), 3.31-3.37 (m, 4H), 2.58 (s, 3H); MS (ESI) m/z: 531.73, calculated for $[M-2PF_6]^{2+}$: 531.15.

Ru-SH. 200 μl TFA and 50 μl TIPS were added to a cooled mixture of compound **5** (8 mg, 0.006 mmol) in 0.5 ml DCM. The mixture was stirred at this temperature for 1h and the solvent was removed at reduced pressure. The residue was purified by reverse-phase HPLC to give 4 mg red powder. Yield: 60.1%. ^{1}HNMR (400 MHz, Acetone-d6) δ (ppm): 10.10 (br, 1H), 9.51 (s, 1H), 9.02 (s, 1H), 8.89 (m, 4H), 8.72 (br, 1H), 8.15-8.24 (m, 4H), 8.03-8.11 (m, 5H), 7.88 (m, 1H), 7.85 (d, *J* = 5.96 Hz, 1H), 7.52-7.61 (m, 4H), 7.40 (d, *J* = 4.56 Hz, 1H), 7.28 (d, *J* = 8.24 Hz, 2H), 7.16 (dd, *J* = 1.84 Hz, 8.24 Hz, 2H), 3.55 (m, 2H), 3.47 (s, 2H), 3.36 (m, 2H), 2.54 (s, 3H); MS (ESI) m/z: 409.99, calculated for $[M-2PF_6]^{2+}$: 410.10.

3.2.2 Enzyme activation

Luminescence measurement. BLRu was dissolved in DMSO to a concentration of 5 mM. The emission spectra were recorded with 450 nm excitation in PBS (pH=7.2).

Singlet oxygen detection. Generation of singlet oxygen species was determined by a $^{1}O_2$ trap, 9,10-anthracenediyl-bis(methylene) dimalonic acid (ABDA).[22] BLRu (5 μM) was mixed with ABDA (30 μM) in PBS buffer and the mixture was irradiated with white light (400-900 nm). Destruction of ABDA was measured from the fluorescence

decrease at 431 nm with 380 nm excitation. The same sample without light irradiation was used as control.

HPLC measurement. BLRu (50 μM) was incubated with TEM-1 Bla in PBS (pH 7.2) at 37 ˚C for 2 h. Then the mixture was subjected to HPLC analysis and the retention time of the released product was compared with that of the synthesized Ru-SH.

Partition coefficient. The *n*-octanol/water partition coefficient was determined as follows. The reagent was dissolved in the premixed *n*-octanol and water (1:1) and shaken for 2 h to achieve the partition equilibrium. Then the mixture was centrifuged (2000 rpm, 10 min) to separate the two phases. After separation, the absorbance of the each phase was determined, from which the concentration was calculated from the calibration curve.

3.2.3 Bacterial imaging and antimicrobial study

Material. Several strains have been used for imaging and photosensitization study, including antibiotic susceptible *S. aureus* (ATCC 29213), antibiotic resistant *B. cereus* (ATCC 13061) and clinically isolated methicillin-resistant *S. aureus* (MRSA, ATCC BAA39 and ATCC BAA44). The penicillin susceptible *E. coli* DH5α (ATCC 53868) without Bla production was used as the negative control. Single colonies of bacterial strains on solid Luria-Bertani (LB) plates were transferred to 5 ml of liquid LB culture medium and grown at 37 ˚C to an OD600 of 0.5. Bacterial cells were harvested by centrifuging and washed with PBS.

Bacterial susceptibility to BLRu and general antibiotics (MIC). The bacterial culture of a single colony was washed and resuspended in PBS buffer to 10^7 CFU/ml.

A 10 μl bacterial solution was added to 1 ml LB solution containing penicillin G, amoxicillin (from 0.5 mg/l to 1024 mg/l) or BLRu (from 0.5 μM to 120 μM) with the final bacteria concentration of 10^5 CFU/ml. The cultures were shaken at 37 ˚C for 24 h and the bacterial growth was determined with naked eye. The reported MIC was the lowest concentration of compound that inhibited cell growth. Each measurement was performed in triplicate.

Detection of Bla in antibiotic resistant strains. The bacterial suspensions (10^6 to 2×10^8 CFU/ml) were lysed in 1 ml of PBS by sonication with a Vibra-Cell Sonics (3 × 10 min), pulsed at 70% max. These bacterial lysates were incubated with BLRu (10 μM) at 37 ˚C for 3h in the dark, then centrifuged to isolate the supernatant for luminescence measurement. All the tests were performed in triplicate.

Imaging of Bla activity in bacterial strains. The bacterial suspensions were incubated with BLRu (10 μM) in the dark for 3 h at 37 ˚C. After washing with PBS, the bacterial cells were spotted on polylysine pretreated glass slides and immobilized by the coverslips. Cell imaging tests were conducted with a Nikon Eclipse TE2000 Confocal Microscope with 488 nm excitation.

Photodynamic antimicrobial chemotherapy. The photodynamic treatment was performed according to the methods previously described.[21] The bacterial suspensions were incubated with different concentrations of BLRu or $Ru(bpy)_3$ in the dark for 3 h at 37 ˚C, then irradiated with white light (400-900 nm) at light doses from 0 to 84 J/cm^2. After irradiation, the bacterial cells were serially diluted in PBS and a 20 μl portion of the diluted mixture was spread on the solid LB agar plate and incubated for

20 hr at 37 ˚C. The formed colonies were counted by the naked eye and divided by that of reference sample with neither probe incubation nor light irradiation to determine the survival fraction.

Cellular uptake of BLRu probe. The uptake study was performed according to the methods previously described.[23] Antibiotic susceptible *S. aureus* (10^8 CFU/ml, 1 ml) was incubated with BLRu or $Ru(bpy)_3$ (10 μM) in PBS buffer at 37˚C for 3h in the dark. After washing with PBS, the bacterial cells were harvested and lysed in 10% SDS aqueous solution overnight at room temperature. The lysates were filtered through a 0.2 μm membrane and recorded the absorbance at 450 nm. The probe concentration was determined according to the calibration curve which was prepared from different concentrations of BLRu or $Ru(bpy)_3$ in 10% SDS solution. All the tests were performed in triplicate.

3.3 Results and discussion

3.3.1 Enzyme activation of Ru(II) probe

Enzyme cleavage of BLRu probe was observed from the 8-fold luminescence enhancement at 645 nm after incubation with TEM-1 Bla at 37˚C for 2 h (Figure 3.3A), which demonstrated the disruption of FRET quenching status by effective enzyme hydrolysis and consequent release of Ru(II) complex. Meanwhile, $^1O_2$ production could also be quenched by the connected BHQ3 moiety through energy transfer or scavenging of the generated $^1O_2$ species.[24] Upon Bla hydrolysis, there was an obvious increase in $^1O_2$ productivity determined by ABDA assay (Figure 3.3B). This recovery of $^1O_2$ production was not complete, probably because of slow enzyme reaction or

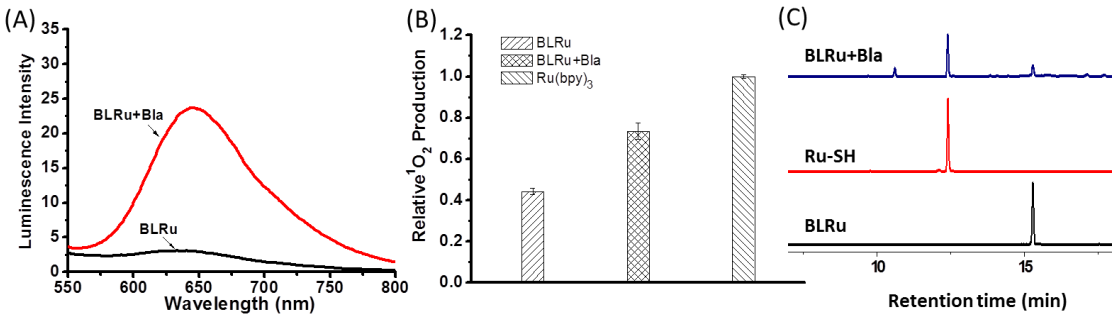

Figure 3.3 (A) β-lactamase activated luminescence emission of BLRu (10 μM). Ex = 450 nm. (B) Singlet oxygen productivity of BLRu (5 μM) before and after enzyme reaction. (C) HPLC analysis of BLRu enzymatic hydrolysis at 450 nm.

consumption of generated $^1O_2$ by the thiol group in the released Ru(II)-containing fragment.[25] To better understand the reaction, the hydrolysis product of BLRu was examined by HPLC analysis, which proved the formation of the proposed enzyme cleavage compound Ru-SH (Figure 3.3C).

Further analysis of BLRu enzyme reaction determined the catalytic constant (k_{cat}) of 16.5 ± 1.1 min^{-1} and Michaelis constant (K_m) of 35.5 ± 2.7 μM (Figure 3.4A). This BLRu probe was also quite stable in PBS with the rate constant of spontaneous

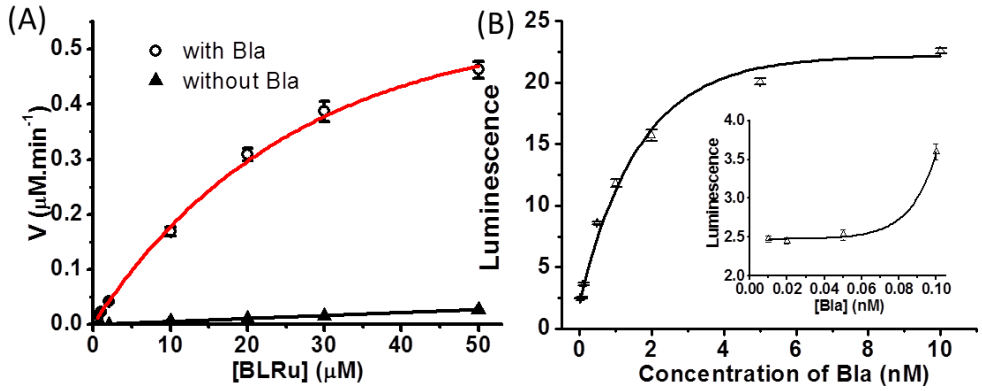

Figure 3.4 (A) Enzyme kinetics of TEM-1 β-lactamase (50 nM) with BLRu at 37˚C. (B) Dependence of BLRu luminescence emission in enzyme concentration. The inset shows the data between 0.01 nM to 0.1 nM.

hydrolysis at 5.4×10^{-4} min^{-1}, thus provided reliable enzyme analysis with detection limit of Bla as low as 0.085 nM (Figure 3.4B).

3.3.2 Bacterial imaging and antimicrobial activity

To detect the endogenous Bla production in resistant strains, the bacterial cells were lysed and incubated with BLRu (10 μM). There was obvious emission enhancement in the antibiotic resistant *B. cereus* and two MRSA strains (ATCC BAA39 and BAA44), while the lysates of antibiotic susceptible *E. coli* and *S. aureus* could not cleave BLRu even at high cell concentrations (Figure 3.5).

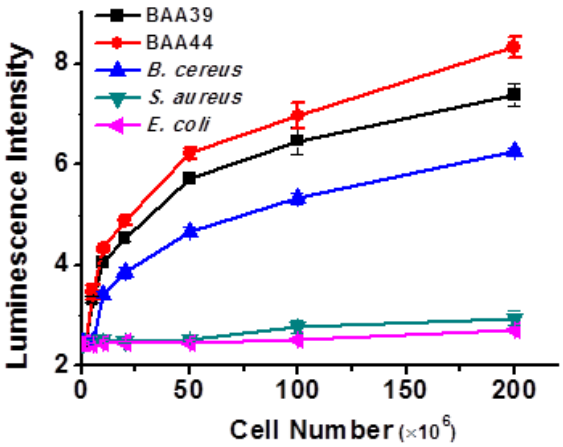

Figure 3.5 BLRu hydrolysis in cell lysates of different bacterial strains.

Encouraged by this result, we investigated the cellular imaging of the resistant strains using a confocal microscope with 488 nm excitation. As shown in Figure 3.6, after incubation of BLRu substrate with the living bacterial cells, strong luminescent signal was observed inside the drug resistant strains including *B. cereus* and two MRSAs. In contrast, the emission was very weak in antibiotic susceptible *S. aureus* and not detectable in the control of *E. coli* DH5α without obvious β-lactamase

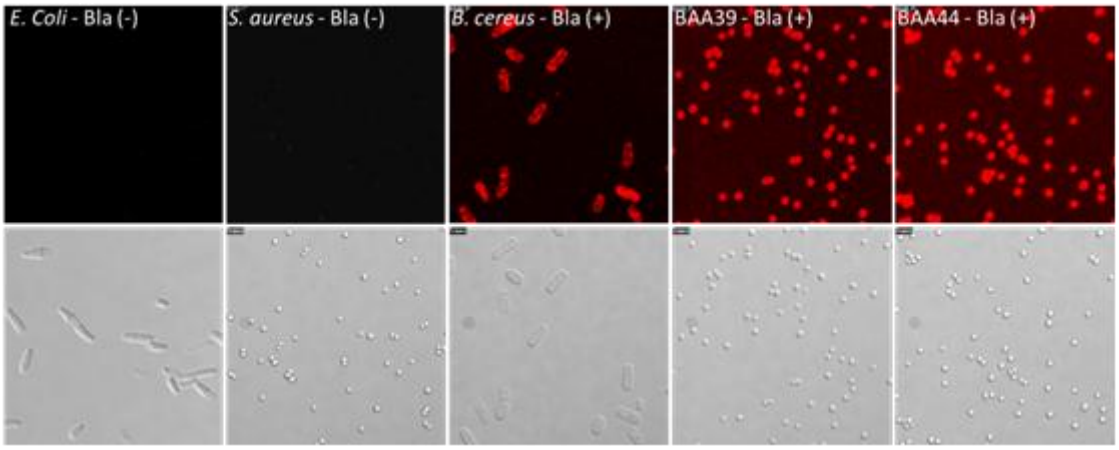

Figure 3.6 Confocal microscopic of fluorescent (top) and differential interference contrast (bottom) images of bacteria incubated with BLRu (10 μM).

production. These results exhibited similar trends of Bla activities as observed in the sonicated bacterial lysates, clearly demonstrated the native capability of BLRu probe to recognize endogenous Bla production in resistant strains.

Photokilling of the antibiotic-resistant strains was investigated by a traditional surface plating method. The resistant *B. cereus* and two clinically isolated MRSA strains were incubated with BLRu for 3h, followed by irradiation with 70 mW/cm^2 white light and spread on LB agar plate for growth. The number of formed colony-forming units (CFU) was divided by that of bacterial samples with neither PS treatment nor irradiation, from which survival fraction was determined. As shown in Figure 3.7A, BLRu displayed effective photosensitization toward the resistant bacteria, where 1 μM of BLRu could lead to over 80% lethality to the MRSA strains after 20 min irradiation (84 J/cm^2). With higher BLRu concentration, the killing efficacy was significantly improved with the bacterial survival decreased by 3 orders of magnitude. At lower light dose of 21 J/cm^2, a relative higher concentration of BLRu (5 μM) was

required for efficient photosensitization of MRSA strains (Figure 3.7B). These results achieved our expectation of killing the resistant bacteria by photodynamic antimicrobial chemotherapy (PACT).

Meanwhile, the PACT studies also exhibited the photoinactivation of antibiotic susceptible *S. aureus* by the partially quenched $^1O_2$ production (Figure 3.7), which was less effective than the resistant *B. cereus* and MRSA strains mostly due to the limited Bla hydrolysis and $^1O_2$ production in this strain. This result was also consistent with the bacterial fluorescent imaging.

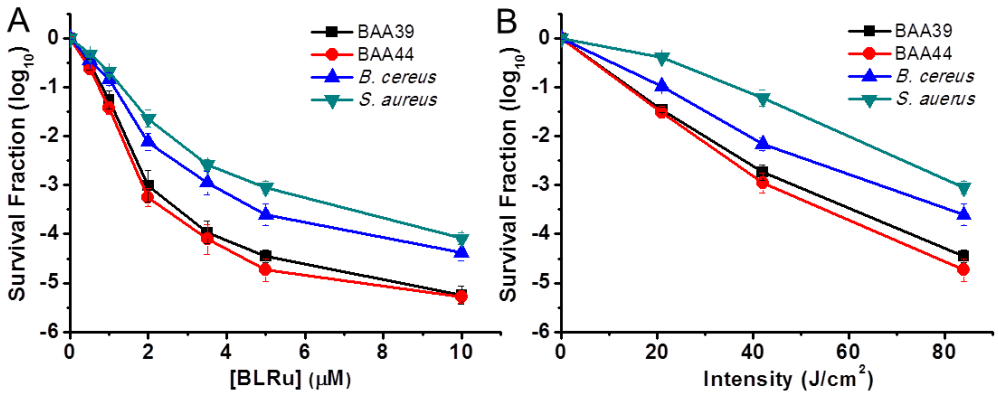

Figure 3.7 Photodynamic inactivation of various bacteria at (A) different BLRu concentration with light intensity of 84 J/cm^2 and (B) different light irradiation with BLRu (5 μM).

This antimicrobial profile was further studied for better understanding the mechanism of bacterial inactivation. First, as BLRu molecule was a derivative of β-lactam antibiotic, it may potentially inhibit bacteria growth as a β-lactam drug and interfere with the photodynamic therapy. Hence the susceptibility of bacterial strains to BLRu probe was examined and compared to normal antibiotics. As shown in Table 3.2, all the tested strains exhibited potent activities to resist BLRu substrate, indicated that

BLRu did not possess native antimicrobial activity and the observed bacterial lethality after irradiation could be mostly attributed to the efficient photosensitization.

Compounds	*E. coli*	*S. aureus*	*B. cereus*	BAA39	BAA44
BLRu	>120 μM (246 mg/l)	≥ 80 μM (164 mg/l)	>120 μM (246 mg/l)	>120 μM (246 mg/l)	>120 μM (246 mg/l)
Penicillin G	48 μM (16 mg/l)	3 μM (1 mg/l)	3.06 mM (1024 mg/l)	1.53 mM (512 mg/l)	1.53 mM (512 mg/l)
Amoxicillin	11 μM (4 mg/l)	5 μM (2 mg/l)	1.40 mM (512 mg/l)	1.40 mM (512 mg/l)	1.40 mM (512 mg/l)

Table 3.2 Antibacterial activities (MICs) of BLRu, penicillin G and amoxicillin.

Second, the cellular localization of ruthenium complex was studied by confocal laser scanning to understand the biological targets of photosensitization. As shown in Figure 3.8, scanning of *B. cereus* at various depths exhibited the almost even distribution of released ruthenium complex throughout the cells, suggesting the possibility that both cellular membranes and DNA molecules were subjected to photosensitization.

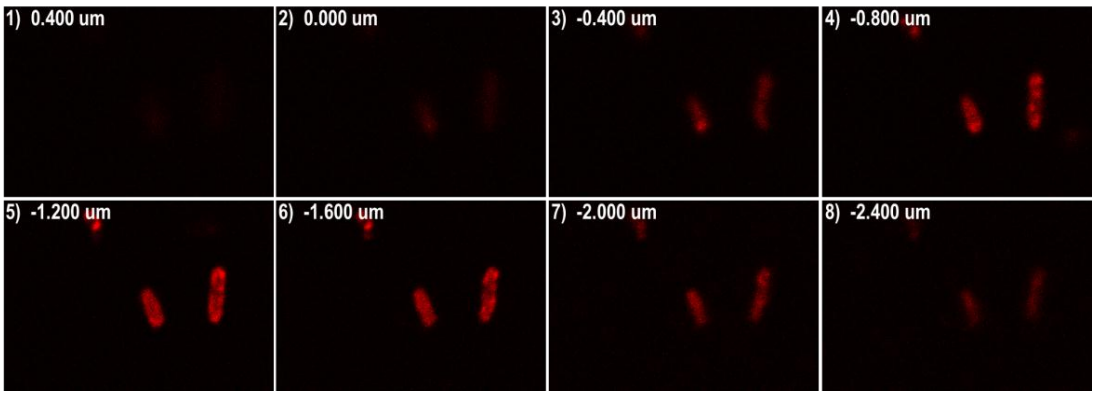

Figure 3.8 Confocal laser scanning of BLRu (10 μM) distribution in *B. cereus* at various depths.

Moreover, the luminescent imaging inside living cells also indicated effective membrane permeability of the BLRu probe and trapping of the released product in bacterial cells. In fact, although good at $^1O_2$ production, $Ru(bpy)_3Cl_2$ complexes were not highly efficient in antibacterial photodynamic therapy.[26] Our experiment also demonstrated much lower lethality of the unmodified $Ru(bpy)_3Cl_2$ to bacterial strains than that of BLRu probe (Figure 3.9A). Due to the short lifetime and limited diffusion distance of $^1O_2$,[12] the significant enhancement of BLRu photosensitization was mostly attributed to its improved cellular uptake, which was clearly proved in the fluorescent imaging of antibiotic resistant bacteria.

In addition, for quantitative analysis, *S. aureus* cells were incubated with ruthenium complexes and lysed with 10% SDS. After filteration, the lysates were collected and the probe concentration was determined from UV-Vis spectrum. The cellular uptake was calculated from the calibration curve, that was 28% for BLRu and 2% for $Ru(bpy)_3Cl_2$ (Figure 3.9B). Further hydrophobicity analysis determined the *n*-octanol/water partition coefficient of BLRu to be 0.294, but the solubility of $Ru(bpy)_3Cl_2$ and released Ru-SH in *n*-octanol was very low.[13] Thus, the BLRu probe with an appropriate hydrophobic/hydrophilic balance could penetrate into cell wall, with the released hydrophilic Ru-SH molecules preferentially trapped inside the cells to perform cellular imaging and photosensitization.

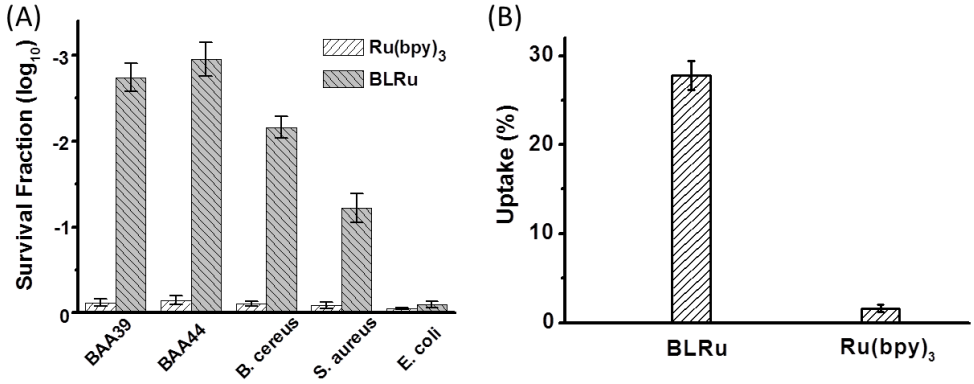

Figure 3.9 (A) Comparison of bacteria photoinactivation in the presence of unmodified $Ru(bpy)_3Cl_2$ (5 μM) or BLRu (5 μM). Light dose: 42 J/cm^2 (B) Comparison of cellular uptake of ruthenium complexes in *S. aureus*.

It should also be mentioned that the photoinactivation of antibiotic susceptible Gram negative *E. coli* strain was difficult because of no Bla expression and the presence of different outer membrane architecture in the Gram negative species as the permeability barrier, thus requires higher concentration of photosensitizers to perform effective PACT (Figure 3.10).

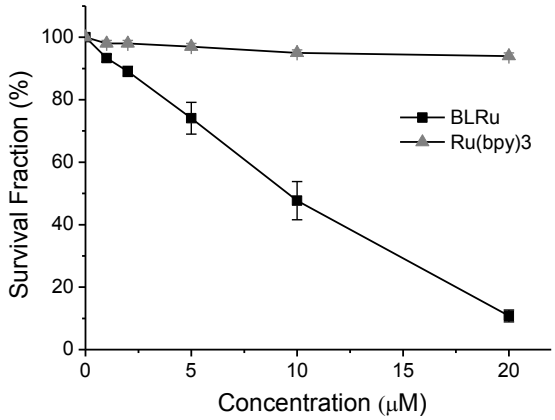

Figure 3.10 Photoinactivation of antibiotic susceptible *E. coli* at different BLRu and $Ru(bpy)_3$ concentration. Light dose: 42 J/cm^2.

3.4 Conclusion

In this chapter, we have presented an easy and effective approach for cellular imaging and photoinactivation of antibiotic resistant bacteria based on a FRET-prequenched ruthenium(II) cephalosporin probe. Confocal fluorescent microscope and photodynamic antimicrobial chemotherapy studies have demonstrated that the luminescent ruthenium (II) cephalosporin derivative could be selectively activated by endogenous β-lactamases, thus provided an intracellular imaging and antibacterial therapy against drug resistant bacterial pathogens.

3.5 Reference

(1) Bugg, T. D. H.; Braddick, D.; Dowson, C. G.; Roper, D. I. *Trends Biotechnol.* **2011**, *29*, 167.

(2) Fisher, J. F.; Meroueh, S. O.; Mobashery, S. *Chem. Rev.* **2005**, *105*, 395.

(3) Sanders, C. C.; Sanders, W. E. *Clin. Infect. Dis.* **1992**, *15*, 824.

(4) Maiti, S. N.; Phillips, O. A.; Micetich, R. G.; Livermore, D. M. *Curr. Med. Chem.* **1998**, *5*, 441.

(5) Xie, H. X.; Mire, J.; Kong, Y.; Chang, M. H.; Hassounah, H. A.; Thornton, C. N.; Sacchettini, J. C.; Cirillo, J. D.; Rao, J. H. *Nat. Chem.* **2012**, *4*, 802.

(6) Kong, Y.; Yao, H. Q.; Ren, H. J.; Subbian, S.; Cirillo, S. L. G.; Sacchettini, J. C.; Rao, J. H.; Cirillo, J. D. *Proc. Nat. Acad. Sci. USA* **2010**, *107*, 12239.

(7) Juris, A.; Balzani, V.; Barigelletti, F.; Campagna, S.; Belser, P.; Vonzelewsky, A. *Coord. Chem. Rev.* **1988**, *84*, 85.

(8) Mei, H. Y.; Barton, J. K. *Proc. Natl. Acad. Sci. U.S.A.* **1988**, *85*, 1339.

(9) Lee, J. Y.; Udugamasooriya, D. G.; Lim, H. S.; Kodadek, T. *Nat. Chem. Biol.* **2010**, *6*, 258.

(10) Maisch, T. *Laser. Med. Sci.* **2007**, *22*, 83.

(11) Maisch, T. *Mini-Rev. Med. Chem.* **2009**, *9*, 974.

(12) Maisch, T.; Baier, J.; Franz, B.; Maier, M.; Landthaler, M.; Szeimies, R. M.; Baumler, W. *Proc. Natl. Acad. Sci. U.S.A.* **2007**, *104*, 7223.

(13) Lei, W. H.; Zhou, Q. X.; Jiang, G. Y.; Zhang, B. W.; Wang, X. S. *Photochem. Photobiol. Sci.* **2011**

(14) Cassidy, C. M.; Tunney, M. M.; McCarron, P. A.; Donnelly, R. F. *J. Photoch. Photobio. B* **2009**, *95*, 71.

(15) Gad, F.; Zahra, T.; Francis, K. P.; Hasan, T.; Hamblin, M. R. *Photoch. Photobio. Sci.* **2004**, *3*, 451.

(16) Tome, J. P. C.; Neves, M.; Tomes, A. C.; Cavaleiro, J. A. S.; Soncin, M.; Magaraggia, M.; Ferro, S.; Jori, G. *J. Med. Chem.* **2004**, *47*, 6649.

(17) Embleton, M. L.; Nair, S. P.; Cookson, B. D.; Wilson, M. *J. Antimicrob. Chemoth.* **2002**, *50*, 857.

(18) Suci, P. A.; Varpness, Z.; Gillitzer, E.; Douglas, T.; Young, M. *Langmuir* **2007**, *23*, 12280.

(19) Embleton, M. L.; Nair, S. P.; Heywood, W.; Menon, D. C.; Cookson, B. D.; Wilson, M. *Antimicrob. Agents Chemother.* **2005**, *49*, 3690.

(20) Strassert, C. A.; Otter, M.; Albuquerque, R. Q.; Hone, A.; Vida, Y.; Maier, B.; De Cola, L. *Angew. Chem., Int. Ed.* **2009**, *48*, 7928.

(21) Xing, C. F.; Xu, Q. L.; Tang, H. W.; Liu, L. B.; Wang, S. *J. Am. Chem. Soc.* **2009**, *131*, 13117.

(22) Qian, H. S.; Guo, H. C.; Ho, P. C. L.; Mahendran, R.; Zhang, Y. *Small* **2009**, *5*, 2285.

(23) Frimannsson, D. O.; Grossi, M.; Murtagh, J.; Paradisi, F.; O'Shea, D. F. *J. Med. Chem.* **2010**, *53*, 7337.

(24) Lovell, J. F.; Liu, T. W. B.; Chen, J.; Zheng, G. *Chem. Rev.* **2010**, *110*, 2839.

(25) Devasagayam, T. P. A.; Sundquist, A. R.; Di Mascio, P.; Kaiser, S.; Sies, H. *J. Photoch. Photobio. B* **1991**, *9*, 105.

(26) Donnelly, R. F.; Fletcher, N. C.; McCague, P. J.; Donnelly, J.; McCarron, P. A.; Tunney, M. M. *Lett. Drug Des. Discov.* **2007**, *4*, 175.

Chapter 4

Activity-based Probes for Detection and Identification of Antibiotic Resistance Proteins

4.1 Introduction

Antibiotic resistance is associated with a number of bacterial proteins as defensive mechanisms, such as destroying the drugs, altering the drug targets or preventing the drug accumulation. Among them, production of β-lactamases is a main mechanism to render bacteria resistance. Blas have different isozymes. They share structural and biochemical similarities; however, they still exhibit differences in biochemical properties such as substrate spectrum and inhibitor specificity, which are important for antimicrobial studies and clinical applications. Construction of the imaging probes for bacterial β-lactamase detection is usually based on the enzyme-substrate interactions. Another strategy for probe design is through the activity-based protein profiling (see Section 1.3.1), which uses inhibitor for specific enzyme labeling and identification. In order to better understand β-lactamase activities in their natural habitat, and more importantly to facilitate the rational design of enzyme inhibitors with potential biomedical or bioimaging applications, an ongoing study aims to develop probes for detection and identification of the antibiotic resistance proteins with this strategy.

4.1.1 β-Lactamases in antibiotic resistance

β-Lactam drugs stop bacteria growth by inactivating penicillin binding proteins that are required for the polymerization and cross-linking of peptidoglycan in cell wall biosynthesis.[1,2] However, the misuse and overuse has fostered many resistant strains,

which developed various mechanisms for surviving, such as production of β-lactamases (Blas) to destroy β-lactam drugs, alteration of drug targets and prevention of drug access through permeation barrier or efflux pump.[3-5] These events exist in microorganisms long before the clinical use of antibiotics, but are selectively developed under the pressure of high-concentration drugs through strain selection and plasmid transfer.

Among them, production of β-lactamases can be found in many pathogenic species including those most seriously infectious stains of *Mycobacterium tuberculosis* and *Staphylococcus aureus*. Up to now, there are four classes of β-lactamases to render bacteria resistance according to the difference in protein structure (Ambler class)[6] or substrate preference (Bush class),[7] where there is a good correspondence between these two classifications (Table 4.1). The Bush classification is based on phenotypic studies, which faces the problem of complexity in substrate specificity and inhibitor susceptibility caused by protein mutations. The Ambler classification reflects the fundamental relationship, in which classes A, C, and D β-lactamases are serine enzymes while class B β-lactamases are metalloenzymes.[8] In general, the serine enzymes deactivate the β-lactam drugs through the acylation and deacylation process (see Section 2.1.4). In contrast, class B β-lactamases use Zn^{2+} to coordinate a water molecule, of which the hydroxyl group is activated to hydrolyze the amide bond of β-lactam ring.

Ambler class	Bush-Jacoby-Medeiros class	Preferred substrates	Representative enzyme
A (serine penicillinases)	2a	Penicillins	PC1
	2b	Penicillins, narrow-spectrum cephalosporins	TEM-1, TEM-2, SHV-1
	2be	Penicillins, narrow-spectrum and extended-spectrum cephalosporins	SHV-2 to SHV-6, TEM-3 to TEM-26, CTX-Ms
	2br	Penicillins	TEM-30, SHV-72
	2c	Penicillins, carbenicillin	PSE-1
	2e	Extended-spectrum cephalosporins	FEC-1, CepA
	2f	Penicillins, Cephalosporins., carbapenems	KPC-2, SME-1, NMC-A
B (metallo-β-lactamases)	3	Most β-lactams, including carbapenems	IMP-1, VIM-1, CcrA, and BcII (B1); CphA (B2); L1 (B3)
C (cephalospo-rinases)	1	Cephalosporins	AmpC, CMY-2, ACT-1
D (oxacillinases)	2d	Penicillins, cloxacillin	OXA-1, OXA-10
Not classified	4		

Table 4.1 β-lactamase classification schemes.[8]

The ability of bacterial β-lactamases to reduce the drug concentration around the PBPs is dependent on several parameters, including the protein location, enzyme kinetics and quantity. Normally, higher level of bacterial Bla can lead to greater resistance. In these strains, the susceptible drugs are destroyed at different kinetics (Table 4.2).

Enzyme class	Source	Location[a]	Molecular mass (kDa)	pI	Relative k_{cat}						
					Benzylpenicillin	Ampicillin	Cefazolin	Cephaloridine	Cefoxitin	Cefotaxime	Imipenem[c]
C	*E. cloacae*	Chr	39.2	8.4	100	5	21,400	5,000	0.43	0.11	0.02
	C. freundii	Chr	39.9		100	21	16,100	2,260	1	0.05	0.05
	E. coli K-12	Chr	39.6	8.7	100	9	333	289	0.44	0.38	0.02
	S. marcescens	Chr	37	9.5	100	0.6	1,730	1,470	0.02	2.3	0.001
	P. aeruginosa	Chr	34	8.4	100	6	—[b]	145	0.015	0.20	0.03
	ACT-1	P	39.4	9.0	100	1.8	1,020	>455	0.67	0.09	0.02
	MIR-1	P	39.2	8.4	100	3.9	—[b]	1,540	4.6	19.3	0.09
	CMY-1	P	39.9	8.0	100	3.5	2,500	1,190	0.38	0.08	0.02
	CMY-2	P	38.8	9.0	100	3.9	—[b]	1,536	1.64	0.29	0.24
A	TEM-2	P	22.0	5.4	100	95	34	315			
	B. licheniformis	Chr	29.5		100	68	14	29			
D	OXA-29	Chr	28.5	>9	100	164	17			0.26	NH

[a] Chr, chromosomal; P, plasmid; [b] Biphasic kinetics; [c] NH, no hydrolysis detected

Table 4.2 *β*-lactamase physical properties and kinetic behavior to antibiotics.[9]

In Gram negative species, the β-lactamases are largely located in periplasmic space,

although some can also be released extracellularly by leakage.[10] Both class A and class C enzymes are commonly encountered, which are expressed constitutively or inducible at different levels according to the strains and culture conditions. In enzyme structure, the active site of class C Bla, such as AmpC, is similar to that of class A β-lactamases. But the class C Blas have relative higher molecular weight and there is a more open binding site in class C enzyme with greater ability to accommodate side chains, thus the cephalosporins with bulkier side chains are preferred substrates.

On the contrary, the Gram positive pathogens usually produce the β-lactamases extracellularly to destroy drugs, although some Blas can also adhere to the cytoplasmic membranes. For example, the resistance in *Staphylococci* is most commonly caused by β-lactamases, which are class A types and usually surface attached to reduce the external drug level. In another Gram positive pathogenic *Mycobacterium tuberculosis*, which causes the lethal tuberculosis and remains the therapeutic challenge due to the resistance to multiple drugs, the production of class A Bla has also been found.[11,12]

Identification of these enzymes is important to ensure the appropriate therapy by avoiding the clinical misuse of labile drugs and recommending the coadministration of Bla inhibitors.[13] Currently, there are three commercially available β-lactamase inhibitors, including clavulanate, tazobactam and sulbactam (Figure 4.1), which can irreversibly bind the enzyme active site with high affinity. In general, class A enzymes are susceptible to these inhibitors with different turnover number (t_n), which is used to evaluate the efficacy of an inhibitor and defined as the number of inhibitor molecules being consumed before inactivating one enzyme molecule. However, these inhibitors

are generally less effective against the Blas belonging to other classes (Table 4.3). In clinical practice, the coadministration of Bla inhibitors can significantly expand the spectrum of antibiotics to the penicillin resistant strains.[13] Meanwhile, the *in vitro* sensitivity of a bacterial isolate to different antibiotics or antibiotic-Bla inhibitor combinations is also valuable as the establishment of such antibiogram can provide detailed information for further comparison and investigation.

β-Lactamase	Ambler class	Clavulanate			Sulbactam			Tazobactam		
		K_I (μM)	IC_{50} (nM)	t_n	K_I (μM)	IC_{50} (nM)	t_n	K_I (μM)	IC_{50} (nM)	t_n
TEM-1	A	0.1	60	160	1.6	900	10,000	0.01	97	140
SHV-1	A	1	12	60	8.6	12,000	13,000	0.07	150	5
SHV-5	A		20			1,800			80	
PC1	A		30	1		80			27	1
CTX-M-2	A		200			2,100			20	
CcrA	B		>500,000	>500,000		>500,000			400,000	4,000
P99	C		>100,000	>500,000		5,600			8.5	50
CMY-2	C	4,365			101			50		
OXA-1	D		1,800			4,700		380	1400	
OXA-2	D		1,400		0.1	140			10	

Table 4.3 Kinetic behavior of selective Blas to Bla inhibitors.

In addition, the resistance caused by Bla production is also highly considered in the development of synthetic antibiotic drugs. For example, in the third generation β-lactam antibiotics, a bulky group, like 2-amino-4-thiazolyl methoxyimino (ATMO) group (Figure 4.1), has been introduced into cephalosporins (e.g. Cefotaxime) or monobactams (e.g. Aztreonam), which forms an unfavorable steric hindrance in the acyl-enzyme intermediate once interacted with Bla protein and prevents the hydrolysis.

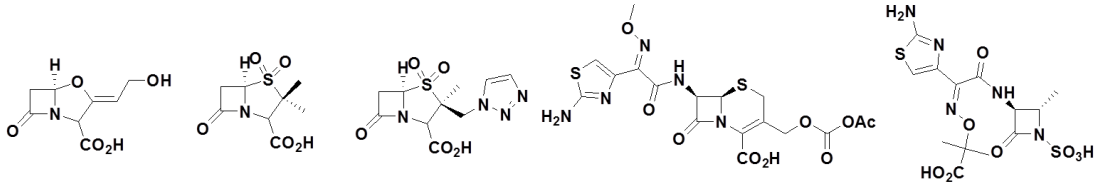

Figure 4.1 Structure of Bla inhibitors and β-lactam antibiotics with steric hindrance.

Thus, knowledge of Bla quantity, distribution and kinetics can contribute to the full understanding of resistance mechanism, also provide valuable antibiogram data to facilitate antimicrobial study.[10,13] To detect and identify these Blas, several methods have been developed with biological or chemical strategies.

4.1.2 Detection and identification method

In microbiological study, the strain's enzyme type is often predicted from its antibiogram when the observed resistance pattern is particular and corresponding to particular β-lactamase. Such interpretive readings can help to ensure the appropriate therapy. However, it is limited in the strains where multiple β-lactamases exist or the antibiogram is poorly established.

Another strategy is utilizing enzyme assays to examine the production of bacterial Bla with resultant chromogenic and/or fluorogenic changes, which are fast, direct and convenient.[14] Such enzyme assays include nitrocefin,[15] CCF2-AM,[16] Fluorocillin™ Green (Invitrogen), nanoparticle based assays,[17,18] etc., which have been successfully used in Bla detection and enzyme inhibitor screening. These probes are designed as Bla substrates with cephalosporin cores. Among them, nitrocefin is more applicable as it can be used as a solution or as disks with characteristic color change from yellow to pink/red upon hydrolysis. With high sensitivity to most β-lactamases, the nitrocefin test has been widely used as a confirmation where the production of Bla in the clinical isolate is suspected.

However, such β-lactamase detection does not provide sufficient information to identify the type of Bla in the isolates. Recently, selective probes have been developed

with the strategy of introducing bulky groups to keep them sensitive to specific Bla in certain pathogenic species but inert to the mostly encountered TEM-1 Bla.[19,20] As these probes are constructed as enzyme substrates with enhanced fluorescent signals, the selectivite detection may still cannot identify the exact type of protein.

Usually, chemical methods for identifying an unknown protein can be achieved by proteomic study, such as activity-based protein profiling (see Section 1.3.1) and peptide mass fingerprinting (PMF).[21] In this method, a protein of interest can be detected by specific probes with labeling events. Further it can be cleaved into smaller peptides, of which the absolute masses are accurately measured and compared to known protein sequences to find the best match. As many frequently encountered Blas have been characterized, it will be relatively easy to confirm the identity of bacterial β-lactamase with this method. However, this approach usually requires an isolated protein as most PMF analyses assume that the cleaved peptides are from a single protein. A sample of protein mixtures will make the analysis much more difficult and cause potential compromise to the results. Recently, several reports utilize the proteomic method to identify the Blas in resistant strains. However, in these studies, the bacterial Bla characterization is dealing with the production of known Bla.[22] In the study of unknown genomic background, the characterization is much more complicated. For example, in a multi-resistant clinical *E. coli* isolate, the mean protein intensity of the proteome is around 1.4E+08, where the protein intensity of Bla is much lower, only at 1.0E+06, and difficult to identify in a mixture.[23]

In this study, we aim to develop a probe for bacterial proteomic study with the

ability to report Bla activity and identify Bla class. The design principle is based on the strategy of activity-based protein profiling with an inhibitor-based probe composed of a targeting group and an analytical handle. The specific bacterial Bla in the proteome can be visualized in gel analysis after labeling, which can be separated for further Mass spectrum identification (Figure 4.2).

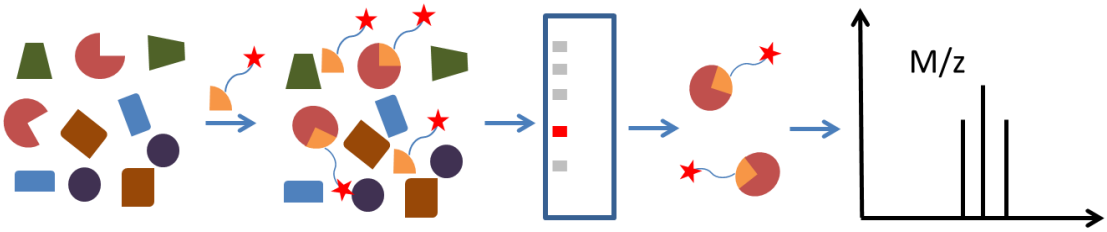

Figure 4.2 Design of activity-based probes for Bla detection and identification.

4.2 Experimental section

4.2.1 Design, synthesis and characterization

In the design of the inhibitor-based probe, we assume that an unfavorable steric hindrance of the acyl-enzyme complex may prevent the deacylation step and trap the enzyme. Such bulky group, like 2-amino-4-thiazolyl methoxyimino (ATMO) group, is common among the third-generation antibiotics with potency to some penicillin resistant strains like *N. gonorrhoeae*. Meanwhile, as the hindrance may be different in various Bla classes, the enzyme inhibition may represent a range of selectivity. In addition, to improve labeling specificity, the sulfide bond in the penicillin structure was oxidized to reduce the binding affinity with penicillin binding proteins.[24]

To examine our hypothesis, we first synthesized compound A and B by connecting ATMO group to the 6-amino of penicillin structure at different oxidation states (Scheme 4.1). Then we synthesized compound C by adding an analytical handle of a

terminal alkyne, which was introduced for fluorescent labeling and identification (Scheme 4.2).

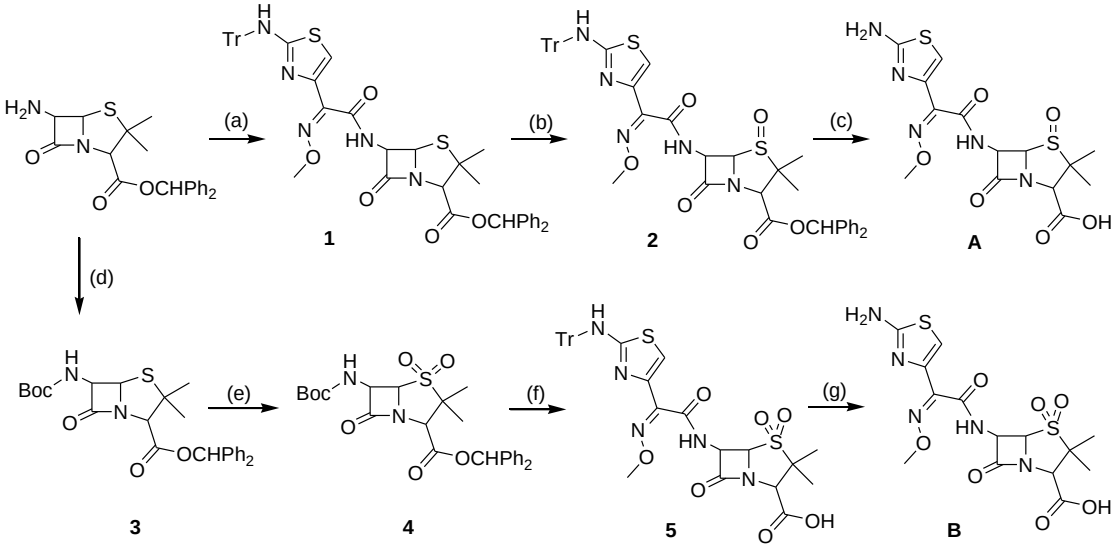

Scheme 4.1 Synthesis of compound A and B. Conditions: (a) Tr-ATMO, HBTU, TEA; (b) m-CPBA; (c) TFA, anisole; (d) $(Boc)_2O$, TEA; (e) $KMnO_4$, AcOH; (f) i) TFA, anisole; ii) Tr-ATMO, $POCl_3$, Py, TEA; (g) TFA, anisole

Compound 1: The diphenylmethyl ester of 6-aminopenicillanic acid (200 mg, 0.52 mmol) was dissolved in 10 ml of DCM. Then 2-triphenylmethylamino-4-thiazolyl methoxyimino acetic acid (Tr-ATMO, 230 mg, 0.52 mmol), HBTU (200 mg, 0.53 mmol) and TEA (100 ul, 0.72 mmol) was added. The mixture was stirred under N_2 atmosphere overnight and concentrated. The residue was purified by column chromatography to give 332 mg of white solid. Yield: 79.1%. ^{1}HNMR (400 MHz, $CDCl_3$) δ (ppm): 7.28-7.38 (m, 26H), 6.94 (s, 1H), 6.88 (d, J = 9.16 Hz, 1H), 6.75 (s, 1H), 5.78 (dd, J = 9.16 Hz, 4.60 Hz, 1H), 5.63 (d, J = 4.60 Hz, 1H), 4.55 (s, 1H), 4.05 (s, 3H), 1.59 (s, 3H), 1.26 (s, 3H); MS (ESI) m/z: calcd for $C_{46}H_{41}N_5O_5S_2$: 807.25; $[M+H]^+$ found: 807.93.

Compound 2: *m*-Chloroperbenzoic acid (62 mg, 85%, 0.30 mmol) was added to a cooled solution of compound **1** (200 mg, 0.25 mmol) in 1 ml of DCM and stirred at 0˚C for 1 hr. Then the mixture was diluted with 40 ml of EA, washed with 10% $NaHCO_3$ and dried over Na_2SO_4. After evaporation, the residue was purified by column chromatography on silica gel to afford 155 mg of white solid. Yield: 75.3%. ^{1}HNMR (400 MHz, $CDCl_3$) δ (ppm): 7.28-7.37 (m, 26H), 6.99 (s, 1H), 6.70 (s, 1H), 6.12 (dd, J = 10.56 Hz, 4.60 Hz, 1H), 5.06 (d, J = 4.60 Hz, 1H), 4.76 (s, 1H), 4.06 (s, 3H), 1.67 (s, 3H), 0.91 (s, 3H); MS (ESI) m/z: calcd for $C_{46}H_{41}N_5O_6S_2$: 823.25; $[M+H]^+$ found: 824.02.

Compound A: To a stirred solution of compound **2** (50 mg, 0.061 mmol) in 300 ul of DCM was added 300 ul of TFA and 150 ul of anisole. The mixture was stirred for 1 hr in ice bath and purified by reverse-phase HPLC to give 13 mg product after lyophilization. Yield: 50.3%. ^{1}HNMR (400 MHz, D_2O) δ (ppm): 7.24 (s, 1H), 6.04 (d, J = 4.56 Hz, 1H), 5.51 (d, J = 4.56 Hz, 1H), 4.62 (s, 1H), 4.10 (s, 3H), 1.73 (s, 3H), 1.35 (s, 3H); MS (ESI) m/z: calcd for $C_{14}H_{17}N_5O_6S_2$: 415.06; $[M+H]^+$ found: 416.20.

Compound 3: The diphenylmethyl ester of 6-aminopenicillanic acid (200 mg, 0.52 mmol) was dissolved in 10 ml of DCM. Then $(Boc)_2O$ (150 ul, 0.65 mmol) and TEA (100 ul, 0.72 mmol) was added. The mixture was stirred for 5 hrs and purified by column chromatography on silica gel to give 223 mg product. Yield: 89.3%. ^{1}HNMR (400 MHz, $CDCl_3$) δ (ppm): 7.31-7.37 (m, 10H), 6.93 (s, 1H), 5.54 (d, J = 4.12 Hz, 1H), 5.47 (m, 1H), 5.25 (m, 1H), 4.51 (s, 1H), 1.62 (s, 3H), 1.45 (s, 9H), 1.26 (s, 3H); MS (ESI) m/z: calcd for $C_{26}H_{30}N_2O_5S$: 482.19; $[M+Na]^+$ found: 505.19.

Compound 4: To a cooled solution of compound **3** (92 mg, 0.19 mmol) in DCM was added acetic acid and $KMnO_4$ (60 mg, 0.38 mmol). The mixture was stirred till the reaction finished. Then the mixture was washed with H_2O_2, and $NaHCO_3$ aqueous solution. After dried, the product was obtained by concentration. Yield: 93.3%. ^{1}HNMR (400 MHz, $CDCl_3$) δ (ppm): 7.31-7.38 (m, 10H), 6.98 (s, 1H), 5.94 (m, 1H), 5.83 (m, 1H), 4.75 (d, J = 4.56 Hz, 1H), 4.57 (s, 1H), 1.52 (s, 3H), 1.45 (s, 9H), 1.08 (s, 3H); MS (ESI) m/z: calcd for $C_{26}H_{30}N_2O_7S$: 514.18; $[M+Na]^+$ found: 537.19.

Compound 5: In a round bottom flask, compound **4** (50 mg, 0.09 mmol) was deprotected with TFA and anisole in DCM. Then the mixture was dried under vacuum for further usage. In another flask, the Tr-ATMO (66 mg, 0.15 mmol) was dissolved in 1 ml of DCM and reacted with $POCl_3$ and pyridine to form acetyl chloride *in situ*. Then this acetyl chloride was added dropwise to the cooled mixture of deprotected compound **4** and 2,6-lutidine in THF. After reacted for 1h, the mixture was diluted with EA, washed with water and acidified with HCl. After evaporation, the residue was recrystallized to give 30 mg crude product, which was used directly without further purification. MS (ESI) m/z: calcd for $C_{33}H_{31}N_5O_7S_2$: 673.17; $[M+H]^+$ found: 673.91.

Compound B: Same procedure as compound **A**. Yield: 60.7%. ^{1}HNMR (400 MHz, D_2O) δ (ppm): 7.14 (s, 1H), 6.01 (d, J = 4.56 Hz, 1H), 5.33 (d, J = 4.56 Hz, 1H), 4.89 (s, 1H), 4.06 (s, 3H), 1.61 (s, 3H), 1.48 (s, 3H); MS (ESI) m/z: calcd for $C_{14}H_{17}N_5O_7S_2$: 431.06; $[M+H]^+$ found: 432.20.

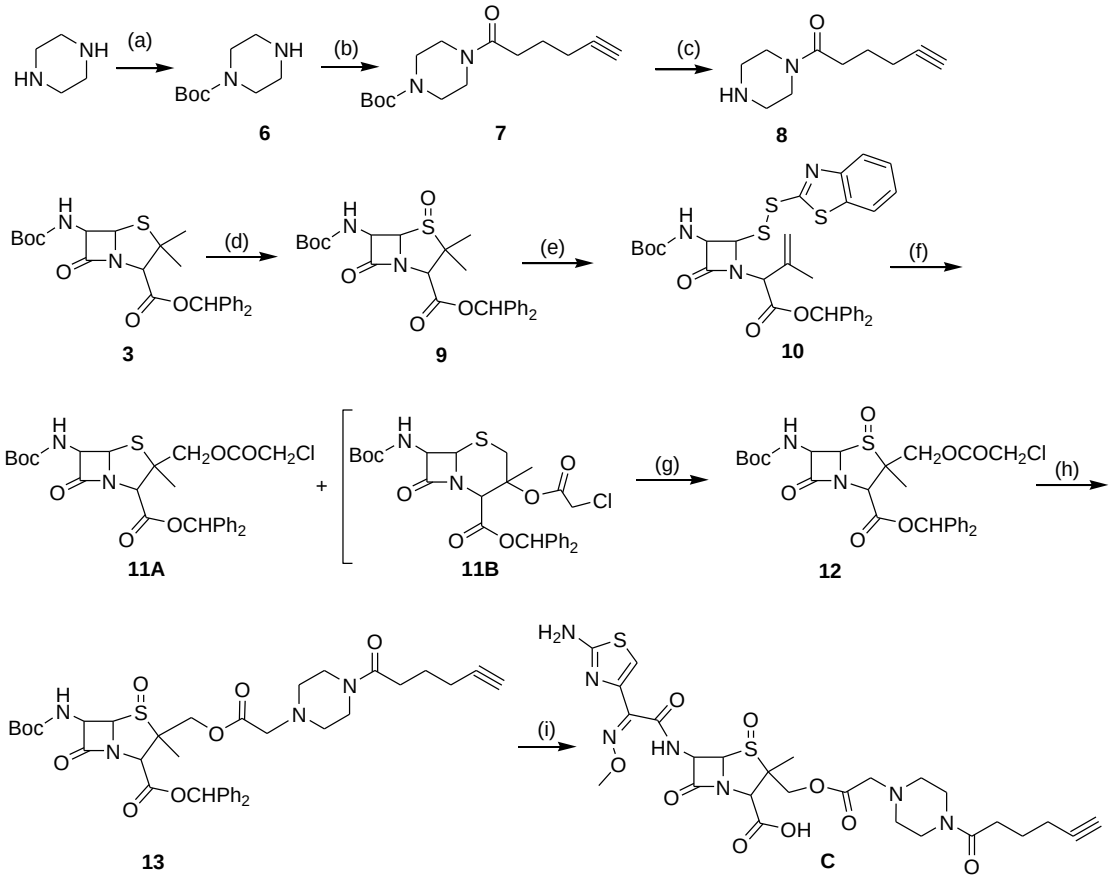

Scheme 4.2 Synthesis of compound C. Conditions: (a) $(Boc)_2O$, DCM; (b) HBTU, 5-hexynoic acid, TEA; (c) TFA, DCM; (d) m-CPBA; (e) 2-mercaptobenzothiazole, toluene; (f) silver acetate, chloroacetic acid; (g) m-CPBA; (h) compound **8**, K_2CO_3, NaI; (i) i) TFA, anisole; ii) Tr-ATMO, $POCl_3$, Py, TEA; iii) TFA, DCM.

Compound 6: $(Boc)_2O$ (0.7 ml, 3 mmol) was added to a stirred solution of piperazine (0.86 g, 10 mmol) in 10 ml of DCM by dropwise. The mixture was stirred overnight and washed with water. The organic layer was separated and dried over sodium sulfate. The solvent was evaporated to give 475 mg of product. Yield: 85.1%. ^{1}HNMR (400 MHz, $CDCl_3$) δ (ppm): 3.38 (m, 4H), 2.80 (m, 4H), 1.46 (s, 9H); MS (ESI) m/z: calcd for $C_9H_{18}N_2O_2$: 186.14; $[M+H]^+$ found: 187.10.

Compound 7: Compound **6** (372 mg, 2.0 mmol) was dissolved in 10 ml of DCM. Then 5-hexynoic acid (224 ul, 2.0 mmol), HBTU (755 mg, 2 mmol) and TEA (700 ul,

5.0 mmol) was added. The mixture was stirred under N_2 atmosphere overnight and concentrated. The residue was purified by column chromatography on silica gel to give 447 mg product. Yield: 79.7%. ^{1}HNMR (400 MHz, $CDCl_3$) δ (ppm): 3.49 (m, 2H), 3.30-3.36 (overlap, 6H), 2.39 (m, 2H), 2.19 (m, 2H), 1.90 (m, 1H), 1.77 (m, 2H), 1.37 (s, 9H); MS (ESI) m/z: calcd for $C_{15}H_{24}N_2O_3$: 280.18; $[M+H]^+$ found: 281.10.

Compound 8: To a stirred solution of compound **7** (40 mg, 0.14 mmol) in 1 ml of DCM was added 300 ul of TFA. The mixture was stirred for 1 hr in ice bath and used directly without further purification.

Compound 9: *m*-Chloroperbenzoic acid (372 mg, 85%, 1.8 mmol) was added to a cooled solution of compound **3** (725 mg, 1.5 mmol) in 3 ml of DCM and stirred at 0˚C for 1 hr. Then the mixture was diluted with 40 ml of EA, washed with 10% $NaHCO_3$ and dried over Na_2SO_4. After evaporation, the residue was purified by column chromatography on silica gel to give 524 mg of white solid. Yield: 70.3%. ^{1}HNMR (400 MHz, $CDCl_3$) δ (ppm): 7.29-7.38 (m, 10H), 6.99 (s, 1H), 6.09 (m, 1H), 5.73 (m, 1H), 5.01 (d, J = 4.60 Hz, 1H), 4.75 (s, 1H), 1.69 (s, 3H), 1.44 (s, 9H), 0.91 (s, 3H); MS (ESI) m/z: calcd for $C_{26}H_{30}N_2O_6S$: 498.18; $[M+Na]^+$ found: 521.23.

Compound 10: To a round bottom flask equipped with a Dean-stark apparatus was added 2-mercaptobenzothiazole (95 mg, 0.57 mmol) and compound **9** (280 mg, 0.56 mmol). The mixture was refluxed in 30 ml of toluene for 3 hrs. After cooling, the solvent was evaporated and the residue was purified by column chromatography on silica gel to afford 290 mg product. Yield: 79.9%. ^{1}HNMR (400 MHz, $CDCl_3$) δ (ppm): 7.87 (d, J = 8.24 Hz, 1H), 7.74 (d, J = 8.24 Hz, 1H), 7.42 (m, 1H), 7.26-7.34 (m, 11H),

6.91 (s, 1H), 5.73 (d, *J* = 9.16 Hz, 1H), 5.51 (d, *J* = 4.60 Hz, 1H), 5.31 (m, 1H), 5.16 (s, 1H), 5.04 (s, 1H), 4.95 (s, 1H), 1.92 (s, 3H), 1.45 (s, 9H); MS (ESI) m/z: calcd for $C_{33}H_{33}N_3O_5S_3$: 647.16; $[M+Na]^+$ found: 670.17.

Compound 11: To a stirred solution of compound **10** (114 mg, 0.18 mmol) in 10 ml of DCM was added silver acetate (65 mg, 0.38 mmol) and chloroacetic acid (765 mg, 8.1 mmol). The mixture was stirred at room temperature for 4 hrs and filtered. The filtrate was concentrated partially and diluted in ethyl acetate. The solution was washed with saturated sodium bicarbonate solution and dried over Na_2SO_4. After concentration and column chromatography, 82 mg of crude product containing **11A** and **11B** was obtained, which was not separable in silica gel and used directly without further purification. MS (ESI) m/z: calcd for **11A** and **11B** $C_{28}H_{31}ClN_2O_7S$: 574.15; $[M+Na]^+$ found: 597.18.

Compound 12: The crude product of compound **11** was dissolved in 1 ml of DCM. Then 43 mg of m-CPBA was added and the mixture was stirred for 1h. After reaction, the mixture was diluted with 20 ml of ethyl acetate, washed with $NaHCO_3$ and dried over Na_2SO_4. The solvent was removed by concentration and the residue was purified by column chromatography on silica gel to give 44 mg product. Yield (two steps): 38.9%. ^{1}HNMR (400 MHz, $CDCl_3$) δ (ppm): 7.32-7.38 (m, 10H), 6.99 (s, 1H), 6.00 (m, 1H), 5.79 (m, 1H), 5.00 (d, *J* = 4.56 Hz, 1H), 4.83 (d, *J* = 11.92 Hz, 1H), 4.74 (s, 1H), 4.63 (d, *J* = 11.92 Hz, 1H), 4.07 (s, 2H), 1.44 (s, 9H), 0.90 (s, 3H); MS (ESI) m/z: calcd for $C_{28}H_{31}ClN_2O_8S$: 590.15; $[M+Na]^+$ found: 613.25.

Compound 13: Compound **12** (44 mg, 0.07 mmol) was added to the crude product of

compound **8** (0.14 mmol) in 5 ml of acetone, followed by addition of potassium carbonate (58 mg, 0.42 mmol) and NaI (10 mg). The mixture was stirred at room temperature for 6 hrs and concentrated. The residue was purified by column chromatography on silica gel to give 30 mg product. Yield: 58.3%. ^{1}HNMR (400 MHz, $CDCl_3$) δ (ppm): 7.32-7.36 (m, 10H), 6.97 (s, 1H), 5.98 (m, 1H), 5.78 (m, 1H), 4.99 (d, *J* = 4.56 Hz, 1H), 4.76 (d, *J* = 11.88 Hz, 1H), 4.73 (s, 1H), 4.54 (d, *J* = 11.88 Hz, 1H), 3.65 (m, 2H), 3.52 (m, 2H), 3.27 (s, 2H), 2.54 (m, 4H), 2.45 (t, *J* = 7.32 Hz, 2H), 2.28 (m, 2H), 1.96 (m, 1H), 1.86 (m, 2H), 1.43 (s, 9H), 0.87 (s, 3H); MS (ESI) m/z: calcd for $C_{38}H_{46}N_4O_9S$: 734.30; $[M+H]^+$ found: 735.37.

Compound C: step i): In a round bottom flask, compound **13** (30 mg, 0.04 mmol) was deprotected with TFA and anisole in DCM, then dried under vacuum for further usage. Step ii): In another flask, the Tr-ATMO (22 mg, 0.05 mmol) was dissolved in 1 ml of DCM and reacted with $POCl_3$ and pyridine to form acetyl chloride *in situ*. Then this acetyl chloride was added dropwise to the cooled mixture of deprotected compound **13** and 2,6-lutidine in THF. After reacted for 1h, the mixture was diluted with EA, washed with water and acidified with HCl. The organic layer was separated, dried over Na_2SO_4 and concentrated. Step iii): This crude product was dissolved in DCM and deprotected with TFA. After reaction, the solvent was removed and the residue was purified by reverse-phase HPLC to give 5 mg product after lyophilization. Yield: 20%. ^{1}HNMR (400 MHz, Acetone-D6) δ (ppm): 8.33 (br, 1H), 8.18 (d, *J* = 9.64 Hz, 1H), 7.18 (s, 1H), 6.14 (m, 1H), 5.50 (d, *J* = 4.56 Hz, 1H), 4.91 (d, *J* = 11.88 Hz, 1H), 4.71 (s, 1H), 4.59 (d, *J* = 11.88 Hz, 1H), 4.04 (s, 3H), 3.91 (s, 3H), 3.76 (overlap, 5H),

3.08-3.15 (m, 4H), 2.50 (t, *J* = 7.32 Hz, 2H), 2.35 (m, 1H), 2.24 (m, 2H), 1.79 (m, 2H), 1.40 (s, 3H); MS (ESI) m/z: calcd for $C_{26}H_{33}N_7O_9S_2$: 651.18; $[M+H]^+$ found: 652.32.

4.2.2 Enzyme inhibition and labeling

Inhibitory activity test. Typically, Bla (~ 0.1 U to benzylpenicillin) was incubated with compound A, B (from 4 to 400 μM) or C (from 50 to 250 μM) for 30 minutes. Then the reaction mixture was added to 1 ml of benzylpenicillin (0.5 mM in PBS) with 1: 200 dilution and the enzymatic hydrolysis of benzylpenicillin was monitored based on the absorbance change at 232 nm.

Enzyme labeling test. The labeling ability was examined with gel electrophoresis. The incubated mixture of 1 μg of Bla and 10 μM of probe C was reacted with 10 μM of Alexa-488-azide in the presence of Cu(I) for 1 hr. Then the reaction mixture was loaded on a 10%-polyacrylamide/SDS gel and subjected for 1 h of separation. The fluorescence was examined on a typhoon scanner with 488 nm excitation and 520 nm emission.

4.3 Results and discussion

The ability of enzyme inhibition was examined with a class A Bla and a class C Bla by measuring the enzymatic hydrolysis of benzylpenicillin as substrate. As shown in Figure 4.3, the enzyme activity of class A Bla was effectively suppressed in the presence of 4 μM of compound A or B, thus proved our hypothesis of introducing the steric hindrance for enzyme inhibition.

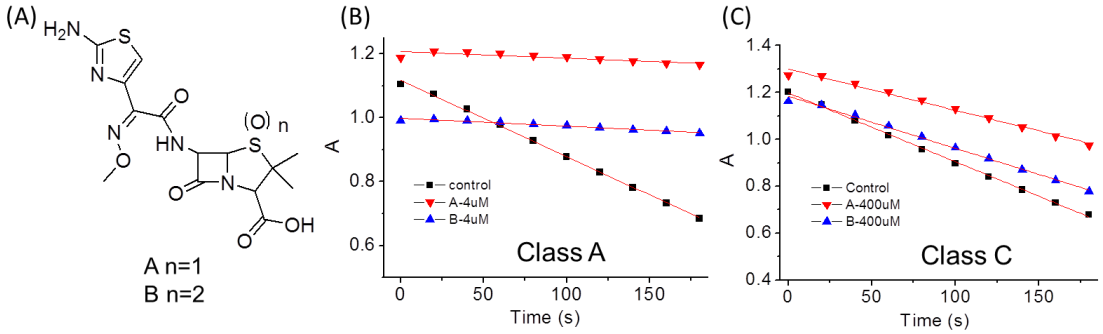

Figure 4.3 (A) Structure of compound A and B. (B) and (C) inhibition of Bla activity by measuring the hydrolysis of benzylpenicillin. (B) class A Bla; (C) class C Bla.

The preliminary result also roughly indicated almost same extent of Bla inhibition in both compounds. In addition, there was no significant inhibition in class C Bla by 400 μM of compound A or B, indicating the selectivity of these probes.

Then we added an analytical handle. Compound C was synthesized by modifying the oxidized ATMO-penicillin with a piperazine group tagged with terminal alkyne, which was introduced for fluorescent labeling and identification (Figure 4.4).

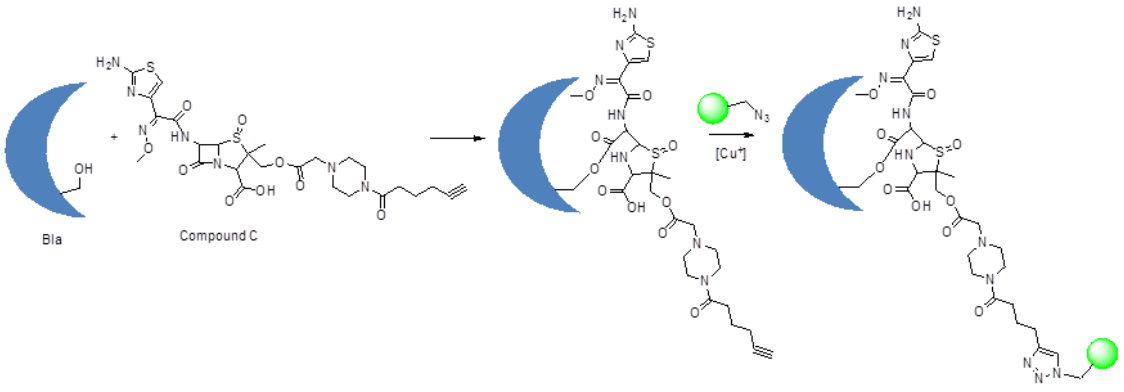

Figure 4.4 Proposed inhibition and labeling of Bla by compound C.

This probe could also inhibit the activity of class A Bla as shown in Figure 4.5A. In addition, the Bla protein could be directly observed from in-gel fluorescence by coupling the incubation mixture with Alexa-488-azide (Figure 4.5B). This preliminary

result proved the design principle of activity-based protein labeling.

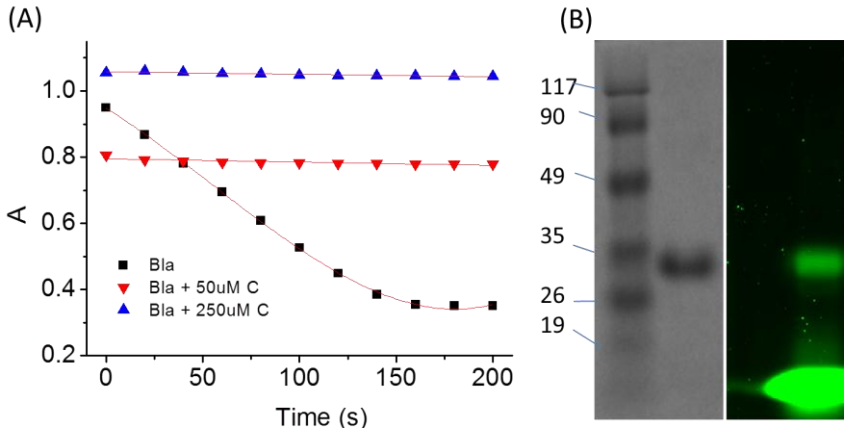

Figure 4.5 (A) Inhibition and (B) labeling of class A Bla by compound C (left: coomassie blue staining, right: fluorescent).

4.4 Future work

This probe displayed the selectivity to class A Bla. Meanwhile, the inhibitor with broader spectrum is also interested for the identification of the protein of interest with unknown type. The labeled protein can be further collected through rapid enrichment by magnetic nanoparticles for further proteomic study and quantitative analysis of inhibitory efficacy. In addition, as this study aims to develop probes for identification of bacterial β-lactamase, it is necessary to study the labeling specificity in bacterial lysates, especially in the presence of penicillin binding proteins. The selective labeling of class A Bla also requires further examination with mixed Blas in fluorescent gel analysis. Meanwhile, with the confirmation of class A β-lactamases in bacterial lysates through in-gel fluorescent image, the labeled protein can be separated and subjected to Mass spectrum analysis for protein identification. Mass spectrum analysis can also provide information about the labeling profile, such as active amino acid residue, to

improve our understanding of enzyme function and enzyme-inhibitor interaction at the molecular level. Further, the Bla inhibition should also be studied in living cells to examine probe membrane permeability and labeling specificity in living conditions. With this probe, it will be easy to determine the type and activity of bacterial *β*-lactamase, which may be helpful to the study of antibiotic resistance.

4.5 References

(1) Scheffers, D. J.; Pinho, M. G. *Microbiol. Mol. Biol. Rev.* **2005**, *69*, 585.

(2) Ghuysen, J. M. *Int. J. Antimicrob. Agents* **1997**, *8*, 45.

(3) Bush, K.; Jacoby, G. A.; Medeiros, A. A. *Antimicrob. Agents Chemother.* **1995**, *39*, 1211.

(4) Bennett, P. M.; Chopra, I. *Antimicrob. Agents Chemother.* **1993**, *37*, 153.

(5) Nikaido, H. *Science* **1994**, *264*, 382.

(6) Ambler, R. P. *Phil. Trans. R. Soc. Lond. B.* **1980**, *289*, 321.

(7) Bush, K.; Jacoby, G. A.; Medeiros, A. A. *Antimicrob. Agents Chemother.* **1995**, *39*, 1211.

(8) Waley, S. G. In *The chemistry of beta-lactams*; Page, M. I., Ed.; Blackie Academic and Professional: London, 1992, p 198.

(9) Jacoby, G. A. *Clin. Microbiol. Rev.* **2009**, *22*, 161.

(10) Livermore, D. M. *Clin. Microbiol. Rev.* **1995**, *8*, 557.

(11) Wang, F.; Cassidy, C.; Sacchettini, J. C. *Antimicrob. Agents Chemother.* **2006**, *50*, 2762.

(12) Kwon, H. H.; Tomioka, H.; Saito, H. *Tubercle Lung Dis.* **1995**, *76*, 141.

(13) Drawz, S. M.; Bonomo, R. A. *Clin. Microbiol. Rev.* **2010**, *23*, 160.

(14) Xing, B. G.; Rao, J. H.; Liu, R. R. *Mini-Rev. Med. Chem.* **2008**, *8*, 455.

(15) Ocallagh.Ch; Shingler, A. H.; Kirby, S. M.; Morris, A. *Antimicrob. Agents Chemother.* **1972**, *1*, 283.

(16) Zlokarnik, G.; Negulescu, P. A.; Knapp, T. E.; Mere, L.; Burres, N.; Feng, L. X.; Whitney, M.; Roemer, K.; Tsien, R. Y. *Science* **1998**, *279*, 84.

(17) Liu, R. R.; Liew, R. S.; Zhou, H.; Xing, B. G. *Angew. Chem., Int. Ed.* **2007**, *46*, 8799.

(18) Jiang, T. T.; Liu, R. R.; Huang, X. F.; Feng, H. J.; Teo, W. L.; Xing, B. G. *Chem. Commun.* **2009**, 1972.

(19) Zhang, J. X.; Shen, Y.; May, S. L.; Nelson, D. C.; Li, S. W. *Angew. Chem., Int. Ed.* **2012**, *51*, 1865.

(20) Xie, H. X.; Mire, J.; Kong, Y.; Chang, M. H.; Hassounah, H. A.; Thornton, C. N.; Sacchettini, J. C.; Cirillo, J. D.; Rao, J. H. *Nat. Chem.* **2012**, *4*, 802.

(21) Pappin, D. J.; Hojrup, P.; Bleasby, A. J. *Curr. Biol.* **1993**, *3*, 327.

(22) Camara, J. E.; Hays, F. A. *Anal. Bioanal. Chem.* **2007**, *389*, 1633.

(23) Tomazella, G. G.; Risberg, K.; Mylvaganam, H.; Lindemann, P. C.; Thiede, B.; de Souza, G. A.; Wiker, H. G. *J. Proteomics* **2012**, *75*, 1830.

(24) English, A. R.; Retsema, J. A.; Girard, A. E.; Lynch, J. E.; Barth, W. E. *Antimicrob. Agents Chemother.* **1978**, *14*, 414.

Chapter 5

Photoactivable Bioluminescent Probes for *in vivo* Bioluminescent Imaging with Spatiotemporal Control

5.1 Introduction

Optical imaging of biomolecule functions and dynamics appreciates the precise control of surrounding microenvironments and regulation of biomolecule activities. One promising strategy for this purpose is through the photocage technology. This approach involves the photoactivation of a caged biomolecule, which is deactivated by the covalent installation of a photolabile group and remains biologically inert before photolysis. With simple irradiation, this strategy can provide spatiotemporal control in the regulation of protein activity, gene expression and cell function. In this chapter, we select the firefly bioluminescence as the target to develop probes with photoactive control due to the importance of this bioluminescent system in small animal imaging.

Firefly luciferase (fLuc) is one of the mostly used bioluminescent reporter genes for *in vivo* imaging of biological pathways.[1] This reporter gene has undergone multiple genetic modifications to achieve high-level expression in mammalian cells and optimized localization of the gene product in cytoplasm.[2] It catalyzes the oxidation of enzyme substrate D-luciferin, which is injected and distributed throughout the entire animal,[3,4] in the presence of endogenous O_2, ATP, and Mg^{2+}. During this process, bioluminescent emission is generated at the peak wavelength of 560 nm (Scheme 5.1, also see Section 1.2.2.3),[5] which is highly efficient with the quantum yield of ~ 41.0% as recently determined by a total-photon-flux spectrometer,[6] affording great sensitivity

for the detection of attomole amounts of luciferase protein.[7] As normal animal cells and tissues do not emit significant light, fLuc bioluminescence has been widely used for biomedical applications like monitoring of infections[8] and cancer progressions with appreciated high sensitivity and low background.[9]

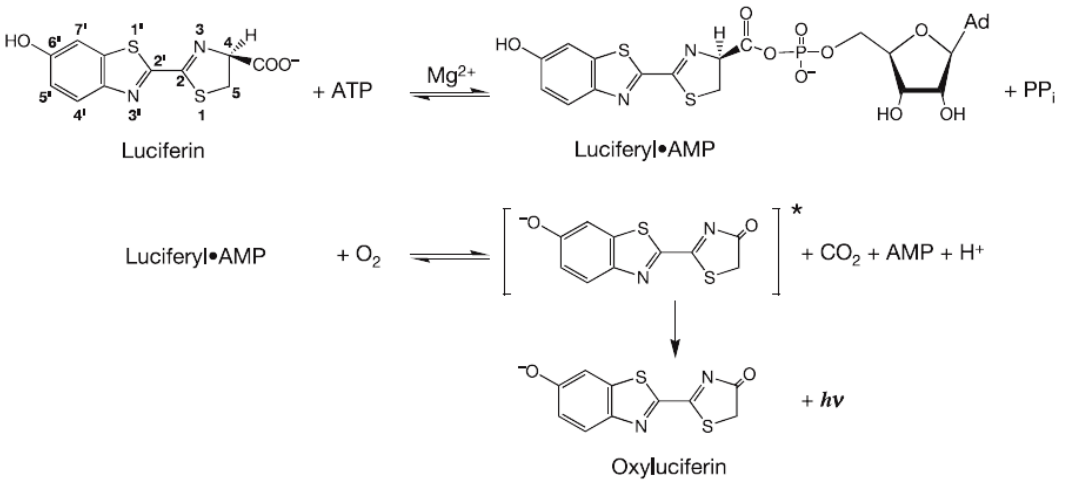

Scheme 5.1 Mechanism of firefly bioluminescence.

Meanwhile, with our understanding of biological mechanisms and functions improves, it has become more and more interesting to track the dynamic properties of bioevents and investigate the intrinsic molecular bases with precise control, which still remains a big challenge due to complicated spatial and temporal organization of living cells and tissues. In order to address this issue, the most notable and promising strategy is the photolysis of photocaged biomolecules, as the activation processes can be triggered by a beam of light with controlled delivery in timing, location, and amplitude (see Section 1.3.2).[10,11] This capability is valuable for the examination of dynamics or spatiotemporal heterogeneity of biochemical events within intact cells where rapid mechanical mixing is not practical.[12]

This photocage technology employs photocaging groups, such as 2-nitrobenzyl (NB) derivatives, which are mostly used due to the compatibleness with a wide variety of functional groups including hydroxyl group, amino group and carboxylic acid, as well as the synthetic easiness and reasonable uncaging kinetics.[13,14] This photoactivation is derived from the phototautomerisation of 2-nitrobenzyl group. During photolysis at the long wave UV (350-400 nm), the NB chromophores are excited electronically to generate the tautomers in aqueous solution, which undergo cyclization reactions to form benzisoxazoline intermediates and finally release the uncaging compounds after ring opening and elimination steps (Figure 5.1).[4] Up to now, more than 40 photocaged biochemicals are commercially available by the installation of 2-nitrobenzyl groups (Table 5.1), which are usually NB derivatives with improved aqueous solubility or uncaging efficiency, such as 2-nitrophenethyl group (NPE), α-carboxy-2-nitrobenzyl group (CNB) and 4,5-dimethoxy-2-nitrophenethyl group (DMNPE).

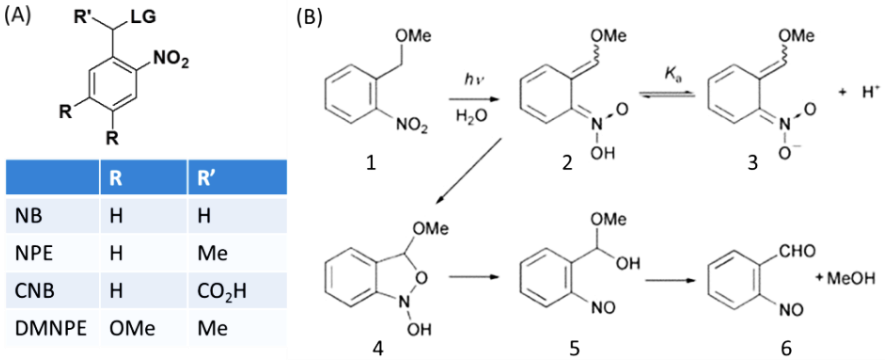

	R	R′
NB	H	H
NPE	H	Me
CNB	H	CO_2H
DMNPE	OMe	Me

Figure 5.1 (A) Structure and (B) activating mechanism of 2-nitrobenzyl photocage groups.

As photoactivation is performed in living cells, the caged compounds must be biologically inert in cellular conditions with essential aqueous solubility and stability.

In some cases, chemical modification of positive or negative charges is performed to improve compound solubility after installation of caging groups.[15] Meanwhile, the chemical bond to connect the photocage group, usually ether, ester, amide, amine or carbamate, must be stable enough to avoid spontaneous release or enzyme hydrolysis by cellular proteins. At the same time, the bond is required to undergo easy photocleavage with fast rate and high efficiency to achieve spatiotemporal control. Actually, it is difficult to determine the release kinetic and efficiency in living conditions due to biological complexity and the fact that most biomolecules are not intrinsically fluorescent and require additional indicators to report the release.[16,17] Although such indicators exist, only a few have been used to characterize the rate of uncaging in living cells,[17,18] probably due to the limited speed of response. Usually, the uncaging property is studied from the photochemistry of caging groups including uncaging quantum efficiency (Φ) and molar extinction coefficient (ε), from which the uncaging cross section ($\Phi \times \varepsilon$) is determined and used to measure the efficiency of uncaging (Table 5.1).

Applied in the development of imaging probes, the caged fluorescent reagents (like bis-CMNB-fluorescein) can display significant signal contrast and huge emission enhancement upon photoactivation, thus have been incorporated into macromolecules to track their movements in living cells upon selective photolysis.[19,20] However, the photocaged probe for *in vivo* bioluminescent imaging is still unachievable since current caged bioluminescent probe is easily hydrolyzed in living cells and not suitable for *in vivo* imaging of luciferase expression by photoactivation (Scheme 5.2).[21]

Caged compound	ϕ	ε (M^{-1} cm^{-1})	$\phi \times \varepsilon$	Rate (s^{-1})	Stability
Calcium chelators					
DM-nitrophen[a,b]	0.18	4,300	774	3.8×10^4	Complete
NP-EGTA[a]	0.23	970	194	6.8×10^4	Complete
nitr-5[b]	0.012	5,500	66	2.5×10^3	Complete
diazo-2[a]	0.03	22,800	1,596	2.3×10^3	Complete
Neurotransmitters					
CNB-Glu[a]	0.14	500	70	4.8×10^4	Fair
CNB-GABA[a]	0.16	500	70	3.6×10^4	Fair
CNB-carbamoylcholine[a]	0.8	430	344	1.7×10^4	Excellent
MNI-Glu[c]	0.085	4,300	366	$\sim 10^5$	Excellent
Phosphates					
NPE-IP_3[a,b]	0.65	430	280	225 and 280	Excellent
NPE-cAMP[b]	0.51	430	219	200	Fair
DMNPE-cAMP[a]	0.05	5,000	250	300	Poor
NPE-cADPribose[a]	0.11	430	271	18	Excellent
NPE-ATP[a,b]	0.63	430	271	90	Excellent
DMNPE-ATP[a]	0.07	5,000	350	18	Fair
Fluorophores					
bis-CMNB-fluorescein[a]	ND	2,000	ND	ND	Complete
DMNB-HPTS [a]	ND	~5,000	ND	ND	Complete

Table 5.1 Commercially available photocaged compounds. [a]From Invitrongen, [b]From Calbiochem, [c]From Tocris.[10]

Meanwhile, as fLuc has a potential disadvantage that the fast consumption of luciferin substrate will lead to unstable signals; the controlled delivery of luciferin probe in living conditions is still highly desired to improve fLuc bioluminecent imaging.

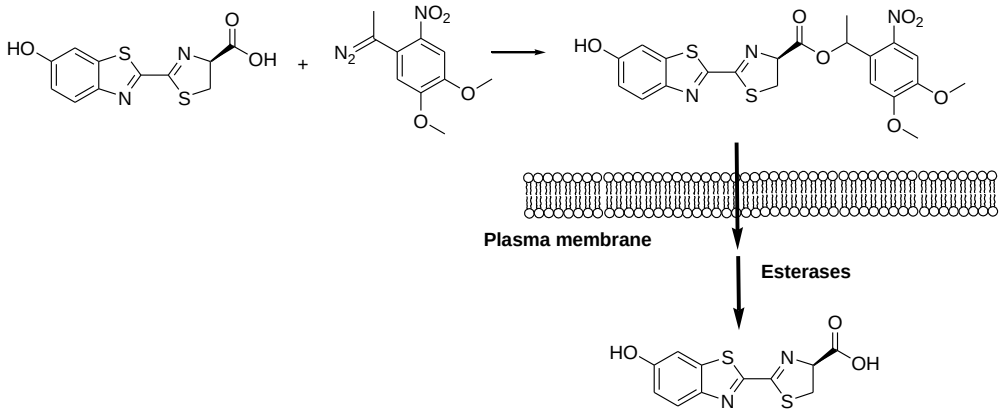

Scheme 5.2 Spontaneous hydrolysis of the caging group in luciferin carboxylic acid.

In order to provide a simple and applicable photocaged firefly luciferase system for efficient bioluminescent measurements in living animals, here we introduce a set of photoactivable luciferin derivatives for detecting firefly luciferase activity *in vivo*.

5.2 Experimental section

5.2.1 Design, synthesis and characterization

As the luciferase reaction involves the fixation of luciferin molecule in the enzyme active site through H-bond interactions (Figure 5.2),[22] chemical modification of the luciferin structure may affect the H-bond and significantly decrease luciferin activity. Previously, the luciferin carboxylic acid was connected with a caging group, but the formed ester bond was found unstable in cellular conditions.[21] In chemistry, it may be more applicable to cage the 6-hydroxy group, as the formed ether bond is theoretically stable to cellular enzymes and not capable of H-bonding to luciferase Arg218.

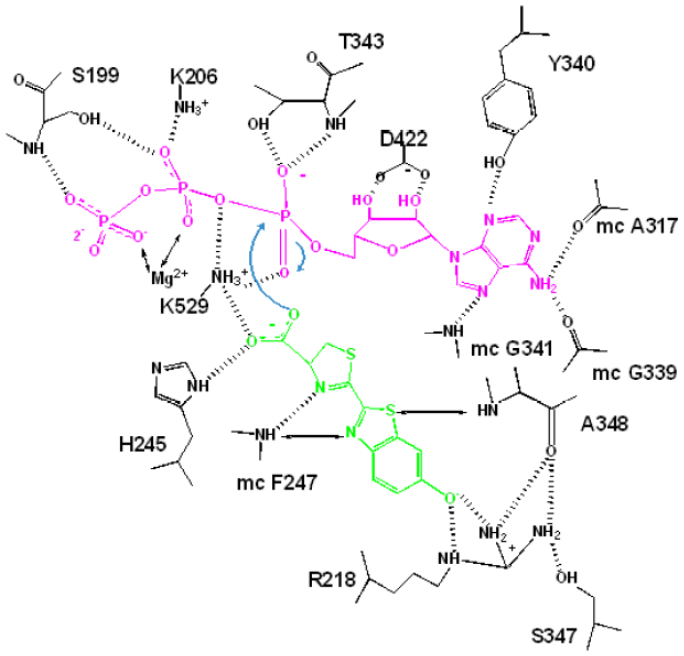

Figure 5.2 Structure of hydrogen bonding between luciferase and luciferin substrate (green), together with ATP (violet) and Mg^{2+}. Dashed lines represent hydrogen bonds.

In this chapter, the luciferin 6-hydroxy group was connected with 2-nitrobenzyl derivatives to block the bioactivity. Photoactivation of the photocaged substrates resulted in the recovery of D-luciferin activity, which was used for imaging luciferase expression in living mice (Scheme 5.3). Combined with photocage technology, the caged luciferin derivatives and fLuc report gene system will provide great opportunity for real-time monitoring of cell functions and dynamics *in vivo*.

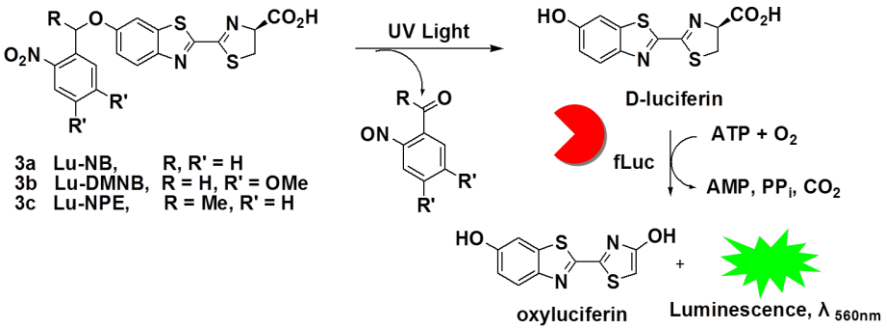

Scheme 5.3 Photoactivation of caged D-luciferin probes for detection of fLuc.

Scheme 5.4 represents the synthetic route for the caged luciferin derivatives. After installing caging groups to 2-cyano-6-hydroxybenzothiazole molecule, the alkylated compounds were directly condensed with D-cysteine to produce the caged luciferin derivatives of **3a**, **3b** and **3c**. The products were characterized by NMR and Mass spectrometry.

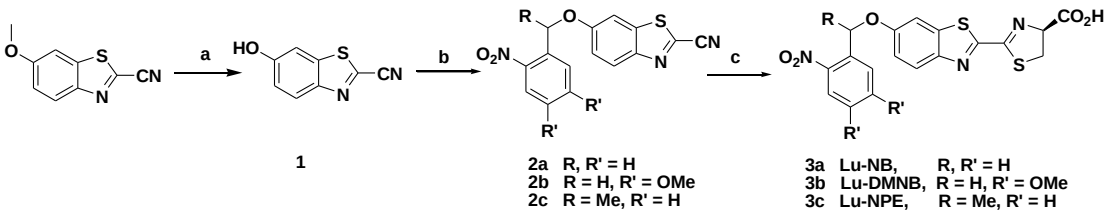

Scheme 5.4 Synthesis of the photocaged D-luciferin derivatives.

Compound 1. In a round bottom flask, pyridine hydrochloride (4 g) was heated to

180 ℃ for half an hour and 2-cyano-6-methoxybenzothiazole (0.200 g, 1.05 mmol) was added. The mixture was then stirred at this temperature for 1h and cooled in ice bath. Then 20 ml of 10% sodium bicarbonate solution was added and the mixture was extracted with EA (15 ml × 3). The combined organic layer was washed with brine, dried over Na_2SO_4 and concentrated. The residue was purified by column chromatography on silica gel using MeOH and DCM (1:20) as eluent to give 0.115 g of white solid. Yield: 62.2%. ^{1}HNMR (DMSO-d6) δ (ppm): 10.59 (br, 1H), 8.06 (d, J = 9.1 Hz, 1H), 7.58 (d, J = 2.3 Hz, 1H), 7.17 (dd, J = 9.1, 2.3 Hz, 1H);^{13}CNMR (MeOH-d4) δ (ppm): 160.6, 147.5, 139.2, 134.1, 126.8, 119.8, 114.5, 107.2; MS (EI): m/z calcd for $C_8H_4N_2OS$ 176.00, found 176.11 $[M]^+$

Compound 2a. 0.053 g of compound **1** (0.30 mmol), 2-nitrobenzylbromide (0.077 g, 0.36 mmol) and potassium carbonate (0.117 g, 0.85 mmol) was refluxed in 5 ml of acetone for 1h. After cooling, the solid was filtered off and the filtrate was concentrated and purified by column chromatography on silica gel with DCM and Hexane (1:3) as eluent to give 0.085 g white solid. Yield: 90.0%. ^{1}HNMR ($CDCl_3$) δ (ppm): 8.22 (d, J = 8.2 Hz, 1H), 8.14 (d, J = 9.2 Hz, 1H), 7.88 (d, J = 7.8 Hz, 1H), 7.72 (d, J = 7.8 Hz, 1H), 7.54 (d, J = 8.2 Hz, 1H), 7.46 (d, J = 2.3 Hz, 1H), 7.36 (dd, J = 2.3, 9.2 Hz, 1H), 5.60 (s, 2H), ^{13}CNMR ($CDCl_3$) δ (ppm): 158.9, 147.5, 147.0, 137.5, 134.3, 134.2, 132.6, 129.0, 128.5, 126.3, 125.4, 118.9, 113.2, 104.6, 67.7; MS (EI): m/z calcd for $C_{15}H_9N_3O_3S$ 311.04, found 311.13 $[M]^+$

Compound 2b. Same procedure as compound **2a**. Yield: 88.6%**.** ^{1}HNMR ($CDCl_3$) δ (ppm): 8.14 (d, J = 9.2 Hz, 1H), 7.80 (s, 1H), 7.48 (d, J = 2.3 Hz, 1H), 7.376-7.39 (m,

1H), 7.31 (s, 1H), 5.60 (s, 2H), 3.97 (s, 3H), 3.98 (s, 3H)**,** ^{13}CNMR ($CDCl_3$) δ (ppm): 158.8, 154.2, 148.3, 147.5, 139.3, 137.5, 134.2, 127.9, 126.3, 118.9, 113.1, 109.3, 108.3, 104.7, 67.9, 56.6, 31.0**;** MS (EI): m/z calcd for $C_{17}H_{13}N_3O_5S$ 371.06, found 371.15 $[M]^+$

Compound 2c. Same procedure as compound **2a**. Yield: 94.5%, ^{1}HNMR ($CDCl_3$) δ (ppm): 8.02-8.06 (m, 2H), 7.73 (m, 1H), 7.60 (m, 1H), 7.44 (m, 1H), 7.19-7.25 (m, 2H), 6.15 (q, J = 6.4 Hz, 1H), 1.75 (d, J = 6.4 Hz, 3H), ^{13}CNMR ($CDCl_3$) δ (ppm): 158.1, 147.6, 147.2, 138.0, 137.4, 134.5, 134.0, 129.0, 127.4, 126.2, 125.2, 119.3, 113.2, 105.5, 72.5, 23.7; MS (EI): m/z calcd for $C_{16}H_{11}N_3O_3S$ 325.05, found 325.08 $[M]^+$

Compound 3a, Lu-NB Compound **2a** (0.040 g, 0.13 mmol) and D-cysteine hydrochloride monohydrate (0.040 g, 0.23 mmol) was added to the mixed solvent of 2 ml of DCM and 2 ml of methanol and stirred till the solid dissolved. Then 0.32 ml of 10% $NaHCO_3$ aqueous solution was added and the mixture was stirred for 15min. Then the mixture was acidified with HCl to pH 2-3 and extracted with DCM (20 ml × 3). The combined organic layer was washed with brine, dried over Na_2SO_4 and concentrated to give product as yellow solid. Yield: 83.4%. ^{1}HNMR (DMSO-d6) δ (ppm): 8.16 (d, J = 7.8 Hz, 1H), 8.08 (d, J = 9.2 Hz, 1H), 7.87 (d, J = 2.3 Hz, 1H), 7.80 (m, 2H), 7.62-7.65 (m, 1H), 7.31 (dd, J = 9.2, 2.3 Hz, 1H), 5.85 (s, 2H), 5.42 (t, J = 9.2 Hz, 1H), 3.66-3.80 (m, 2H); ^{13}CNMR(DMSO-d6) δ (ppm): 171.7, 164.9, 158.9, 157.9, 148.0, 147.9, 137.6, 134.7, 132.7, 129.8, 129.7, 125.5, 125.4, 118.0, 106.5, 78.6, 67.5, 35.3; MS (ESI): m/z calcd for $C_{18}H_{13}N_3O_5S_2$ 415.03, found 416.64 $[M+H]^+$

Compound 3b, Lu-DMNB Same procedure as compound **3a**. Yield: 87.6%. ^{1}HNMR (DMSO-d6) δ (ppm): 8.08 (d, J = 9.2 Hz, 1H), 7.91 (d, J = 2.8 Hz, 1H), 7.74 (s, 1H), 7.38 (s, 1H), 7.34 (dd, J = 9.2, 2.8 Hz, 1H), 5.52 (s, 2H), 5.39-5.43 (m, 1H), 3.87 (s, 3H), 3.88 (s, 3H), 3.65-3.77 (m, 2H); ^{13}CNMR (DMSO-d6) δ (ppm): 171.7, 164.8, 158.9, 158.0, 153.8, 148.5, 148.0, 140.2, 137.6, 127.3, 125.4, 118.0, 111.8, 108.8, 106.6, 78.8, 67.8, 56.8, 56.6, 35.3; MS (ESI): m/z calcd for $C_{20}H_{17}N_3O_7S_2$ 475.05, found 476.31 $[M+H]^+$

Compound 3c, Lu-NPE Same procedure as compound **3a**. Yield: 75.8%. ^{1}HNMR ($CDCl_3$) δ(ppm): 9.43 (br, 1H), 8.00 (d, J = 8.2 Hz, 1H), 7.92 (d, J = 9.2Hz, 1H), 7.73 (d, J = 7.4 Hz, 1H), 7.56 (t, J = 7.4 Hz, 1H), 7.38(t, J = 7.8 Hz, 1H), 7.18 (s, 1H), 7.07 (d, J = 9.2 Hz, 1H), 6.11 (q, J = 6.0 Hz, 1H), 5.37-5.42 (m, 1H), 3.67-3.77 (m, 2H), 1.70 (d, J = 6.0 Hz, 3H); ^{13}CNMR ($CDCl_3$) δ (ppm): 173.8, 167.5, 158.0, 156.9, 148.0, 147.4, 138.4, 137.8, 134.4, 128.7, 127.4, 125.5, 125.0, 117.7, 106.3, 72.2, 53.6, 35.1, 23.6; MS (ESI): m/z calcd for $C_{19}H_{15}N_3O_5S_2$ 429.05, found 430.57 $[M+H]^+$

5.2.2 Photoactivation of caged luciferin derivatives

Photoactivation in cuvette. A 5-mm path quartz cell containing caged luciferin derivative (1 μM, in 10 mM PBS containing 0.05% DMSO as cosolvent) was illuminated at 365 nm for a short period of time.

HPLC analysis and uncaging cross section determination. After photolysis, the uncaging products were confirmed by HPLC analysis on a C-18 reverse phase column with an isocratic mixture of 50% acetonitrile and 50% water containing 0.1% TFA as eluent. The absorbance at 325 nm was used to monitor the caged substrates and

photolysis products. The unmodified D-luciferin was used as standard.

To determine the uncaging cross section ($\Phi^*\varepsilon$), the caged compounds (50 μM in PBS) were irradiated at 365 nm and their disappearance was monitored in terms of peak area from HPLC analysis. The compound of 2-nitrobenzyl alcohol with known quantum yield (Φ_{365}=0.45) was used as standard.[23] The percentage of remained substrate [%] was plotted versus irradiation time [sec]. Each plot was fitted to a linear equation and the slope (k^{sample}, $k^{standard}$) was determined. Thus the disappearance quantum yield (Φ_{365}) of **3a**, **3b** and **3c** was calculated according to the following equation: $\Phi_{365}^{sample}/\Phi_{365}^{standard} = \varepsilon_{365}^{standard} k^{sample}/ (\varepsilon_{365}^{sample} k^{standard})$. Together with the molar extinction coefficient (ε_{365}) obtained from the UV-Vis spectra, the uncaging cross section ($\Phi^*\varepsilon$) was determined.

In vitro bioluminescence measurement. After 1min UV irradiation of caged luciferin solution (final concentration: 12.5 μM), a mixture containing firefly luciferase, ATP and $MgCl_2$ was added with a final concentration of 75 μg/ml, 1 mM and 2.5 mM respectively. The bioluminescence intensity was recorded on a luminometer (20/20n Luminometer; Turner BioSystems, Sunnyvale, CA, USA). The bioluminescence of samples before UV irradiation was also measured as control.

Cell lysis assay. C6 glioma cell line was bought from American Type Culture Collection (ATCC No.: CCL-107) and maintained in F-12K medium containing 10% FBS. Transfection of fLuc gene was carried out by another lab member. PGL3 control plasmid was purchased from Promega containing SV40 promoter, enhancer and firefly luciferase reporter gene. C6 glioma cell line was transfected with PGL3 control

plasmid using Lipofectamine 2000 (Invitrogen). After that, the transfected cells were lysed and added into a mixture containing uncaged compound (12.5 μM), ATP (1 mM) and $MgCl_2$ (2.5 mM) for bioluminescence measurement and determination of luciferase expression.

5.2.3 Photoactivation in living cells

Cell fluorescent imaging. The cell culture of fLuc transfected C6 glioma cells were plated in a 35-mm-diameter glass-bottomed dish (MatTek) and incubated with 25 μM of caged compound for 1hr in an incubator. The cells were then washed with PBS (2 ml) twice and illuminated with UV light. After exposure, fluorescence imaging was acquired with a confocal microscope (Nikon, Eclipse TE2000-E).

Cytotoxicity assays. According to the cell imaging procedure, fLuc transfected C6 glioma cells were incubated with caged luciferin derivatives and followed by 1min UV irradiation. The cytotoxicity was evaluated by an MTT assay.[24]

In vivo bioluminescent imaging. All experiments with live animals were carried out by cooperators in Stanford University. Nude mice were implanted with fLuc transfected C6 cells in the left ear and right shoulder for ten days. After implantation, the mice were anesthetized, transferred to the light-tight chamber of IVIS 200 (Xenogen) and injected with the caged luciferin derivatives intraperitoneally or via tail vein. Followed with UV irradiation in the left ear, the bioluminescent images were acquired. As a control, the tumor in the right shoulder was not irradiated. In comparison, same amount of free D-luciferin was injected into another mouse to identify the luciferase activity.

5.3 Results and discussion

5.3.1 Photoactivation of luciferin bioactivity

In this work, the uncaging is performed with a 365 nm UV light. A prerequisite is the light absorption of the caged luciferin derivatives at this wavelength. As shown in Figure 5.3A, these three derivatives all have obvious absorption at the uncaging wavelength, thus ensures effective photoactivation. The caged compounds were then irradiated for 1 min and the uncaging products were confirmed by HPLC analysis (Figure 5.3B). Obviously, upon brief irradiation, luciferin was released at retention time of 1.6 min, together with the photolysis product of 2-nitrosobenzaldehydes, such as the peak of 6.7 min in compound **3b**, which was further confirmed by Mass spectrum.

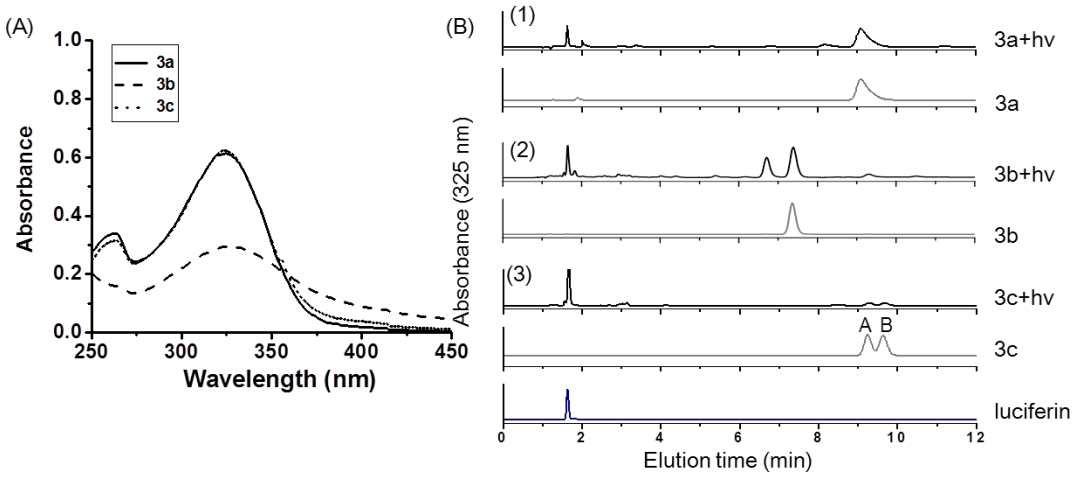

Figure 5.3 (A) Absorption spectra of caged luciferin derivatives (5 μM) in PBS buffer (pH 7.2) with path length of 5 mm. (B) HPLC analysis of photolysis products with free luciferin as reference. In spectrum of **3c**, two diastereomers (peak A and B) were observed due to two chiral centers in this molecule.

It was also found that the photolytic efficiency of these three compounds was

different. The uncaging quantum yield (Φ_{365}) was then determined from HPLC analysis of the disappearance of caged compound upon photolysis. As shown in Figure 5.4, uncaging of these three compounds was comparable to the standard 2-nitrobenzyl alcohol (Φ_{365} = 0.45). Together with the molar extinction coefficient (ε_{365}) obtained from the UV-Vis spectra, the uncaging cross sections ($\Phi^*\varepsilon$) of the caged luciferin derivatives were determined (Table 5.2). Among them, compound **3c** containing NPE-caged group displayed most efficient uncaging, that was consistent with the observations in previous studies.[25]

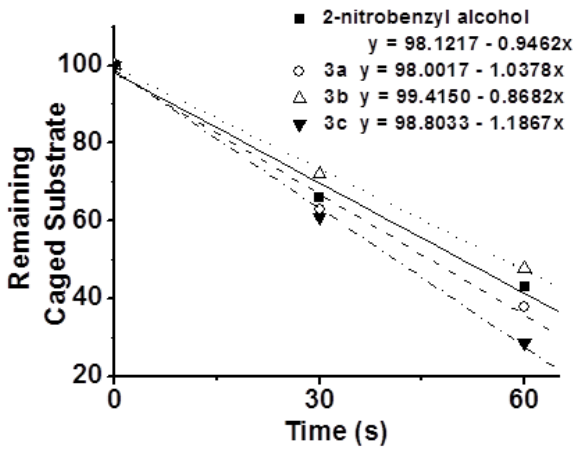

Figure 5.4 Remaining caged substrates versus irradiation time.

	3a	**3b**	**3c**
Φ_{365}	0.69	0.35	0.63
ε_{365}	4304	6864	5280
$\Phi^*\varepsilon$	2970	2402	3326

Table 5.2 Photochemical properties of caged luciferin derivatives.

Photoactivation of the caged luciferin was also examined with bioluminescence measurement by the fLuc assay containing ATP, Mg^{2+} and fLuc. As shown in Figure

5.5A, there was almost no luminescence signal (at the level of 50~100 a.u.) in the caged derivatives before photolysis, proved our hypothesis of blocking the luciferin bioactivity completely by caging the 6-hydroxy group. Upon 1 min UV photolysis, the photoactivation switched on the luciferin bioactivity with robust bioluminescence emission (at the level of 10^7 a.u.). Similar result was also observed in the fLuc transfected C6 cell lysates, where brief photolysis could easily activate the bioluminescence and the signal was also dependent on the cell number (Figure 5.5B). Among the three compounds, substrate **3c** exhibited the highest bioluminescent signal under same irradiation, mostly due to the highest uncaging cross section. As a negative control, incubation of the same cell lysates with the caged substrates did not produce any bioluminescent signal without irradiation, demonstrating that the caged bioluminescent substrates were stable to cellular proteins and able to identify fLuc activities by the fast and convenient cell lysis upon photoactivation.

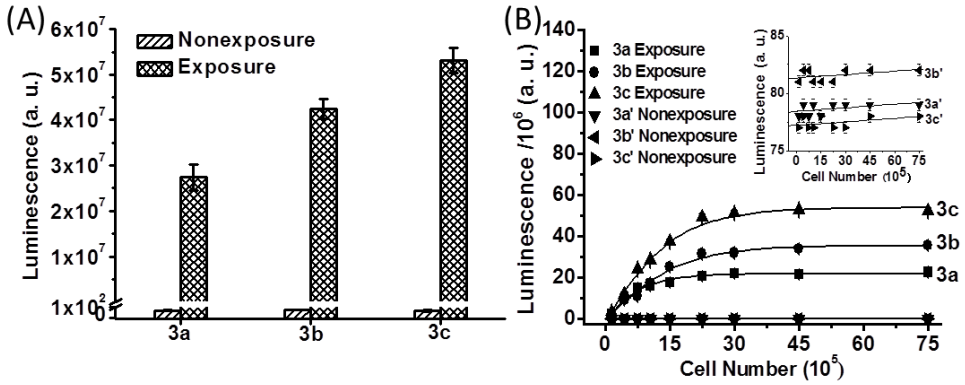

Figure 5.5 (A) Photoactivation of the bioluminescent activity of caged compounds (12.5μM). (B) Bioluminescence intensity in cell lysates. Irradiation time is 1 min.

5.3.2 In vivo photoactivation

For in vivo bioluminescent imaging, the membrane permeability is a prerequisite for

living cell applications. Fortunately, the luciferin molecule is intrinsically fluorescent, thus offers simple and direct observation of the cell permeability through fluorescent imaging. In these compounds, the fluorescent property was largely quenched by the nitrobenzyl group mostly due to photoinduced electron transfer. And upon photolysis, strong fluorescence enhancement was observed in the caged derivatives, indicating the release of free luciferin and the recovery of fluorescence (Figure 5.6). Among them, compound **3c** afforded the greatest fluorescence enhancement, same as the result from uncaging cross section and bioluminescence test.

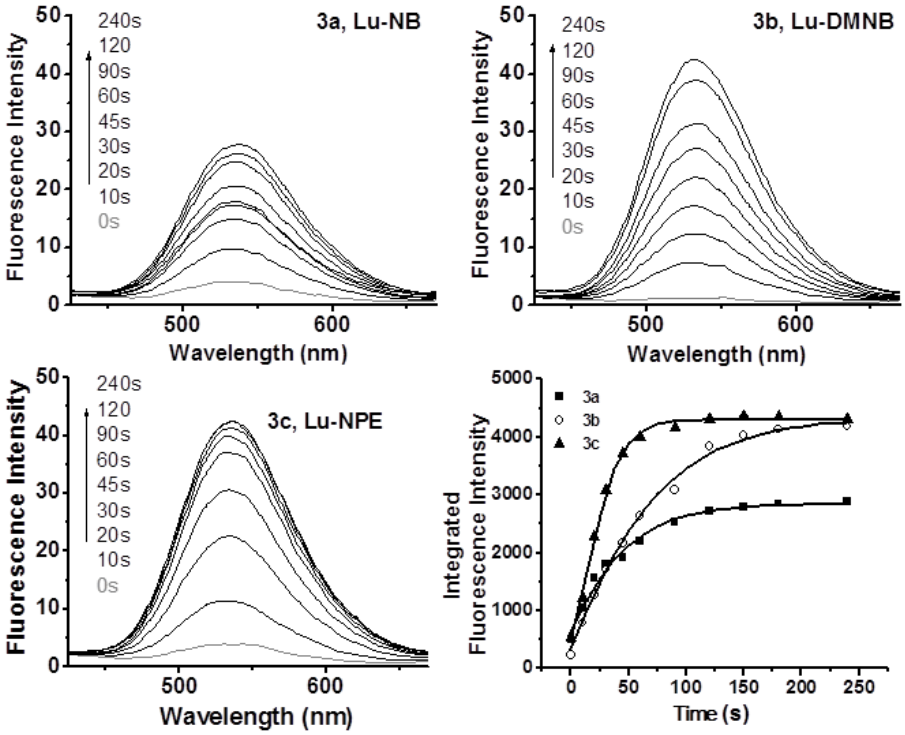

Figure 5.6 Increase of fluorescence intensity after irradiating the caged luciferin derivatives for short periods of time. Ex = 350 nm.

Then the probe cell penetration and photoactivation was monitored in living cells with fluorescent imaging. As shown in Figure 5.7, before photoactivation, the caged compound **3c** displayed very weak fluorescence signal in the C6 glioma cells due to

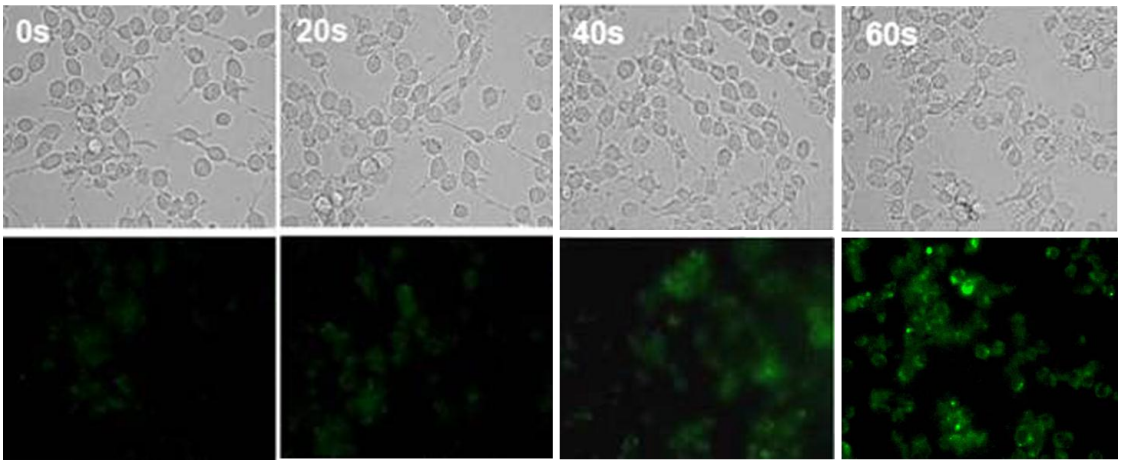

Figure 5.7 Fluorescent imaging of C6 glioma cells incubated with compound **3c** upon irradiation with different time.

effective quenching. Upon brief UV irradiation, the released luciferin revealed bright fluorescence signals inside the cytoplasm with increased illumination time, thus proved the cell penetration. In addition, the other two probes can also exhibit different extent of photoactivation in living cells, mostly because of the difference in uncaging cross section (Figure 5.8).

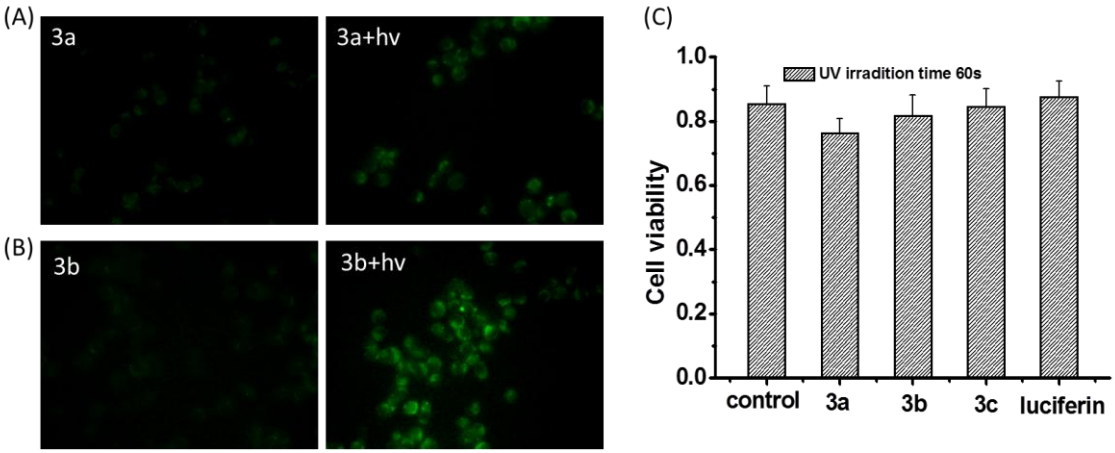

Figure 5.8 Fluorescent imaging of C6 glioma cells incubated with **3a** (A) and **3b** (B) (25 μM) for 1 min irradiation. (C) Cell viability of compound **3a**, **3b**, **3c** and luciferin with 1 min irradiation. Cells without compound incubation were used as control.

Meanwhile, the cell toxicity study using MTT assay showed that there was no obvious toxicity during probe incubation and brief irradiation (Figure 5.8C), demonstrating that the photoactivation of the caged bioluminescent probes did not induce obvious cellular damage. Hence the living cell imaging studies clearly indicated the good cell membrane permeability for cellular photoactivation.

With these results, we studied the in vivo bioluminescent measurements. Typically, 1×10^5 of C6 cells stably transfected with fLuc were injected into the left ear of a nude mouse and 8×10^5 same cells into the right shoulder of the same mouse for ten days of tumor implantation. Then the mice were intraperitoneally injected with 3mg of NPE-caged luciferin (**3c**) for bioluminescent imaging. As shown in Figure 5.9A1, without irradiation, no emission signal was observed in the mouse due to the luciferin activity was blocked by the caged groups. Selective irradiation of the left ear could lead to a strong emission localized in the tumor with irradiation (Figure 5.9A2), where the emission peaked at 20 minutes post-injection and irradiation, and gradually decreased over one hour. Meanwhile, bioluminescent signal was not observed in right shoulder tumor because no irradiation was applied (Figure 5.9A2). This specific bioluminescence signal was also confirmed with ex vivo imaging of the sacrificed mouse (Figure 5.9B). In comparison, same amount of free D-luciferin was injected into a mouse with resultant significant emission in both tumors (Figure 5.9A3), indicating similar fLuc activities in these tumors. Thus the observed signal contrast of compound **3c** upon photolysis was definitely attributed to the photoactivation of luciferin bioactivity, clearly confirmed the capability of caged bioluminescent probes

for imaging the luciferase expression in the living animals.

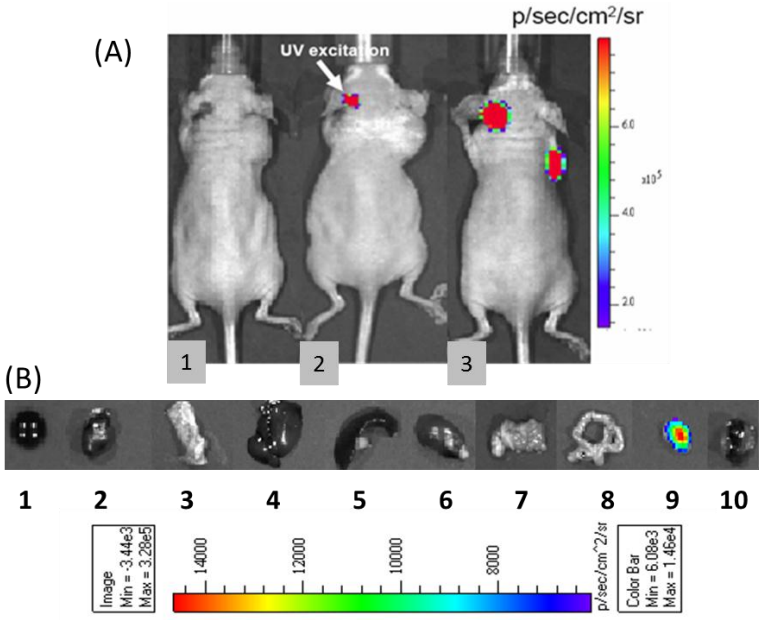

Figure 5.9 (A) In vivo bioluminescent imaging of fLuc activity in living mice. The tumors were implanted in mice by injection of C6-fLuc cells in the left ear and right shoulder. (1) **3c** injection without UV irradiation; (2) **3c** injection and 4 min UV irradiation on left ear tumor only; (3) D-luciferin injection. (B) Ex vivo bioluminescent imaging. (1) blood, (2) heart, (3) lung, (4) liver, (5) spleen, (6) kidney, (7) stomach, (8) intestine, (9) UV-activated tumor, (10) non-activated tumor.

5.4 Conclusion

In this chapter, we have presented the development of new photoactivable bioluminescent probes for imaging firefly luciferase activity in living animals. Combined with photocage technology, these caged luciferin derivatives with preferred stability and membrane permeability, exhibit rapid release of D-luciferin probes with highly controlled spatial and temporal resolution upon brief irradiation and confer robust bioluminescent signals with minimum background. These caged bioluminescent probes will offer great opportunities for real-time imaging of cellular functions *in vivo*.

5.5 Reference

(1) Wilson, T.; Hastings, J. W. *Annu. Rev. Cell Dev. Biol.* **1998**, *14*, 197.

(2) Sherf, B. A.; Wood, K. V. *Promega Notes* **1994**, *49*, 14.

(3) Rehemtulla, A.; Stegman, L. D.; Cardozo, S. J.; Gupta, S.; Hall, D. E.; Contag, C. H.; Ross, B. D. *Neoplasia* **2000**, *2*, 491.

(4) Lipshutz, G. S.; Gruber, C. A.; Cao, Y. A.; Hardy, J.; Contag, C. H.; Gaensler, K. M. L. *Mol. Ther.* **2001**, *3*, 284.

(5) Branchini, B. R.; Southworth, T. L.; Khattak, N. F.; Michelini, E.; Roda, A. *Anal. Biochem.* **2005**, *345*, 140.

(6) Ando, Y.; Niwa, K.; Yamada, N.; Enomot, T.; Irie, T.; Kubota, H.; Ohmiya, Y.; Akiyama, H. *Nat. Photonic.* **2008**, *2*, 44.

(7) Lundin, A. In *Bioluminescence and Chemilunescence: Status Report*; Szalay, A., Kricka, L. J., Stanley, P. E., Eds.; John Wiley: Chichester, UK, 1993, p 291.

(8) Doyle, T. C.; Burns, S. M.; Contag, C. H. *Cell. Microbiol.* **2004**, *6*, 303.

(9) Greer, L. F.; Szalay, A. A. *Luminescence* **2002**, *17*, 43.

(10) Ellis-Davies, G. C. R. *Nat. Methods* **2007**, *4*, 619.

(11) Mayer, G.; Heckel, A. *Angew. Chem., Int. Ed.* **2006**, *45*, 4900.

(12) Shao, Q.; Xing, B. G. *Chem. Soc. Rev.* **2010**, *39*, 2835.

(13) Adams, S. R.; Tsien, R. Y. *Annu. Rev. Physiol.* **1993**, *55*, 755.

(14) Pelliccioli, A. P.; Wirz, J. *Photochem. Photobiol. Sci.* **2002**, *1*, 441.

(15) Wang, L. J.; Corrie, J. E. T.; Wootton, J. F. *J. Org. Chem.* **2002**, *67*, 3474.

(16) Grynkiewicz, G.; Poenie, M.; Tsien, R. Y. *J. Biol. Chem.* **1985**, *260*, 3440.

(17) Bannwarth, M.; Correa, I. R.; Sztretye, M.; Pouvreau, S.; Fellay, C.; Aebischer, A.; Royer, L.; Rios, E.; Johnsson, K. *Acs Chem. Biol.* **2009**, *4*, 179.

(18) Walker, J. W.; Reid, G. P.; McCray, J. A.; Trentham, D. R. *J. Am. Chem. Soc.* **1988**, *110*, 7170.

(19) Mitchison, T. J. *J. Cell Biol.* **1989**, *109*, 637.

(20) Theriot, J. A.; Mitchison, T. J.; Tilney, L. G.; Portnoy, D. A. *Nature* **1992**, *357*, 257.

(21) Yang, J. W.; Thomason, D. B. *Biotechniques* **1993**, *15*, 848.

(22) Deluca, M. *Adv. Enzymol. Relat. Areas Mol. Biol. Cell* **1976**, *44*, 37.

(23) Cummings, R. T.; Krafft, G. A. *Tetrahedron Lett.* **1988**, *29*, 65.

(24) Choi, Y. H.; Liu, F.; Kim, J. S.; Choi, Y. K.; Park, J. S.; Kim, S. W. *J. Control. Rel.* **1998**, *54*, 39.

(25) Kobayashi, T.; Urano, Y.; Kamiya, M.; Ueno, T.; Kojima, H.; Nagano, T. *J. Am. Chem. Soc.* **2007**, *129*, 6696.

Summary and Perspective

In this thesis, the author describes the development of novel optical imaging probes for biological study. In chapter 2 and chapter 3, the strategy of bio-activatable targeting is used in the rational design of imaging probes to facilitate the study of antibiotic resistance. In chapter 4, the strategy of activity-based protein profiling is used in the development of novel probes for identification of antibiotic resistance protein. In chapter 5, the photocage strategy is employed in the development of photoactivable bioluminescent probes.

Chapter 2 presents the *β*-lactamase activated probes for covalent labeling of antibiotic resistant bacteria through the introduction of quinone-methide intermedium for fluorescent labeling. With *β*-lactamase as endogenous reporter, this method can provide quantitative analysis of the resistant bacterial population by flow-cytometry; also allow single-cell detection and direct observation of bacterial enzyme activity in resistant species, thus may be useful in the study of resistance mechanism or new drug development.

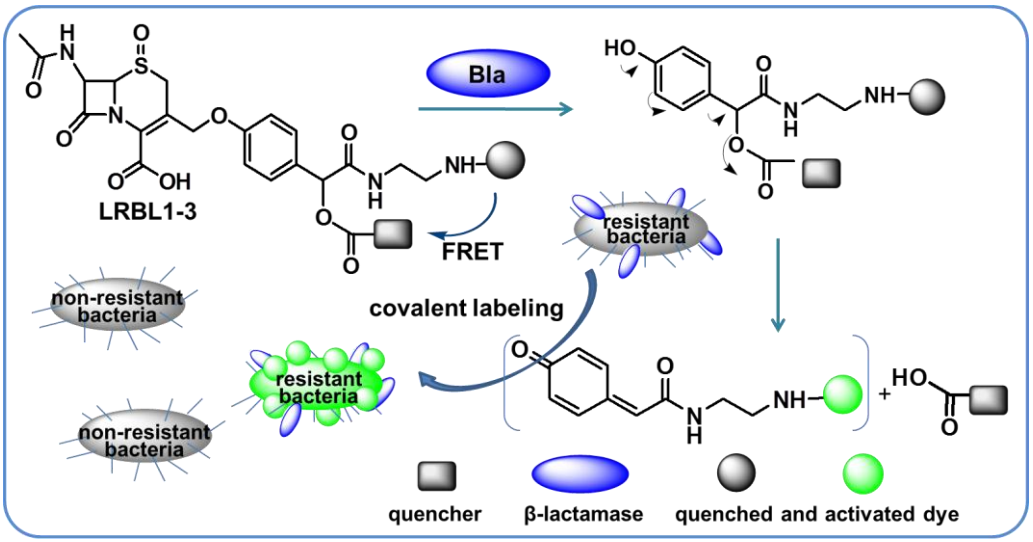

Chapter 3 presents a luminescent Ru(II) probe for intracellular imaging and photokilling of drug resistant bacteria. In this study, the strategy of activatable imaging with photosensitizer is employed, where endogenous β-lactamase is used as reporter. By combining the β-lactam activity and ruthenium photosensitization, this method can clearly image the antibiotic resistance in Gram positive pathogenic strains and kill these resistant strains through photolysis, which may be useful in clinical applications.

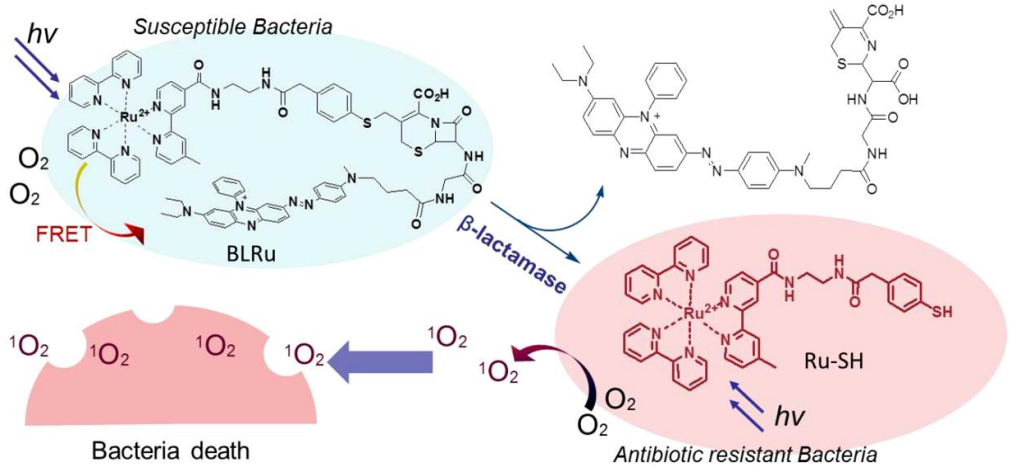

Chapter 4 presents the preliminary results of an ongoing study on the development of activity-based probes for labeling and identification of bacterial β-lactamases. This study uses Bla inhibitors to specifically label the antibiotic resistance proteins and facilitate the proteomic analysis, which may be useful in microbiological study or preclinical investigation.

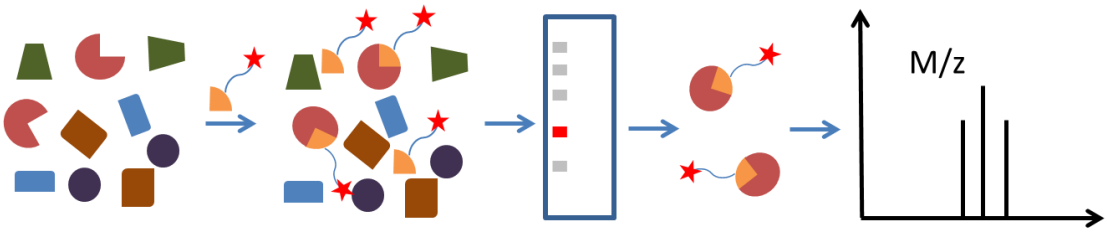

Chapter 5 presents the development of photocaged bioluminescent probes for

imaging the expression of firefly luciferase *in vivo* with photoactivation. With the photocage technology, these caged bioluminescent probes can be activated upon brief irradiation and generate bioluminescent signals with minimum background, which may offer great opportunities for real-time imaging of biological events *in vivo*.

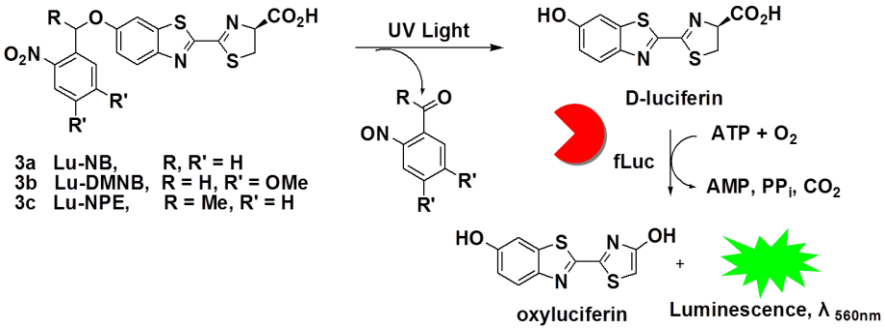

In conclusion, these probes were successfully developed to detect and image the biological targets with specificity and sensitivity. Construction of these probes is dependent on the molecular basis of the biological events to ensure signal specificity, also employs the strategy of pre-quenching to provide high sensitivity. Furthermore, particular functions are also involved in the probe design to confer appreciated features and extend the imaging approach, such as labeling capability to improve the signal contrast, photocage activity to provide spatiotemporal control, inhibitor-based labeling for protein profiling and photosensitizing property for selective bacteria killing. These functions will provide powerful tools in biological study.

Meanwhile, there are still some important points missing from discussion, which may be worth of further study. First, the approaches of photocage technology and photosensitization utilize the UV light or visible light for photolysis, which is limited in tissue penetration. In this consideration, two-photon photolysis powered by paired

IR photons is more appreciated due to the greatly improved penetration and three-dimensional resolution of IR light in the light-scattering media.[1,2] However, in these probes, the 2-nitrophenyl caging group and $Ru(bpy)_3$ photosensitizer are not good at two-photon absorption, which can be improved by chemical modification such as installing the functional groups with higher two-photon absorptions and uncaging cross sections.[1-3] Alternatively, these probes can be conjugated with upconverting nanoparticles, which absorb IR light and emit UV and visible light.[4] With this method, our group has successfully demonstrated the applicability of uncaging the bioluminescent probes in vivo with IR light.[5] Second, the long lifetime of ruthenium luminescence may be suitable for fluorescence lifetime imaging microscopy (FLIM),[6] which is based on the exponential decay rate of fluorescence signal rather than the emission intensity, with the advantage as minimizing the light scattering across the tissue.[7] As the Bla sensitive ruthenium probe is developed with FRET to quench the luminescence intensity, the non-radiative energy transfer will also decrease the emission lifetime. Thus the FLIM based FRET measurement will allow the BLRu probe to discriminate the enzyme activity and avoid the variations in probe concentration and emission intensity across the living sample.

References:

(1) Pawlicki, M.; Collins, H. A.; Denning, R. G.; Anderson, H. L. *Angew. Chem., Int. Ed.* **2009**, *48*, 3244.

(2) Furuta, T.; Wang, S. S. H.; Dantzker, J. L.; Dore, T. M.; Bybee, W. J.; Callaway, E. M.; Denk, W.; Tsien, R. Y. *Proc. Nat. Acad. Sci. USA* **1999**, *96*, 1193.

(3) Poon, C. T.; Chan, P. S.; Man, C.; Jiang, F. L.; Wong, R. N. S.; Mak, N. K.; Kwong, D. W. J.; Tsao, S. W.; Wong, W. K. *J. Inorg. Biochem.* **2010**, *104*, 62.

(4) Haase, M.; Schafer, H. *Angew. Chem., Int. Ed.* **2011**, *50*, 5808.

(5) Yang, Y. M.; Shao, Q.; Deng, R. R.; Wang, C.; Teng, X.; Cheng, K.; Cheng, Z.; Huang, L.; Liu, Z.; Liu, X. G.; Xing, B. G. *Angew. Chem., Int. Ed.* **2012**, *51*, 3125.

(6) Svensson, F. R.; Abrahamsson, M.; Stromberg, N.; Ewing, A. G.; Lincoln, P. *J. Phys. Chem. Lett.* **2011**, *2*, 397.

(7) Bastiaens, P. I. H.; Squire, A. *Trends Cell Biol.* **1999**, *9*, 48.

Publications

(1) Q. Shao, Y. Zheng, X.M. Dong, K. Tang, X.M. Yan, B.G. Xing; *A Covalent Reporter of β-Lactamase Activity for Fluorescent Imaging and Rapid Screening of Antibiotic Resistant Bacteria*, Chem. Eur. J. 2013, , 19, 10903;

(2) Q. Shao, B. G. Xing; *Enzyme Responsive Luminescent Ruthenium (II) Cephalosporin Probe for Intracellular Imaging and photoinactivation of Antibiotics Resistant Bacteria*, Chem. Commun. 2012, 48, 1739;

(3) Q. Shao, B.G. Xing; *Photoactive molecules for applications in molecular imaging and cell biology*, Chem. Soc. Rev. 2010, 39, 2835;

(4) Q. Shao, T.T. Jiang, G. Ren, Z. Cheng, B.G. Xing; *Photoactivable Bioluminescent Probes for Imaging Luciferase Activity*, Chem. Commun. 2009, 4028*;*

(5) Y. M. Yang, Q. Shao, R. Deng, C. Wang, T. Xue, K. Chen, Z. Cheng, L. Huang, X. Liu, B. G. Xing; *In vitro and in vivo Uncaging and Bioluminescent Imaging through Photocaged Upconversion nanoparticles*, Angew. Chem. Intl. Ed. 2012, 51, 3125;

(6) Q. Shao, Y.M. Yang, B.G. Xing; *Molecular Imaging Probes for Cancer Research, Chapter 14: Chemistry of Optical Imaging Probes*, World Science. 2012;

(7) J.X. Aw, Q. Shao, Y.M. Yang, T.T. Jiang, C.Y. Ang, B.G. Xing; *Synthesis and Characterization of 2-(2'-hydroxy-5'-chlorophenyl)-6-chloro-4(3H)-Quinazolinone Based Fluorogenic Probes for Cellular Imaging of Monoamine Oxidases*, Chem. Asian J. 2010, 5, 1317;

(8) Q. Shao, B.G. Xing; *Intracellular imaging and photoinactivation of the antibiotic resistant bacteria by a ruthenium-modified cephalosporin probe responsive to*

endogenous β-lactamase 244th ACS National Meeting & Exposition, Philadelphia, PA, United States, August 19-23, 2012, ORGN-488.